Clemson University
TigerPrints

All Theses | Theses

12-2018

Intermittent Estimation of Volumetric Mass Transfer Coefficient Using Offgas Sensor Data for Continuous OUR Estimation for CHO Cell Culture

Swadeel Deepak Gaad
Clemson University, swadeelgaad@gmail.com

Follow this and additional works at: https://tigerprints.clemson.edu/all_theses

Recommended Citation
Gaad, Swadeel Deepak, "Intermittent Estimation of Volumetric Mass Transfer Coefficient Using Offgas Sensor Data for Continuous OUR Estimation for CHO Cell Culture" (2018). *All Theses*. 2984.
https://tigerprints.clemson.edu/all_theses/2984

This Thesis is brought to you for free and open access by the Theses at TigerPrints. It has been accepted for inclusion in All Theses by an authorized administrator of TigerPrints. For more information, please contact kokeefe@clemson.edu.

Intermittent estimation of volumetric mass transfer coefficient using offgas sensor data for continuous OUR estimation for CHO cell culture

---

A Thesis
Presented to
the Graduate School of
Clemson University

In Partial Fulfillment
of the Requirements for the Degree
Master of Science
Electrical Engineering

---

by
Swadeel Deepak Gaad
August 2018

Accepted by:
Dr. Richard Groff, Committee Chair
Dr. Sarah Harcum
Dr. Rod Harrell

Abstract

For the last several years drugs based on monoclonal antibodies have been manufactured using Chinese Hamster Ovaries (CHO) cells by the bio-pharmaceutical industries to treat cancer and other autoimmune diseases. Several control strategies are used to increase the productivity and efficiency in bio-pharmaceutical manufacturing. Cell growth can be controlled by adjusting the feed rate based on oxygen uptake rate of the cells in the bioreactor. Determining the volumetric mass transfer coefficient and oxygen saturation concentration is vital in correctly estimating oxygen uptake rate. Thus, a robust and efficient method to determine volumetric mass transfer coefficient and oxygen saturation concentration, which uses common industrial sensors, is desired.

In this thesis, a new method to determine volumetric mass transfer coefficient is proposed and implemented on simulated and laboratory experiments. Using this method, volumetric mass transfer coefficient can be calculated independently of oxygen saturation concentration. The fitting parameters required to estimate volumetric mass transfer coefficients are estimated using only the estimated oxygen mole ratio of input gas, the measured oxygen mole ratio of the off-gas and the dissolved oxygen concentration in the bioreactor. A modified version of Savitzky-Golay filtering is used to determine the change in oxygen concentration in the bioreactor liquid. Another algorithm is used to reduce the variations between estimated OUR ($\widehat{OUR}$) and OUR_{linfit} signal to estimate the oxygen saturation concentration in the liquid. Finally, both these signals are used to estimate final OUR signal.

The performance of these algorithms were validated by simulated experiments and lab experiments. A Simulink model was used to simulate bioreactor experiments and the values obtained after implementing the algorithm on simulated experiment data were compared with known values from the Simulink model to verify algorithm accuracy. High accuracy was obtained in all the simulated experiments even in presence of noise. The variation and noise in estimated OUR was

significantly reduced when these algorithms were employed. The algorithm could also be used in cases when there were sudden gas mix changes by estimating OUR using parameters estimated just prior to the gas mix change. The algorithm was applied to laboratory experiments and it showed consistent results over short periods of time. Since the oxygen saturation concentration is important information required to estimate OUR and control the growth rate of cells, these algorithms have the potential of proving useful in implementing robust controller to increase the productivity and efficiency of the monoclonal antibody manufacturing process using CHO cells.

Dedication

I dedicate this work to my parents for their constant support and encouragement throughout my life. All that I am or hope to be I owe it to my parents.

I dedicate this work to my advisers, without whom it was not possible to complete this thesis. Dr. Groff, you were always available and I learned a lot during our brainstorming sessions, more than any book could ever teach me. I owe you a debt of gratitude for answering all my questions with patience and enthusiasm.

I dedicate this work to MATLAB for it allowed me to record, modify and visualize signals and explore biological processes using mathematics.

Acknowledgments

I would like to express my sincere appreciation to my research advisor, Dr. Richard Groff, for his continuous guidance. I would like to thank Dr. Sarah Harcum for introducing me to the area of bio-process engineering with patience and enthusiasm and allowing me to have a free reign in her lab. Also, I would like to thank Dr. Rod Harrell for his valuable inputs and advices.

I would like to sincerely thank Shahin Lashkari for introducing me to bioreactor controls and teaching me the valuable skills required to run bioreactor experiments. I would like to thank Dan Odenwelder and Tom Caldwell for helping me perform bioreactor experiments in the lab.

Table of Contents

List of Tables

List of Figures

Chapter 1

Introduction

Over the past few years in bio-pharmaceutical industry, Chinese Hamster Ovaries (CHO) cells are used as host cell lines for recombinant therapeutic protein manufacturing. Through genetic engineering, these cells can be readily modified, and these host cell lines show robust growth in large scale bioreactors. CHO cells are used to produce various therapeutic proteins to treat cancer, autoimmune diseases and neurological disorder[Al-Rubeai et al., 2015].

Large scale bioreactors are used to produce CHO cells and the associated protein in large quantities. To ensure proper growth and high protein production, it is important to control various aspects of the bioreactor, such as temperature, pH, dissolved oxygen (DO) [Brunner et al., 2016]. Additionally, feeds to the culture are added to ensure that the cells are neither starved nor overfed.

Several control strategies are used to accomplish feeding nutrients. One of the control strategy relies on accurate estimation of the oxygen uptake rate (OUR) to determine the metabolic state of the cells [Pepper, 2015]. OUR is the rate at which oxygen is consumed by the cells in the bioreactor. The metabolic state of the cells is used to control the glucose feed rate, specifically.

Knowledge of the oxygen saturation concentration (C^*_{cal}) in the bioreactor liquid and the Oxygen transfer rate (OTR) is necessary to estimate OUR. OTR is the rate at which Oxygen is transferred from the sparge gas to the bioreactor liquid. This work estimates mass transfer coefficient k_La to calculate oxygen transfer rate (OTR) and provides an estimate of oxygen saturation concentration (C^*_{cal}) in the bioreactor liquid using an estimation of oxygen mole ratio in the input gas, measurement of the oxygen mole ratio in the off-gas and the dissolved oxygen concentration in the liquid.

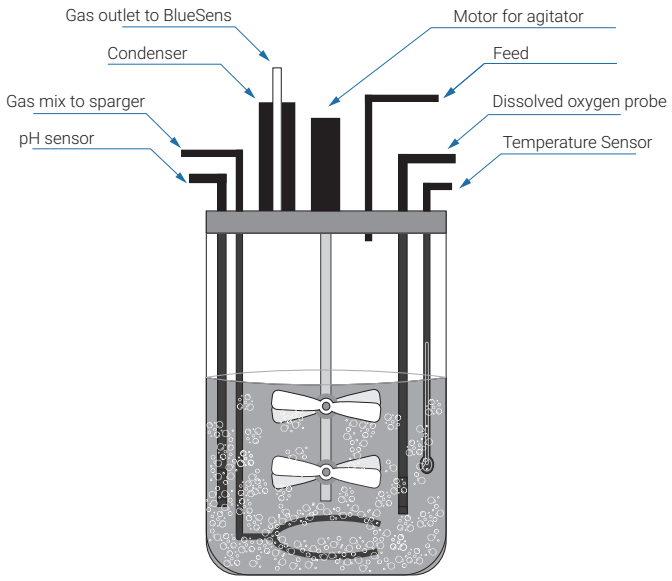

Figure 1.1: Schematic diagram of a basic bioreactor system. Bioreactors are used to manufacture therapeutic proteins using CHO cells or other cells. Several sensors are used to monitor the process.

1.1 Bioreactor Overview

Bioreactors are used to cultivate suspension of cells to produce therapeutic proteins under controlled conditions to facilitate biochemical processes within the cell. A bioreactor is a cylindrical vessel equipped with various sensors and devices which help maintain favorable and contamination free conditions for rapid growth of cells and high protein production. Under optimum conditions, the cells are able to perform their desired function of protein production and produce limited impurities from by-products. Figure 1.1 shows a schematic of typical bioreactor. Enriched air (Air and oxygen mixed) and carbon dioxide are pumped into the bioreactor through a ring sparger. The sparger is a metal tube with a horseshoe shaped ring at its end. This ring has multiple holes for sparge gas to escape into the liquid. A motor operated shaft with impeller blades stir (i.e. agitate) the liquid. Stirring the liquid increases oxygen transfer rate. The impeller blades breaks down bubbles thus increasing surface area and oxygen transfer rate. Agitation also aids in maintaining a temperature control. Metal baffles along the walls of the bioreactor prevent vortex formation.

A metal head plate is used to seal the bioreactor and connect various sensors to the bioreactor. It also serves as an interface for inlet and outlet for the gases and feeds. A water jacket, heating

blanket or dip tube can be used to maintain the culture temperature. A condenser attached to the head plate cools the exhaust gas to reduce evaporation.

Often a digital control unit (DCU) interface is used to regulate the fermentation process by controlling the environment inside the bioreactor. Various sensors such as temperature sensor, pH sensor and dissolved oxygen (DO) probe are connected to the DCU. Pumps can also be used to control feed rates of nutrients.

Initially, the cells grow using the nutrients available in the initial culture media. This phase is called batch phase. Once these nutrients are depleted, additional nutrients are fed into the bioreactor using the pumps. This phase is called fed-batch phase. Throughout the process, it is important to provide sufficient oxygen to the cells to ensure that the cells are in aerobic (oxidative) metabolism state. Initially, air can meet the oxygen demand and stir speed can be increased to increase the OTR as needed to meet the oxygen demand. pre-determined percentage. When the stir speed cannot be increased further, due to biological restrictions, enriched air can be used to meet the OUR demands of the cells.Thus, stir speed and the mole ratio of oxygen in the input stream are increased whenever there is an increased demand for oxygen in the bioreactor.

1.2 Relationship between OTR, OUR and $\dot{C}$

Oxygen transfer rate (OTR) is the rate at which oxygen is transferred from the sparge gas to the bioreactor liquid. Oxygen uptake rate (OUR) is the rate at which oxygen is consumed by the cells in the bioreactor liquid. $\dot{C}$ is the rate of change in the dissolved oxygen concentration in the liquid. The relationship between oxygen uptake rate (OUR), oxygen transfer rate (OTR) and change in the oxygen concentration in the bioreactor liquid ($\dot{C}$) can be expressed as,

$$\dot{C} = OTR - OUR \tag{1.1}$$

In previous work [Mayyan, 2017] using Escherichia-coli, the oxygen uptake rate (OUR) and the oxygen transfer rate (OTR) were nearly equal. That is,

$$OTR \approx OUR \tag{1.2}$$

Thus, $\dot{C}$ was sufficiently low and could be ignored while calculating OUR from OTR. How-

ever, for mammalian cells, the cell growth rate is much lower and OUR cannot be estimated by using equation 1.2. Thus an estimation of $\dot{C}$ is desired. $\dot{C}$ can be expressed as

$$\dot{C} = C^*_{cal} * (\frac{\dot{DO}}{100}) \tag{1.3}$$

Where, C^*_{cal} is oxygen saturation concentration for the culture in the bioreactor at calibration. Thus, to determine $\dot{C}$ it is necessary to obtain an estimation of C^*_{cal}.

1.3 Purpose of oxygen saturation concentration in metabolism control

To increases the production yield for CHO cells in the bioreactor, the nutrient feed has to be controlled. To achieve bioreactor control a continuous online estimation of oxygen uptake rate (OUR) is desired. For correct estimation of OUR an estimation of oxygen saturation concentration is required.

If the amount of substrate in the bioreactor culture is very high i.e., the cells might shift to overflow metabolism and produce lactate [Doverskog et al., 1997], [Friesewinkel et al., 2010] and ammonia [Ljunggren and Häggström, 1992], [Friesewinkel et al., 2010]. Both lactate and ammonia have an inhibitory response [Doverskog et al., 1997], [Ljunggren and Häggström, 1992] for growth and therapeutic protein production in the bioreactor. So it is desirable to minimize the production of these waste products. For E-coli cells maximum growth rate can be achieved if the cells are kept at the boundary of oxidative and overflow metabolism [Pepper, 2015]. To apply this control strategy to CHO cells, online estimation of OUR is necessary in the more complex media. For accurate estimation of OUR, it is vital to accurately determine saturation concentration of oxygen in the CHO cell cultures.

Previous work designed and implemented an OUR controller for E-coli using an an off-gas sensor to estimate oxygen transfer rate (OTR). The OUR controller used a real-time online estimator [Wang, 2014] and was used by [Pepper, 2015] in his control algorithm. The OTR was estimated using dissolved oxygen measurements from the DO probe and a continuously updated mass transfer coefficient (k_La) using off-gas sensor. This 1^{st} generation estimator was limited to using only air as input gas. This limited the maximum E-coli cell density that could be achieved. A further

improvement on the estimator design developed by [Mayyan, 2017] and used by [Lashkari, 2017] involved the ability to increase the oxygen mole ratio in the sparge air. This allowed E-coli to be cultured to higher cell densities by appropriately adapting the feed rate.

In summary, an estimate of OUR is required to implement control strategies that rely on sensing metabolic changes in the cells. To estimate OUR, an estimate of the OTR, and oxygen saturation concentration at calibration, C^*_{cal}, was required. In this thesis, a method to obtain continuous online estimation of OUR is designed. This involves estimating OTR by estimating k_La and $\dot{C}$ by estimating C^*_{cal}.

In chapter 2 there is a discussion about prior work to estimate OTR and OUR. Chapter 2 includes methods to increase OTR. In chapter 3 new algorithms to estimate mass transfer coefficient and oxygen saturation concentration at calibration are discussed. Chapter 3 also includes details about the bioreactor experiment setup. In chapter 4, the Simulink simulation used to design and test the algorithms is discussed. In chapter 5, the algorithm results for experiment data are presented. Chapter 6 presents the conclusion and the future work.

1.4 Thesis statement

To estimate OUR by fitting the relationship between k_La and stir speed (N) and estimating the dissolved oxygen saturation concentration at calibration (C^*_{cal}) using offgas sensor data and dissolved oxygen measurements.

Chapter 2

Background

This chapter discusses several methods to estimate the oxygen transfer rate (OTR). These methods include (i) The dynamic method (ii) Off-gas sensor method (iii) The chemical method. OTR was estimated by using the OTR_{offgas} measurements from the off-gas sensor for bioreactors with E-coli cell culture. This chapter briefly talks about the adaptive estimator used to estimate OUR using OTR_{offgas} measurements.

2.1 Prior work

2.1.1 Techniques to increase oxygen transfer rate:

To meet the oxygen demand of the increasing number of cells in the bioreactor culture OTR must be increased. The four major techniques to increase oxygen transfer rate are:

1. By increasing the stir speed of the impeller blades
2. By pressurizing the bioreactor.
3. By increasing the oxygen mole ratio in the input gas.
4. By using chemical methods.

Increasing stir speed increases the oxygen transfer rate from the gas stream to the bioreactor culture by increasing the amount of time the gas bubbles are in contact with the liquid. Agitation also breaks down the gas bubbles into smaller bubbles thereby increasing the surface area in contact with the liquid. This increases the rate at which oxygen from the input gas stream is transferred

into the liquid. CHO cells have very thin thermodynamically controlled and self-assembled plasma membrane [Hu et al., 2011]. High stir speed can cause sheer stress on this membrane which can lead to cell death [Nasser and El-Moghaz, 2010]. Thus, an upper limit is placed on the stir speed.

OTR can also be increased by pressurizing the bioreactor [Lara et al., 2011]. According to gas laws, pressure is directly proportional to the number of moles, assuming volume and temperature is constant. Since the bioreactor can be maintained at a fixed temperature and the volume of liquid does not change by a large amount instantaneously, mole ratio of oxygen in the bioreactor can be increased by increasing the pressure. In this work, a glass bioreactor was used. Hence, it was not possible to increase the pressure in the bioreactor much.

By increasing the oxygen mole ratio in the input gas, the oxygen transfer rate can be increased [Castan et al., 2002]. The oxygen percentage in the input gas can be steadily increased by increasing the oxygen mass flow rate. By increasing the oxygen mass flow rate and decreasing the flow rate of house air, mole ratio of oxygen in the input gas is increased. This increases the oxygen transfer rate from the gas stream to the bioreactor culture.

One example of a chemical method to increase OTR is to add a perfluorocarbon emulsion to the bioreactor media.[Ju et al., 1991]. The subsequent experiments showed an enhancement in the oxygen transfer rate of the media. To intermittently predict k_La a continuous estimation of OTR is required. However, this method does not allow for an online and continuous measurement of OTR. This limits the use of this method in this work.

2.1.2 Methods to compute volumetric mass transfer coefficient

Oxidative metabolism is desirable to produce good quality recombinant therapeutic protein using CHO cells. Sufficient amounts of dissolved oxygen are required in the culture to ensure that the cells have enough oxygen to operate under oxidative metabolism. The oxygen uptake rate is a good indicator of the metabolism state of the cells in the bioreactor [Pepper, 2015]. As indicated by equation 1.1, to estimate OUR an estimate of OTR and C^*_{cal} is desired. Thus an accurate estimation of OTR is required to estimate the metabolic state of the bioreactor culture. Oxygen transfer rate is expressed as,

$$OTR = k_La \times (C^* - C) \tag{2.1}$$

Where, k_La is the mass transfer rate of oxygen in the liquid $[h^{-1}]$, C^* is the oxygen saturation

concentration in the liquid $[gL^{-1}]$ and C is the dissolved oxygen concentration in the liquid $[gL^{-1}]$. To estimate OTR, it is important to determine k_La. Several methods are proposed to estimate k_La.

In experiments performed for this work, cells were always present in the bioreactor. Cells actively change the composition of the culture media through out the processes. The cells consume oxygen which alters the concentration of oxygen in the bioreactor culture. Thus, methods which only compute k_La in the presence of cells were considered.

One direct way of measuring k_La involves the use of gas sensors connected to the inflow and outflow of the bioreactor. By measuring the total gas flow at the inlet and outlet of the bioreactor and measuring the mole ratio of oxygen at the inflow and the outflow of the bioreactor, k_La can be estimated [Redmon et al., 1983]. This method requires two gas sensors to determine the mole ratio of oxygen in the input and off-gas. A modification of this method to calculate OTR is used to determine the feed rate for increased production yield [Goldrick et al., 2018]. A further improved method uses OTR to obtain a continuous online estimation of OUR [Fontova et al., 2018].This method, however, had high error rates.

Another method consist of shutting down gas flow to the bioreactor [Bandyopadhyay et al., 1967]. OUR is computed as a function of decreasing slope of the dissolved oxygen concentration. When the gas flow is turned back on, dissolved oxygen concentration in the culture increases. Using this time profile of decreasing and increasing DO concentration k_La is computed. There are two major drawbacks for this method. First, the time response of the DO probe must be taken into consideration. Mammalian cells like CHO cells are extremely fragile and susceptible to change in its environmental conditions, stopping or decreasing the input oxygen mole ratio can potentially kill these cells [Riet, 1979]. A later upgrade to this method suggested by[Badino et al., 2000] accounted for the time response of the DO probe. This allowed a more accurate measurement of k_La but did not sufficiently counter the potential harm caused by cutting off input gas to the CHO cells in the bioreactor.

The underlying reason for stopping gas inflow momentarily before restarting it again is to obtain a time versus dissolved oxygen profile of absorption-desorption cycle to calculate k_La as a perturbed signal. Thus, another method proposes that does not require switching off the inflow gas completely. Instead, fluctuates the DO by increasing and decreasing the oxygen mole ratio in the input gas. However, this subjects the CHO cells to oxidative stress [Handlogten et al., 2018]. Similar results can be obtained by applying small stir speed change to increase or decrease DO

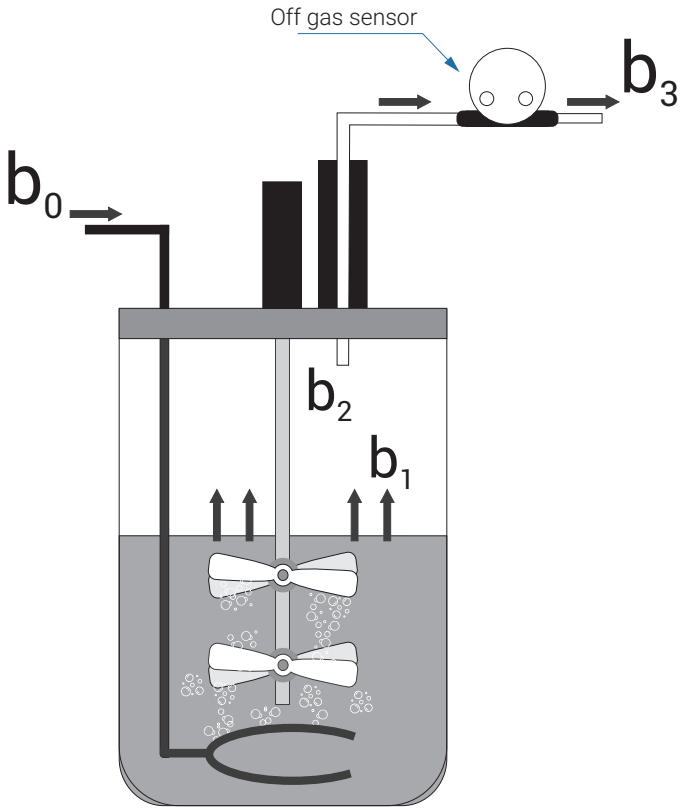

Figure 2.1: Flow direction of gas through the bioreactor system. b_0, b_1, b_2, b_3 are the oxygen mole ratios of oxygen in the input gas, gas exiting the liquid, gas in the head-space and measured by the off-gas sensor.

[Patel and Thibault, 2009]. However, unwarranted increase in stir speed subjects the CHO cells to mechanical sheering [Hu et al., 2011]. In [Hu et al., 2011] the stir speed was varied between 450 rpm and 550 rpm for a 2L vessel which resulted in a negetive effect on cell viability and growth. In this work the stir speed was kept between 80 rpm to 320 rpm to avoid decrease in cell viability fue to sheer stress.

2.1.3 OTR and OUR computation

As explained in section 1.3, to increase protein production in the bioreactor, an estimation of OUR ($\widehat{OUR}$) $[gL^{-1}h^{-1}]$ is required to implement the control strategy used by [Lashkari, 2017].

Using equation 1.1 OUR can be expressed as

$$OUR = OTR - \dot{C} \tag{2.2}$$

Thus, an estimation of OTR ($\widehat{OTR}$) $[gL^{-1}h^{-1}]$ and an estimation of change in the dissolved oxygen concentration in the liquid ($\hat{\dot{C}}$) is necessary to compute $\widehat{OUR}$. Figure 2.1 schematically shows the direction of gas flow through the bioreactor system and peripherals. b_0 [mol/mol] is the oxygen mole ratio in the input gas. Further, the gas escapes at the surface of the liquid. The mole ratio of oxygen here is denoted by b_1 [mol/mol]. This gas mixes with the gas in the head-space which has an oxygen mole ratio of b_2. Finally, the gas escapes through the gas outlet of the bioreactor. The mole ratio of the gas coming out of the bioreactor or off-gas is measured by the off-gas sensor and it is denoted by b_3 [mol/mol].

Equation 2.2 can be rewritten as,

$$\widehat{OUR} = \widehat{OTR} - \hat{\dot{C}} \tag{2.3}$$

To calculate OUR, OTR has to be calculated. OTR can be calculated from the off-gas sensor. It is expressed as [Wang, 2014],

$$OTR_{ideal} = \left(\frac{M_f P}{V_1 R T} \right) \times \left(b_0 - b_1 \right) \tag{2.4}$$

Where, M_f is the mass flow rate (L/h), P is the absolute pressure (atm) in the bioreactor, V_1 is the volume of the liquid (L), R is the gas constant (L atm/K mol) and T is the temprature (Kelvin). b_0 can be calculated and b_3 is measured by the off-gas sensor. However, it is difficult to obtain direct measurements for b_1. It is generally assumed that b_1 is equal to b_3. However, headspace and sensor dynamics heavily filter b_1. Analysis of the head-space mixing dynamics and the measurement delays in the off-gas sensor readings show that b_1 is not equal to b_3. The oxygen concentration dynamics for the bioreactor are,

$$\frac{d}{dt} b_2 = \frac{M_f}{V_2} \left(b_1 - b_2 \right) \tag{2.5}$$

$$\frac{d}{dt}b_3 = \frac{1}{\tau_2}(\, b_2 - b_3) \tag{2.6}$$

The signal b_1 is heavily filtered by a time constant $\tau_1 = \frac{V_2}{M_f}$. The measurement delay of the off-gas sensor further filters the headspace signal b_2 by a time constant τ_2. The value of this time constant for BlueSens off-gas sensor is 55 seconds [Aehle, 2010]. This filtering effects are considered while modelling the OTR estimator. Thus, the modified version of off-gas OTR is calculated as,

$$OTR_{offgas} = (\, \frac{M_f P}{V_1 RT}) \times (\, b_0 - b_3) \tag{2.7}$$

Physically, OTR can be modeled using equation 2.1 as,

$$OTR = k_L a \times (\, DF) \tag{2.8}$$

The term $(C^* - C)$ is denoted as DF (short for driving force) [Mayyan, 2017]. The mass transfer coefficient or $k_L a$ is a function of stir speed and numerous physical parameters such as pressure, temperature and salinity [Dorresteijn et al., 1994]. In this work, $k_L a$ is modeled as a function of stir speed. Thus,

$$k_L a = \alpha_0 + \alpha_1(\, N - N_0) \tag{2.9}$$

Where N is stir speed (rpm), N_0 is a constant chosen as a value in the middle of the range of stir speeds and α_0 and α_1 are fitted parameters. α_0 and α_1 have to be updated as the fermentation progresses to account for changes in dissolved oxygen (DO), b_0 and other physical parameters. Equating equations 2.7 and 2.8 we get,

$$b_1 = b_0 - \frac{V_1 RT(C^* - C)}{M_f P}\alpha_0 - \frac{V_1 RT(C^* - C)(N - N_0)}{M_f P}\alpha_1 \tag{2.10}$$

By rearranging equations 2.5 and 2.6 and substituting equation 2.10 equation 2.11 is obtained.

$$\begin{bmatrix} \dot{b_3} \\ \dot{b_2} \end{bmatrix} = \begin{bmatrix} \frac{-M_f}{V_2} & 0 \\ \frac{1}{\tau_2} & \frac{-1}{\tau_2} \end{bmatrix} x + \begin{bmatrix} \alpha_0 & \alpha_1 & b_0 \\ 0 & 0 & 0 \end{bmatrix} \begin{bmatrix} \frac{-V_1 RT(C^* - C)}{V_2 P} \\ \frac{-V_1 RT(C^* - C)(N - N_0)}{V_2 P} \\ \frac{M_f}{V_2} \end{bmatrix} \tag{2.11}$$

$$y = \begin{bmatrix} 1 & 0 \end{bmatrix} \begin{bmatrix} b_3 \\ \bar{b_2} \end{bmatrix} \tag{2.12}$$

b_2 is the oxygen mole ratio of gas in the headspace. $\bar{b_2}$ is the mean of b_2 and $\dot{\bar{b_2}}$ is the differentiation of $\bar{b_2}$. These values are calculated as a part of the state space equations. However, these values are not needed to use this model. Hence, the output is multiplied by an observable matrix as shown in equation 2.12.

Based on [Narendra and Annaswamy, 2012], the value of $\hat{\alpha}_0$ and $\hat{\alpha}_1$ can be estimated using an adaptive estimator. The details of this method are provided in [Pepper, 2015] and [Wang, 2014]. A slight modification of this method was presented by [Mayyan, 2017] and used by [Lashkari, 2017] where α_0 and N_0 were assumed to be zero.

After determining the unknown parameters of the linear system ($\hat{\alpha}_0$ and $\hat{\alpha}_1$), OTR and OUR can be estimated as

$$\widehat{OTR} = (\hat{\alpha}_0 + \hat{\alpha}_1(N - N_0))(C^* - C) \tag{2.13}$$

and equation 2.3 can be used to determine $\widehat{OUR}$ as,

$$\widehat{OUR} = \widehat{OTR} - \dot{C} \tag{2.14}$$

In summary, dissolved oxygen (DO) sensor and off-gas sensors were used to estimate OTR and OTR_{offgas}. These signals were then used to design an adaptive estimator which can provide an online estimation of OUR. This method minimizes the filtering effects due to head-space dynamics and off-gas sensor delay by using OTR measurements obtained using DO measurements. Equations 2.7 and 2.8 are used extensively in this work to estimate a modified version of k_La.

Chapter 3

Experimental Setup and Research Design

This chapter presents the experimental setup used to perform the bioreactor experiments. Separate Simulink blocks were used to control the bioreactor signals, such as the oxygen mole ratio in the input gas (b_0), stir speed (N) and the feed rate. Additionally, this chapter also discusses and compares the two algorithms developed to estimate OTR and C^*_{cal} by formulating least squares problem and using normal equations.

3.1 Experimental Setup

The experimental setup can be subdivided into two subsystems:

1. Gas mix control
2. Stir Speed and Feed control

3.1.1 Gas mix Control

A schematic diagram of this control setup for the bioreactor is shown in figure 3.1:

The experiment requires continuous supply of three gases, house air, oxygen and carbon dioxide from compressed gas tanks. The flow-rate of these gases was controlled by three mass flow controllers (GFC-17, AALBORG). Each mass flow controller is calibrated for the respective input

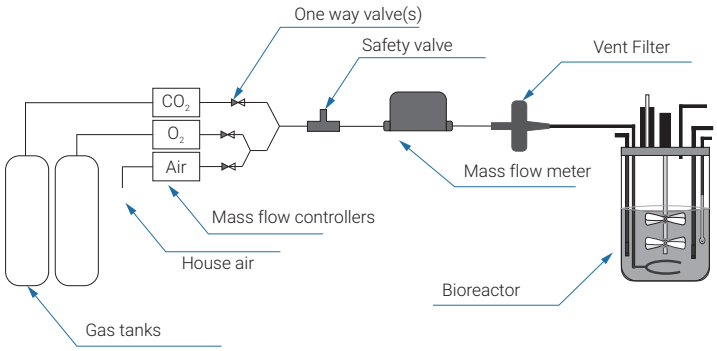

Figure 3.1: Gas mix control setup for the bioreactor.

gas by the manufacturer and have an accuracy of ± 1% of the full scale. The range of each mass flow controller and the corresponding absolute error is listed in Table 3.1:

Sr. No.	Gas Type	Flow range (mL/min)	Flow error (mL/min)
1	Air	0 to 100	± 1
2	Oxygen	0 to 100	± 1
3	Carbon dioxide	0 to 10	± 0.1

Table 3.1: List of MFC mass flow ranges and corresponding errors.

One-way valves are connected at the exit of all mass flow controller to ensure that there is no back-flow of gases. Simulink signals was used to control the mass flow controllers using a Quanser Q8 board. A safety valve was used to protect the bioreactor. A mass flow meter was used to measure the total mass flow into the bioreactor. Before the gas enters the bioreactor, a vent filter (0.2μm, Sartorius) was used to sterilize the gas.

The gases were sparged using a ring sparger. Propeller blades were used. The unconsumed oxygen and other gases escape at the water and air interface into the headspace. This gas mixes in the headspace before being measured by the off-gas sensor (Bluesens, Germany). A condenser was used at the outlet of the bioreactor to reduce evaporation of the media. The off-gas sensor determined the mole ratio of oxygen in the gas that exited the bioreactor.

3.1.2 Stir Speed and Feed Control

A schematic diagram of stir speed and feed control is shown in the figure 3.2: A stir speed controller block from Simulink is used to control the motor connected to the stirring rod. This

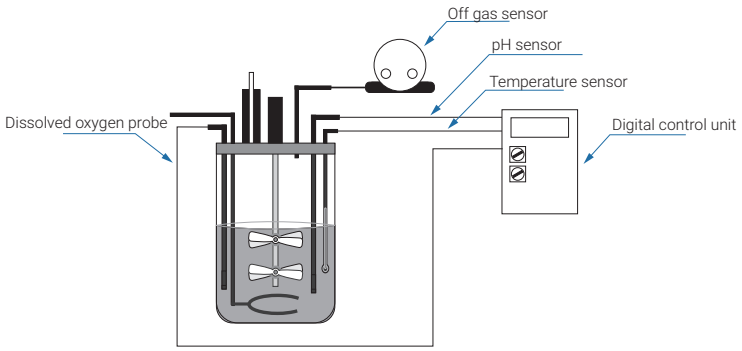

Figure 3.2: Stir speed and feed control setup for the bioreactor.

stirring rod has two impeller blades. The stir speed is controlled (either increased or decreased) based on the dissolved oxygen (DO) probe reading.

The DO probe consists of a probe head featuring a semipermeable membrane and electrolyte solution. The electrolyte solution reacts with oxygen to produce electrons. These electrons give rise to a current which is measured by the DO probe. The semi-permeable membrane is used to ensure that only oxygen molecules are permitted to enter the probe head so that other molecules don't interfere with the chemical reaction.

The DO probe is calibrated at the beginning of each experiment. Calibration of DO probe is relative to the oxygen saturation concentration at the inlet gas stream. For example, the DO probe could be calibrated with 100% air which contains about 21% oxygen where this reading is taken a "100". First, a gas flow of 95% house air and 5% carbon dioxide is established by sending appropriate voltage signals to the mass flow controllers. Once a steady state is reached, the DO is calibrated at 100%. Similarly, a DO probe could be calibrated with 95% air and 5% Carbon-dioxide. In the later case oxygen level is 19.95% versus 21% in the former case. However, both are called saturation or "100%". For the work described in this thesis, the DO probe was calibrated with 95% air and 5% CO_2.

Under normal circumstances, nitrogen gas is pumped in the bioreactor to calibrate the DO reading for 0%. However, the media used in the experiments can be altered if carbon dioxide mole ratio in the input gas is reduced to 0. Thus,the DO probe is disconnected to calibrate DO reading for 0%.

Pumps present on the DCU were used to control the feed rate. In these experiments, feed

rate was manually set. A pulse width modulator (PWM) block in Simulink sets the pump rate depending on the feed rate calculated offline. The DCU is also used to control and maintain the culture temperature. The details of the feeding procedure are discussed in section 5.1.1

3.2 New approach to estimate mass transfer coefficient

As discussed earlier, oxygen transfer rate can be modeled using Equation 2.1 as

$$OTR = k_L a(C^* - C)$$

As discussed earlier, $k_L a$ is the mass transfer coefficient and it can be expressed as,

$$k_L a = (\alpha_0 + \alpha_1(N - N_0)) \tag{3.1}$$

Where, α_0 and α_1 are the fitting parameters which are used to model $k_L a$ as a linear function of stir speed. C^* is the oxygen saturation concentration in the bioreactor liquid and can be expressed as,

$$C^* = C^*_{cal}\frac{b_0}{b_{0i}} \tag{3.2}$$

C is the dissolved oxygen concentration in the bioreactor liquid and it can be modeled as,

$$C = C^*_{cal}\frac{DO}{100} \tag{3.3}$$

Using equations 3.1, 3.2 and 3.3 equation 2.1 can be expressed as,

$$OTR = (\alpha_0 + \alpha_1(N - N_0))(C^*_{cal}\frac{b_0}{b_{0i}} - C^*_{cal}\frac{DO}{100}) \tag{3.4}$$

where C^*_{cal} is oxygen saturation concentration (gL^{-1}), b_0 is the mole ratio of oxygen in the input gas, b_{0i} is the mole ratio of oxygen in the initial input gas and DO is the dissolved oxygen [%] measured by the dissolved oxygen probe. Initially, $b_0 = b_{0i}$. Thus, using Equation 3.4, OTR can be estimated once the fitting parameters, α_0 and α_1, are estimated.

One major drawback of this method to calculate OTR is that driving force or $(C^* - C)$ is calculated without prior knowledge of oxygen saturation concentration of the liquid (C^*_{cal}). For

CHO cells the OUR is lower. Thus, a low OTR is sufficient to maintain DO at the desired level. This makes oxygen transfer rate (OTR) comparable to $\dot{C}$ for CHO cells. Thus, $\dot{C}$ is not equal to zero. $\dot{C}$ can be expressed as,

$$\dot{C} = C^*_{cal}\frac{\dot{DO}}{100} \tag{3.5}$$

Hence, $\dot{C}$ has to be calculated to calculate OUR and C^*_{cal} is required to calculate $\dot{C}$ as shown in equation 3.5. A wrong estimate of C^*_{cal} would provide a wrong estimate of OTR, $\dot{C}$ and OUR.

Thus, to minimize this error, we have to calculate OTR without explicitly using C^*_{cal}. In other words, the fitted parameters have to be estimated in such a way that C^*_{cal} is not explicitly used to calculate OTR. Equation 3.4 for OTR can be modified as,

$$OTR = (\alpha_0 + \alpha_1(N - N_0)) \times C^*_{cal} \times (\frac{b_0}{b_{0i}} - \frac{DO}{100}) \tag{3.6}$$

Thus,

$$OTR = (\alpha_0 C^*_{cal} + \alpha_1 C^*_{cal}(N - N_0))(\frac{b_0}{b_{0i}} - \frac{DO}{100}) \tag{3.7}$$

Rewriting $\alpha_0 C^*_{cal}$ as $\bar{\alpha}_0$ and $\alpha_1 C^*_{cal}$ as $\bar{\alpha}_1$,

$$OTR = (\bar{\alpha}_0 + \bar{\alpha}_1(N - N_0))(\frac{b_0}{b_{0i}} - \frac{DO}{100}) \tag{3.8}$$

It is important to note here that $\bar{\alpha}_0$ and $\bar{\alpha}_1$ are not averages. They are defined as product of α_0 & C^*_{cal} and α_1 & C^*_{cal} respectively.

Equation 3.8 is same as equation 3.4. However, equation 3.8 doesn't use C^*_{cal} explicitly to determine OTR. Instead the fitting parameters $\bar{\alpha}_0$ and $\bar{\alpha}_0$ will be estimated such that they account for C^*_{cal}.

Thus,

$$OTR = (\bar{\alpha}_0 + \bar{\alpha}_1(N - N_0)) \times (\overline{DF}) \tag{3.9}$$

Where, $\overline{DF}$ is the new driving force. It can be mathematically defined using equation 3.9 and 3.8 as,

$$\overline{DF}(t) = (\frac{b_0(t)}{b_{0i}} - \frac{DO(t)}{100}) \tag{3.10}$$

The new version of k_La can be estimated using normal equations. Recounting equation 2.4,

$$OTR_{ideal} = (\frac{M_fP}{V_1RT}) \times (b_0 - b_1) \tag{3.11}$$

The equation for the unknown quantity b_1 can be calculated by equating equations 2.4 and 3.9,

$$b_1 = b_0 - \bar{\alpha}_0 \frac{V_1RT}{M_fP}\overline{DF} - \bar{\alpha}_1 \frac{V_1RT}{M_fP}(N - N_0)\overline{DF} \tag{3.12}$$

To account for filtering caused by headspace mixing delay and off-gas sensor dynamics, we can pass signal from equation 3.12 through two low pass filters with time constants $\tau_1 = \frac{V_2}{M_f}$ and τ_2 for headspace mixing delay and off-gas sensor delay respectively. For the bioreactor used in this work, V_2 or the headspace volume was 1.1 liters. With a massflow of 3 L/h, the headspace time constant was calculated as $\tau_1 = \frac{V_2}{M_f}$. Thus $\tau_1 = 1320$ seconds.The other time constant as obtained from the off-gas sensor manual as $\tau_2 = 55$ seconds.

Thus, a filtered version of equation 3.12 can be written as,

$$\hat{b_3} = b_0(filt) - \bar{\alpha}_0 \frac{V_1RT}{M_fP}\overline{DF}_{filt} - \bar{\alpha}_1 \frac{V_1RT}{M_fP}(N - N_0)\overline{DF}_{filt} \tag{3.13}$$

Where $\hat{b_3}$ is the estimated oxygen mole ratio of oxygen measured by the off-gas sensor. The oxygen mole ratio directly measured by the sensor and the estimated value of this mole ratio are almost equal. Thus, $\hat{b_3} \approx b_3$. Further, in this work the data with no gasmix change was used to estimate all the parameters. Thus, $b_0(filt) \approx b_0$

Using this information, equation 3.13 can be rewritten as

$$b_3 = b_0 - \bar{\alpha}_0 \frac{V_1RT}{M_fP}\overline{DF}_{filt} - \bar{\alpha}_1 \frac{V_1RT}{M_fP}(N - N_0)\overline{DF}_{filt} \tag{3.14}$$

Simplifying equation 3.14,

$$b_0 - b_3 = \bar{\alpha}_0 \frac{V_1RT}{M_fP}\overline{DF}_{filt} + \bar{\alpha}_1 \frac{V_1RT}{M_fP}(N - N_0)\overline{DF}_{filt} \tag{3.15}$$

Rearranging,

$$\frac{M_f P}{V_1 RT}(b_0 - b_3) = \bar{\alpha}_0 \overline{DF}_{filt} + \bar{\alpha}_1 (N - N_0)\overline{DF}_{filt} \tag{3.16}$$

Thus,

$$\frac{M_f P}{V_1 RT}(b_0 - b_3) = (\bar{\alpha}_0 + \bar{\alpha}_1 (N - N_0))\overline{DF}_{filt} \tag{3.17}$$

The left hand side of equation 3.17 can be calculated using sensor data. It represents the filtered version of OTR_{ideal} through two low pass filters with time delay $\tau_1 = \frac{V_2}{M_f}$ and τ_2 for headspace mixing delay and off-gas sensor delay respectively.Thus,

$$OTR_{offgas} = \frac{M_f P}{V_1 RT}(b_0 - b_3) \tag{3.18}$$

Similarly, equation 3.8 can be passed through the same series of low pass filters to obtain the right hand side of equation 3.17. Thus,

$$OTR_{filt} = (\bar{\alpha}_0 \overline{DF}_{filt} + \bar{\alpha}_1 (N - N_0)\overline{DF}_{filt}) \tag{3.19}$$

Rewriting equation 3.17 using equation 3.18 and 3.19

$$OTR_{offgas} = (\bar{\alpha}_0 \overline{DF}_{filt} + \bar{\alpha}_1 (N - N_0)\overline{DF}_{filt}) \tag{3.20}$$

Normal equations can be used to estimate the two unknown parameters of equation 3.20. Equation 3.20 is of the form, $y = af_1(x) + bf_2(x)$. Where, $y = OTR_{offgas}$, $f_1(x) = \overline{DF}_{filt}$, $f_2(x) = ((N - N_0)\overline{DF}_{filt})$ and a & b are $\bar{\alpha_0}$ and $\bar{\alpha_1}$ respectively.

Thus, $\bar{\alpha}_0$ and $\bar{\alpha}_1$ can be estimated using normal equations as,

$$\hat{\bar{\alpha}} = (A^T A)^{-1} A^T B \tag{3.21}$$

Where,

$$\hat{\bar{\alpha}} = \begin{bmatrix} \hat{\bar{\alpha}}_0 \\ \hat{\bar{\alpha}}_1 \end{bmatrix} \tag{3.22}$$

$$A = \begin{bmatrix} D\bar{F}_{filt}(1) & (N-N_0)D\bar{F}_{filt}(1) \\ D\bar{F}_{filt}(2) & (N-N_0)D\bar{F}_{filt}(2) \\ \vdots & \vdots \\ D\bar{F}_{filt}(T) & (N-N_0)D\bar{F}_{filt}(T) \end{bmatrix} \tag{3.23}$$

$$B = \begin{bmatrix} OTR_{offgas}filt(1) \\ OTR_{offgas}filt(2) \\ \vdots \\ OTR_{offgas}filt(T) \end{bmatrix} \tag{3.24}$$

Once the value of $\bar{\alpha}_0$ and $\bar{\alpha}_1$ are determined, OTR can be calculated using equation 3.8 as,

$$\hat{OTR} = (\hat{\bar{\alpha}}_0 + \hat{\bar{\alpha}}_1(N-N_0)) \times (\overline{DF}) \tag{3.25}$$

3.3 New approach to estimate oxygen saturation concentration

As seen in section 3.2, $\bar{\alpha_0}$ and $\bar{\alpha_1}$ can be estimated and $\widehat{OTR}$ can be calculated without explicitly knowing the value of oxygen saturation concentration at calibration (C^*_{cal}) using equation 3.9. Recalling equation 2.2, oxygen uptake rate can be modeled as

$$OUR = OTR - \dot{C} \tag{3.26}$$

Oxygen uptake rate is the rate at which the cells in the bioreactor consume oxygen and oxygen transfer rate is the rate at which oxygen is transferred from gas state to liquid state. Expanding equation 2.2,

$$OUR = OTR - C^*_{cal}\frac{\dot{DO}}{100} \tag{3.27}$$

In this work, the stir speed is persistently varied. This increases the variation in oxygen transfer rate (OTR). Oxygen uptake rate (OUR) is not directly dependent on stir speed variation. Persistent agitation of DO by artificially changing stir speed, in theory, should not change OUR.

Thus, over short time periods, OUR variations are very low.

Thus, we need to estimate a value for C^*_{cal} such that variations in OUR are reduced to a minimum value. An estimate of OUR ($\widehat{OUR}$) can be calculated using equation 3.25, and 2.2 as,

$$\widehat{OUR} = \widehat{OTR} - \widehat{C^*_{cal}}\frac{\dot{DO}}{100} \tag{3.28}$$

Equation 3.28 can be rewritten as

$$\widehat{OUR} = \widehat{OTR} + \widehat{C^*_{cal}}\Big(\frac{-\dot{DO}}{100}\Big) \tag{3.29}$$

$\widehat{C^*_{cal}}$ should be estimated such that the variations in $\widehat{OUR}$ were reduced to a minimum value. To estimate this value, variance of $\widehat{OUR}$ is minimized. Thus,

$$\widehat{C^*_{cal}} = \text{argmin}(\text{variance}(\widehat{OUR})) \tag{3.30}$$

The mathematical formula can be derived by first determining the variance of $\hat{OUR}$. Thus,

$$\text{var}(\widehat{OUR}) = \frac{1}{(N-1)}\sum_{i=1}^{N}[\widehat{OUR}(i) - \overline{\widehat{OUR}}]^2 \tag{3.31}$$

Where $\overline{\widehat{OUR}}$ is mean of $\widehat{OUR}$. Expanding equation 3.31 further,

$$\text{var}(\widehat{OUR}) = \frac{1}{(N-1)}\sum_{i=1}^{N}[\widehat{OUR}(i)^2 + \overline{\widehat{OUR}}^2 - 2\widehat{OUR}(i)\overline{\widehat{OUR}}] \tag{3.32}$$

Which simplifies to,

$$\text{var}(\widehat{OUR}) = \frac{1}{(N-1)}\Big[\sum_{i=1}^{N}\widehat{OUR}(i)^2 - N\Big(\overline{\widehat{OUR}}\Big)^2\Big] \tag{3.33}$$

Using equation 3.29 to find the mean of $\widehat{OUR}$,

$$\overline{\widehat{OUR}} = \overline{\widehat{OTR}} + \widehat{C^*_{cal}}\overline{\Big(\frac{-\dot{DO}}{100}\Big)} \tag{3.34}$$

Squaring equation 3.34 on both sides

$$\left(\widehat{\overline{OUR}}\right)^2 = \left[\widehat{\overline{OTR}} + \widehat{C^*_{cal}}\left(\overline{\frac{-\dot{DO}}{100}}\right)\right]^2 \tag{3.35}$$

$$\implies \left(\widehat{\overline{OUR}}\right)^2 = \left[\left(\widehat{\overline{OTR}}\right)^2 + \left(\widehat{C^*_{cal}}\right)^2\left(\overline{\frac{-\dot{DO}}{100}}\right)^2 + 2\widehat{C^*_{cal}}\left(\widehat{\overline{OTR}}\right)\left(\overline{\frac{-\dot{DO}}{100}}\right)\right] \tag{3.36}$$

Also, using equation 3.34,

$$\sum_{i=1}^{N}\left(\widehat{OUR}(i)\right)^2 = \sum_{i=1}^{N}\left[\widehat{OTR}(i) + \widehat{C^*_{cal}}\left(\frac{-\dot{DO}(i)}{100}\right)\right]^2 \tag{3.37}$$

$$\sum_{i=1}^{N}\left(\widehat{OUR}(i)\right)^2 = \sum_{i=1}^{N}\left[\left(\widehat{OTR}(i)\right)^2 + \left(\widehat{C^*_{cal}}\right)^2\left(\frac{-\dot{DO}(i)}{100}\right)^2 + 2\widehat{C^*_{cal}}\left(\widehat{OTR}(i)\right)\left(\frac{-\dot{DO}(i)}{100}\right)\right] \tag{3.38}$$

Substituting equations 3.36 and 3.38 in 3.33

$$\begin{aligned}\mathrm{var}(\widehat{OUR}) =& \frac{1}{(N-1)}\left[\left[\sum_{i=1}^{N}\left(\widehat{OTR}(i)\right)^2 - N\left(\widehat{\overline{OTR}}\right)^2\right] + 2\widehat{C^*_{cal}}\left[\sum_{i=1}^{N}\left(\widehat{OTR}(i)\right)\left(\frac{-\dot{DO}(i)}{100}\right)\right.\right. \\ & \left.\left. - N\left(\widehat{\overline{OTR}}\right)\left(\overline{\frac{-\dot{DO}}{100}}\right)\right] + \left(\widehat{C^*_{cal}}\right)^2\left[\sum_{i=1}^{N}\left(\frac{-\dot{DO}(i)}{100}\right)^2 - N\left(\overline{\frac{-\dot{DO}}{100}}\right)^2\right]\right]\end{aligned} \tag{3.39}$$

Equation 3.39 is differentiated and equated to zero to find the value of $\widehat{C^*_{cal}}$ which minimizes equation 3.39. Thus, the value of $\widehat{C^*_{cal}}$ which minimizes equation 3.39 is given by,

$$\widehat{C^*_{cal}} = \frac{-\left[\sum_{i=1}^{N}\left(\widehat{OTR}(i)\right)\left(\frac{-\dot{DO}(i)}{100}\right) - N\left(\widehat{\overline{OTR}}\right)\left(\overline{\frac{-\dot{DO}}{100}}\right)\right]}{\left[\sum_{i=1}^{N}\left(\frac{-\dot{DO}(i)}{100}\right)^2 - N\left(\overline{\frac{-\dot{DO}}{100}}\right)^2\right]} \tag{3.40}$$

Equation 3.40 is derived based on a fundamental assumption that the OTR is constant (has zero slope) over short time periods. This allows for $\widehat{C^*_{cal}}$ estimation by minimizing the variation in $\widehat{OUR}$ with respect to a straight line with zero slope. However, experiments conducted in this work

showed that even over short periods of time a linear fit of $\widehat{OUR}$ did not have zero slope. Thus, to calculate a more reasonable estimate of $\widehat{OUR}$ and $\widehat{C^*_{cal}}$, the variations between $\widehat{OUR}$ and a linear fit of OUR ($\widehat{OUR}_{linfit}$) has to be minimized.

By using equations 3.25, 3.29 and 3.40, an initial estimate of $\widehat{OUR}$ can be obtained. $\widehat{OUR}$ can then be used to obtain $\widehat{OUR}_{linfit}$ using least squares method. Thus slope (m) and y-intercept (b) of $\widehat{OUR}_{linfit}$ can be obtained using,

$$x = (A^T A)^{-1} A^T B \tag{3.41}$$

Where,

$$x = \begin{bmatrix} m \\ b \end{bmatrix} \tag{3.42}$$

$$A = \begin{bmatrix} t_1 - t_0 & 1 \\ t_2 - t_1 & 1 \\ \vdots & \vdots \\ t_T - t_{T-1} & 1 \end{bmatrix} \tag{3.43}$$

$$B = \begin{bmatrix} \widehat{OUR}(1) \\ \widehat{OUR}(2) \\ \vdots \\ \widehat{OUR}(T) \end{bmatrix} \tag{3.44}$$

$\widehat{OUR}_{linfit}$ has a non-zero slope and it can be used to minimize the variation in $\widehat{OUR}$ and get a reasonable estimate of $\widehat{C^*_{cal}}$. Thus the new formulation for estimating $\widehat{C^*_{cal}}$ will be,

$$\widehat{C_{cal}}^* = \text{argmin}(\text{variance}(\widehat{OUR} - \widehat{OUR}_{linfit})) \tag{3.45}$$

By going through a derivation similar to derivation of equation 3.40, an estimation for $\widehat{C^*_{cal}}$

is obtained as,

$$\widehat{C^*_{cal}} = \frac{-\left[\sum_{i=1}^{N}\left((\widehat{OTR}(i) - \widehat{OUR}(i)_{linfit})\right)\left(\frac{-\dot{DO}(i)}{100}\right) - N\left(\overline{(\widehat{OTR} - \widehat{OUR}_{linfit})}\right)\left(\overline{\frac{-\dot{DO}}{100}}\right)\right]}{\left[\sum_{i=1}^{N}\left(\frac{-\dot{DO}(i)}{100}\right)^2 - N\left(\overline{\frac{-\dot{DO}}{100}}\right)^2\right]} \tag{3.46}$$

Equation 3.46 finds a value of $\widehat{C^*_{cal}}$ which minimizes the variation between $\widehat{OUR}$ and $\widehat{OUR}_{linfit}$. Using equations 3.25, 3.29 and $\widehat{C^*_{cal}}$ from equation 3.46 $\widehat{OUR}$ can be estimated as,

$$\widehat{OUR} = \widehat{OTR} + \widehat{C^*_{cal}}\left(\frac{-\dot{DO}}{100}\right) \tag{3.47}$$

In summary, $\widehat{OTR}$ and $\widehat{C^*_{cal}}$ are separately estimated using the two algorithms developed in this chapter. These algorithms were applied to experimental data obtained from culturing CHO cells in lab bioreactors, as well as from bioreactor simulations. Further, the accuracy of these algorithms was verified by comparing the known parameters from simulations with the estimated parameters obtained from the algorithm. The consistency of these algorithms was determined by comparing results obtained by applying these algorithms to experiment data over several sub-data sets.

Chapter 4

Bioreactor Simulations

The algorithms to estimate k_La and C^*_{cal} presented in chapter 3 were tested using a simulation environment implemented in Simulink. Values of α_0 and α_1 were set at a constant value using OTR_{offgas} data. Similarly the value of C^*_{cal} was fixed at an arbitrary value between C^*_{cal} of pure water and C^*_{cal} of sea water at T=310K. OUR signal was modeled as an exponentially increasing function to simulate exponentially growing culture. It's magnitude and exponential constants were obtained as an estimate of previously calculated experimental OUR obtained using OTR_{offgas}. The purpose of this simulation was to apply the algorithm formulated in chapter 3 and check the accuracy of the output values against known values. Detail description of the simulation and the corresponding results are discussed in this chapter.

4.1 Simulation Design

By keeping certain parameters constant and focusing on modelling and updating signals that were significant for the algorithm developed in chapter 3, the algorithm was checked for accuracy. The main purpose of this simulation was to check the algorithm against a known set of data. For example, the algorithm to estimate OTR by fitting k_La as a linear function of stir speed estimated the fitting parameters α_0 and α_1. These fitting parameters were kept at a known constant value throughout the simulation. After the simulation was over, these fitting parameters were compared with the estimated fitting parameters obtained by the algorithm to determine algorithm accuracy. Similar computation was performed for C^*_{cal}. Other parameters such as massflow, temperature,

pressure etc were kept constant since they remained relatively constant in the lab experiments. Several parameters were kept constant in the simulation. This list of parameters is shown in Table 4.1. In Table 4.1, b_{oi} is the oxygen mole ratio in the input gas at calibration. Further, initial conditions for several signals were set depending on the experiments performed in the lab. The list of the variables and their initial values is given in Table 4.2. In Table 4.2, $C_{initial}$ is the oxygen concentration in the liquid at calibration.

Sr. No.	Simulation parameter	Value
1	α_0	2.5
2	α_1	0.0085
3	C^*_{cal}	0.005 (g/L)
4	Temperature	310.15 K
5	Pressure	0.998 atm
6	Liquid Volume (V_1)	0.5 L
7	Headspace volume (V_2)	1.1 L
8	Massflow	3 L/h
9	Gas Constant	0.082057 ($LatmK^{-1}mol^{-1}$)
10	b_{oi}	0.1990

Table 4.1: List of predefined constant parameters used in simulation

Sr. No.	Simulation signal	Initial Value
1	DO	100%
2	Stir Speed	100 rpm
3	CO_2 percentage	5 %
4	Air percentage	95 %
5	O_2 percentage	0 %
6	$C_{initial}$	0.005 g/L

Table 4.2: List of signals and their initial values

OUR was modeled as an exponential function to represent an increase in oxygen consumption over time due to cell growth as shown in equation 4.1.

$$OUR = ae^{bt} \tag{4.1}$$

The values for a and b were estimated using a section of OUR data computed from experiments (a = 0.015 and b = 1×10^{-6}). Once these parameters were fixed, a series of simulations were executed.

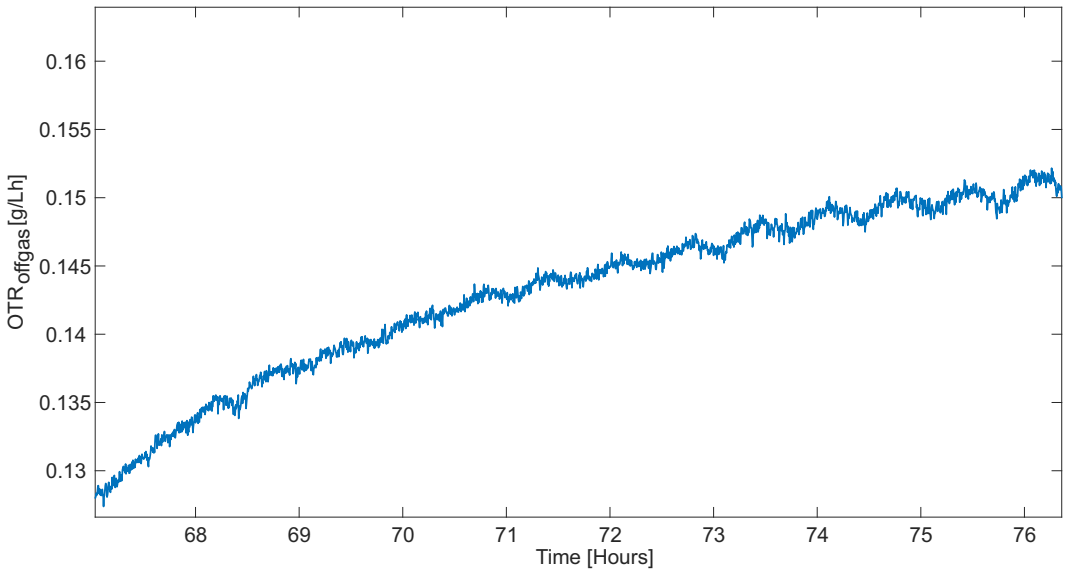

Figure 4.1: OTR_{offgas} signal used to estimate OUR for bioreactor simulations

4.1.1 Simulation flow diagram

The simulation follows a set of programmed instructions that estimate the dissolved oxygen concentration in the bioreactor and update bioreactor signals based on this estimation. A flow diagram for the simulation is shown in figure 4.2.

First, oxygen mole ratio of the input gas (b_0) was calculated as,

$$b_0 = (Air\%) \times 0.2095 + (O_2\%) \times 1 \tag{4.2}$$

Second, driving force (DF) was calculated as shown in equation 4.3. Initial values of DO and b_0 were used to calculate initial driving force. These parameters were automatically updated as the simulation progressed.

$$DF = \left[C^*_{cal}\left(\frac{b_0}{b_{0i}}\right) - C^*_{cal}\left(\frac{DO}{100}\right)\right] \tag{4.3}$$

Thus,

$$\implies DF = (C^* - C)$$

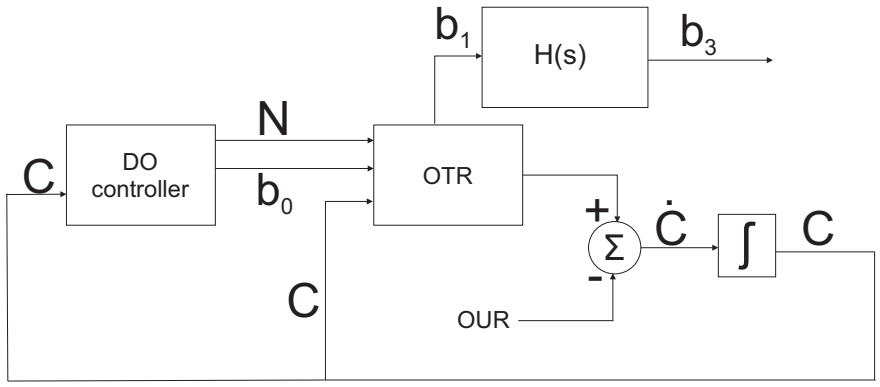

Figure 4.2: Flow diagram of bioreactor simulations

Where C^* is the oxygen saturation concentration in the liquid (gL^{-1}) and C is the dissolved oxygen concentration in the liquid (gL^{-1}). The mass transfer coefficient is calculated as

$$k_L a = \Big(\alpha_0 + \alpha_1 N\Big) \tag{4.4}$$

Finally, oxygen transfer rate (OTR) is calculated using equation 4.3 and equation 4.4,

$$OTR = k_L a \times DF \tag{4.5}$$

The rate of change of oxygen concentration in the bioreactor liquid is modeled as the difference between oxygen transfer rate (OTR) and oxygen uptake rate (OUR),

$$\dot{C} = OTR - OUR \tag{4.6}$$

By integrating $\dot{C}$, a measurement of instantaneous oxygen concentration in the bioreactor liquid (C) is obtained,

$$C = \int_{t_{i-1}}^{t_i} \dot{C} dt \tag{4.7}$$

The dissolved oxygen concentration obtained using equation 4.7 is used to update dissolved oxygen (DO),

$$DO = C\frac{100}{C^*_{cal}} \tag{4.8}$$

The updated DO measurement serves two purposes. First, it is used to update driving force given by equation 4.3. Second, updated DO measurement is used to update three signals. (i) Air percentage, (ii) Oxygen percentage and (iii) Stir Speed.

This update logic depends on two signal values, DO and Stir Speed. A pseudo-code for updating the Air and Oxygen percentages in the input gas and the stir speed is shown below:

```
If (DO >= lowerDOlim and DO < upperDOlim)
        Do nothing
ElseIf (DO < 40 and Stir <= 300)
        Increase Stir Speed;
elseif (DO < 40 and Stir > 300)
        Increase oxygen percentage
        Decrease air percentage
elseif (DO > upperDOlim and Stir > 100)
        Decrease Stir Speed
end
```

The upper and lower DO limits in this simulation were set to 50% and 40% respectively. These signals are updated after every 15 seconds. Thus, depending on the DO measurement, b_0 and stir speed were updated. The updated values of b_0 and stir speed are used to update k_La and driving force (DF). This updated values of driving force and k_La were used to update OTR. After the simulation is over, the data is sampled at 15 seconds interval and stored.

The oxygen mole ratio at the liquid-air interface (b_1) can be calculated as,

$$b_1 = b_0 - \alpha_0\frac{V_1RT}{M_fP}DF - \alpha_1\frac{V_1RT}{M_fP}NDF \tag{4.9}$$

The offgas oxygen mole ratio (b_3) can be simulated by filtering equation 4.9. This filtering

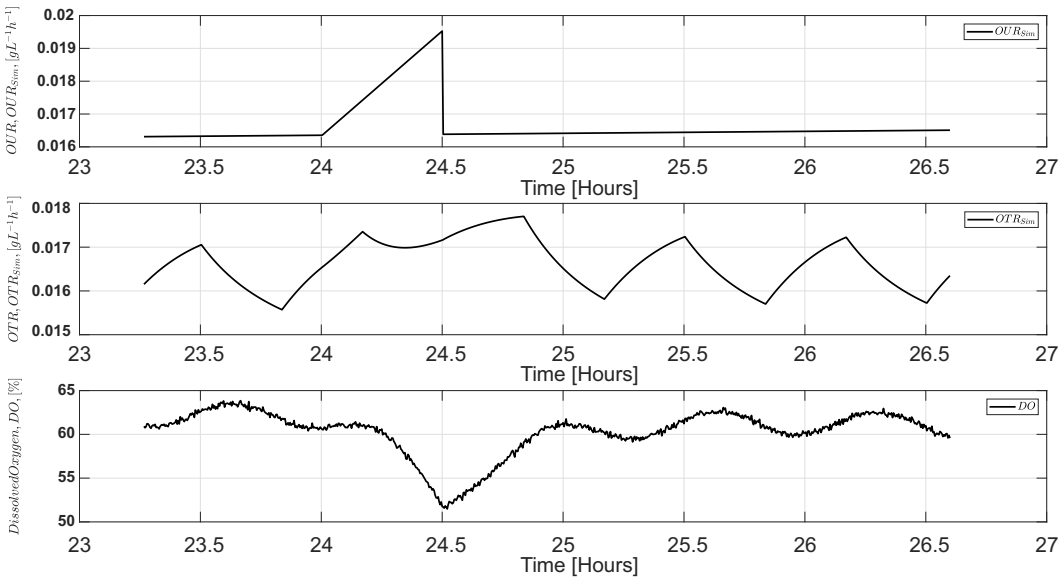

Figure 4.3: OUR, OTR and DO signals during a ramp event for simulated data. OUR signal is artificially increased by 20% to simulate instances when DO gets perturbed due to feeding or taking a sample.

process involves passing the b_1 signal through two low pass filters as explained in section 3.2. These low pass filters will have time constants $\tau_1 = 22$ minutes for head space mixing delay and $\tau_2 = 55$ seconds for offgas sensor dynamics respectively. A full diagram of this Simulink model is provided in appendix A.

Simulink also had a probe capability. By adding an external ramp signal to OUR, the DO was artificially perturbed. Figure 4.3 depicts the change in OUR, OTR and DO caused due to a ramp event. The ramp event which causes a sudden change in OUR simulates a feed pulse. This created a series of disturbances in simulated sensor readings. This allowed the investigation of effects of sudden changes in DO caused due to various events such as taking a sample or gas mix change on the algorithm. The ramp increased OUR by around 20%. In the bioreactor, a sudden gas mix change changes DO creating a spike in the DO signal. If the algorithm discussed in chapter 3 is applied to this curve, there was a possibility of higher error in the parameter estimation. However, it was possible to use parameters determined in an earlier data segment without any perturbation to estimate a more reasonable OUR signal. This hypothesis was tested using the probe signal.

To ensure that the least squares problem is well formed and to ensure that none of the

matrices involved in finding the fitting parameters were singular, persistent excitation was provided to the DO signal by adding a triangular wave to the stir speed signal. This triangular wave had time period of 40 minutes and it changed the stir speed signal by ±20 rpm. In the bioreactor experiment DO changes very slowly. This makes $\dot{DO} \approx 0$. This in turn makes $\dot{C} \approx 0$. However, as discussed earlier, for mammalian cells growth rate is low and thus $OTR \neq OUR$. Thus $\dot{C}$ is not zero. Thus to ensure that $\dot{C} \neq 0$, DO is artificially varied by continuously varying stir speed.

4.1.2 Adding noise to the simulation

The signals measured during experiments with the bioreactor have associated measurement noise. However, the signals obtained using simulation do not have noise. The algorithm developed in chapter 3 has to work in the presence of noise. Thus to closely resemble the signals acquired during experiments, a noise model was developed and added to the Simulink signals.

A Gaussian noise model with mean = 0 and standard deviation = 0.2107 is used to simulate noise in DO probe reading. This variance is obtained by measuring the error between measured DO and estimated DO ($\widehat{DO}$) for one of the experiments (Experiment 14). Square root of variance provided the standard deviation which was used in the noise model. In this model a set of DO readings were obtained when stir speed was constant (No zigzag) and just prior to a feeding event. During this time period DO increases to ensure that the cells did not encounter any sudden decreases in DO due to cell growth or other physical disturbances to the system that might decrease the DO. DO levels below 20% saturation can cause mammalian cells harm and death. Stir speed was also manually set to a value slightly higher than the previous operating value. Using this data, the slope (m) and y-intercept (b) of $\widehat{DO}$ were calculated as

$$x = (A^T A)^{-1} A^T B \tag{4.10}$$

Where,

$$x = \begin{bmatrix} m \\ b \end{bmatrix} \tag{4.11}$$

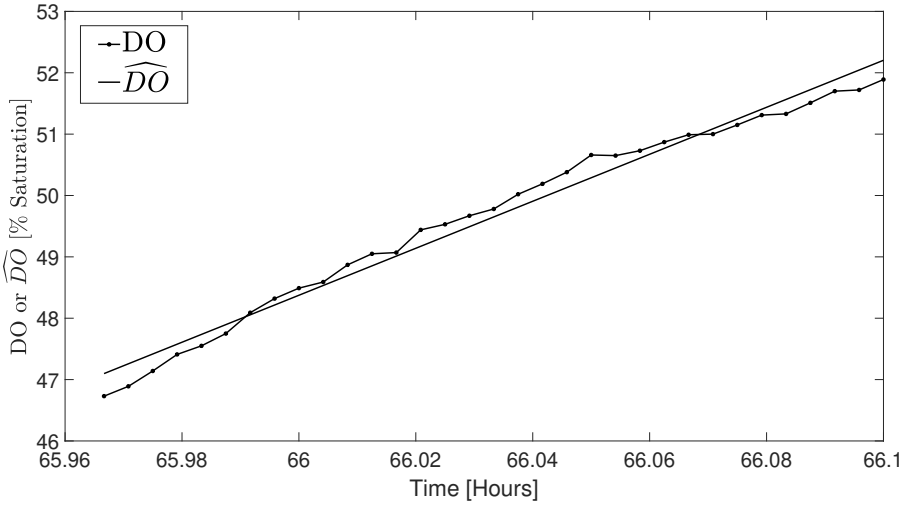

Figure 4.4: $\widehat{DO}$ and DO profiles used in simulation. $\widehat{DO}$ is a linear estimate of DO. The DO signal was obtained from experimental data and was used to model the noise for DO signals in simulation.

$$A = \begin{bmatrix} t_1 - t_0 & 1 \\ t_2 - t_1 & 1 \\ \vdots & \vdots \\ t_T - t_{T-1} & 1 \end{bmatrix} \tag{4.12}$$

$$B = \begin{bmatrix} DO(1) \\ DO(2) \\ \vdots \\ DO(T) \end{bmatrix} \tag{4.13}$$

Using the values obtained using Equation 4.10, $\widehat{DO}$ were calculated as

$$\widehat{DO}(i) = m(t_i - t_{i-1}) + b \tag{4.14}$$

The two signals, DO and $\widehat{DO}$, are shown in figure 4.4

The DO noise (DO_{noise}) signal can then be calculated as

$$DO_{noise} = \widehat{DO} - DO \tag{4.15}$$

The standard deviation of DO_{noise} can be calculated using MATLAB function `std`. The dissolved oxygen (DO) signal with and without superimposed noise is shown in Figure 4.5.

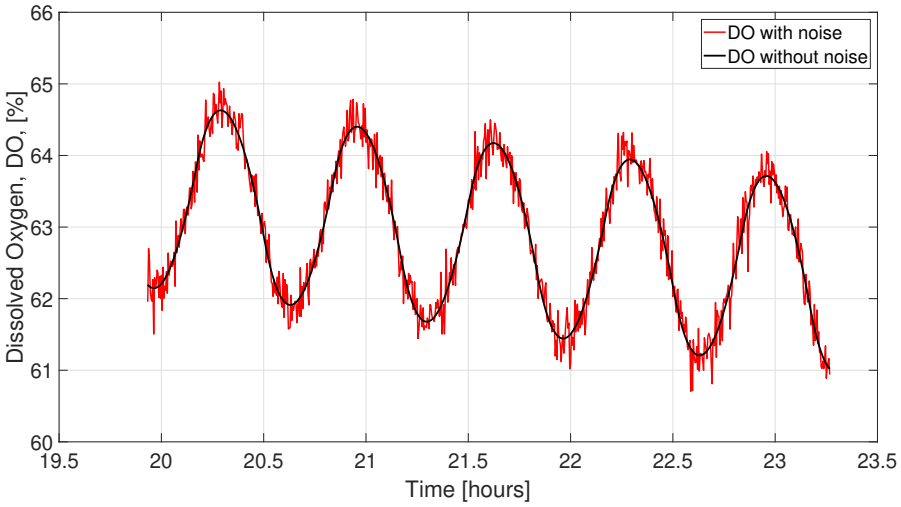

Figure 4.5: DO signal profile with and without noise. Experiment data was used to determine the noise model to use in the simulation.

4.1.3 Noise in $\dot{DO}$ calculation and Savitzky-Golay filtering

There are several methods that can be used to compute $\dot{DO}$ to obtain $\dot{C}$. A direct way to compute $\dot{DO}$ is to use the MATLAB function `diff`, however, the `diff` function computes the derivative by simply dividing the difference between two consecutive data points with the difference between the two consecutive times. Another method to compute $\dot{DO}$ is by using Savitzky-Golay filtering.

Savitzky-Golay filtering method fits a low order polynomial to sequential subsets of data. These polynomial coefficients are used to calculate the filtered value of the signal in the middle of the data set. In the modified version of Savitzky-Golay filtering used in this work, the polynomial coefficients were used to calculate the filtered value of the signal for the last data point in the subset. This modification was used to allow for real time estimates. Calculating the signal value for the data point at the end of the the data set is similar to using past data points to calculate the signal value for the next data point.

In this work a second order polynomial is used to estimate $\dot{DO}$ using the modified Savitzky-

Golay filtering method. This polynomial can be expressed as,

$$DO(t_i) = a_2(t_i)^2 + a_1 t_i + a_0 \tag{4.16}$$

The coefficients of this polynomial can be calculated by formulating a least squares problem. Thus if there are "n" data points in the data subset,

$$x = (A^T A)^{-1} A^T B \tag{4.17}$$

Where,

$$x = \begin{bmatrix} a_2 \\ a_1 \\ a_0 \end{bmatrix} \tag{4.18}$$

$$A = \begin{bmatrix} (t_{-n})^2 & t_{-n} & 1 \\ (t_{-(n-1)})^2 & t_{-(n-1)} & 1 \\ \vdots & \vdots & \\ (-2)^2 & -2 & 1 \\ (-1)^2 & -1 & 1 \\ 0 & 0 & 1 \end{bmatrix} \tag{4.19}$$

$$B = \begin{bmatrix} DO(-n) \\ DO(-(n-1)) \\ \vdots \\ DO(0) \end{bmatrix} \tag{4.20}$$

The filtered value of DO at DO(0) were found by using the matrices 4.18, 4.19 and 4.20 and evaluating equation 4.16

$$DO(0) = a_0 \tag{4.21}$$

$\dot{DO}$ can be calculated by differentiating equation 4.16. Thus,

$$\dot{DO}(t_i) = 2a_2(t_i) + a_1 \tag{4.22}$$

Finally using matrices 4.18, 4.19 and 4.20 and evaluating equation 4.22,

$$\dot{DO}(0) = a_1 \tag{4.23}$$

The Savitzky-Golay filtering process is repeated for the entire data and a filtered version of DO and $\dot{DO}$ is obtained. The comparison plots of filtered and unfiltered DO and $\dot{DO}$ are shown in Figure 4.6 and 4.7 respectively.

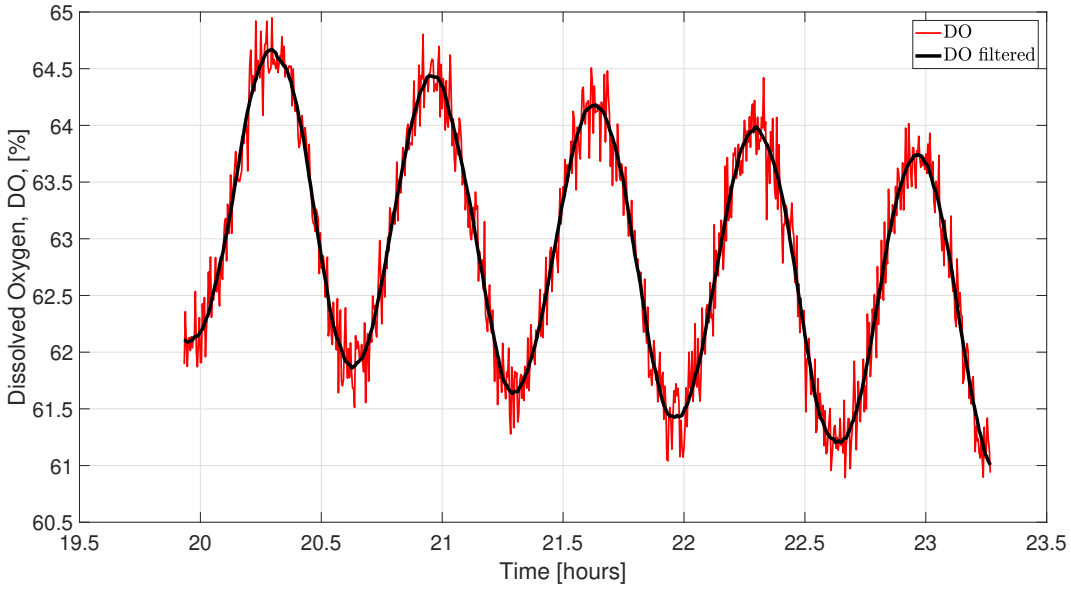

Figure 4.6: The filtered and unfiltered DO signal obtained from simulation. Savitzky-Golay filtering was used to obtain the filtered DO signal.

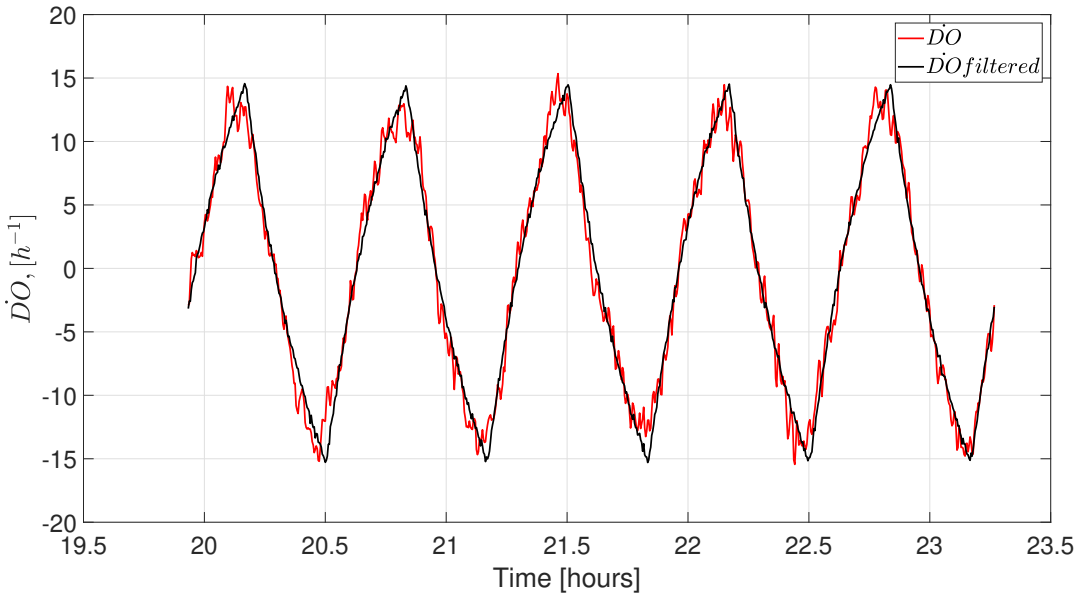

Figure 4.7: The filtered and unfiltered $\dot{DO}$ signal obtained from simulation. Savitzky-Golay filtering was used for obtain the filtered $\dot{DO}$ signal.

4.2 Simulation output

As discussed in section 4.1, several signals were obtained from the simulation. The stir speed variation with a traingular wave superimposed on it is shown in Figure 4.8. The oxygen mole ratio in the input gas b_0 and output gas b_3 (measured by offgas sensor) are shown in Figure 4.10. As expected b_3 increases when b_0 increases and $b_3 < b_0$. Figure 4.9 shows the three mole ratios b_0, b_1 and b_3 plotted together. There is no variation in b_0. However, b_1 and b_3 reflect the variations due to stir speed variations shown in Figure 4.8. As expected b_3 is a filtered version of b_1.

As seen in Figure 4.11 the OTR signal has high variation due to continuously varying stir speed. The OUR signal has comparatively low variation since OUR should not be affected due to artificial changes in stir speed. OUR signal increases over time due to increase in cell numbers in the bioreactor due to cell growth. The simulated OUR and OTR signals in case of a ramp event is shown in Figure 4.12.

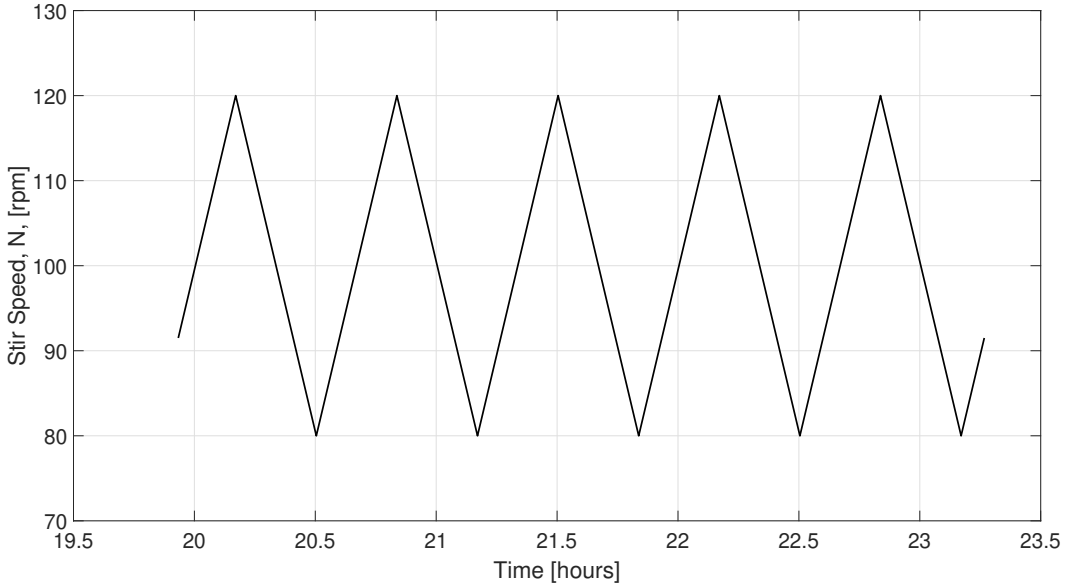

Figure 4.8: Stir speed profile using triangular wave.

4.3 Calculating k_La and C^*_{cal} using simulation data

As discussed in section 4.1, the simulation was designed to keep fitting parameters i.e. α_0 and α_1 constant. Thus, α_0 and α_1 values used for simulation were known. Similarly, the value of C^*_{cal} was kept at a known constant value throughout the simulation. Using the algorithm developed in section 4.1 and simulated sensor signals like DO and b_3, estimated values of α_0 and α_1 ($\widehat{\alpha_0}$ and $\widehat{\alpha_1}$) were calculated. Similarly, using the new algorithm developed in chapter 3, an estimate of C^*_{cal} ($\widehat{C^*_{cal}}$) was calculated. These calculated values were then compared with known values used in the simulation to verify the accuracy and consistency of the algorithm.

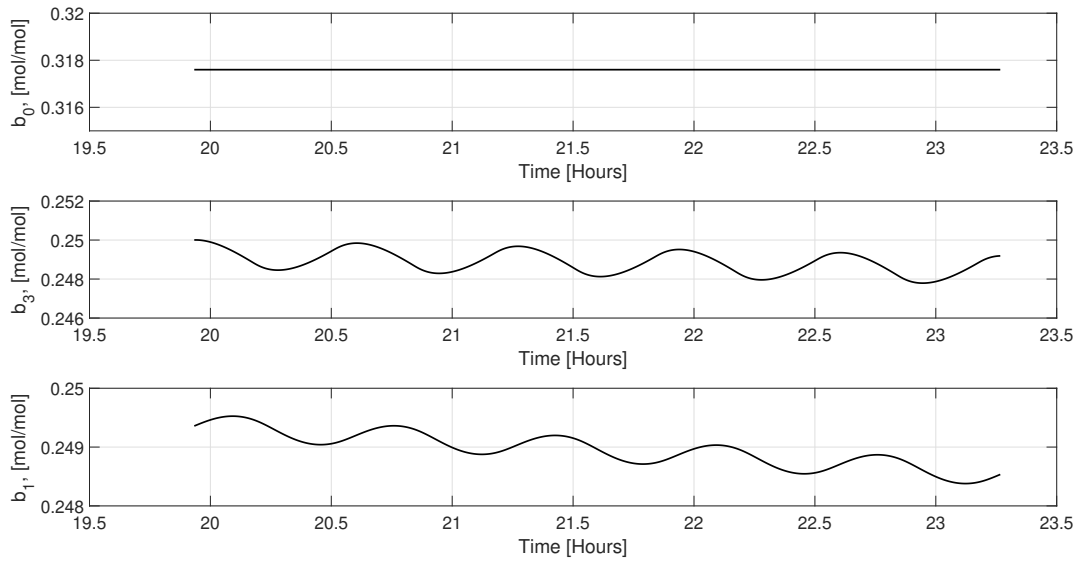

Figure 4.9: Mole ratio profile showcasing mass transfer characteristics in the bioreactor. b_3 is a filtered version of b_1.

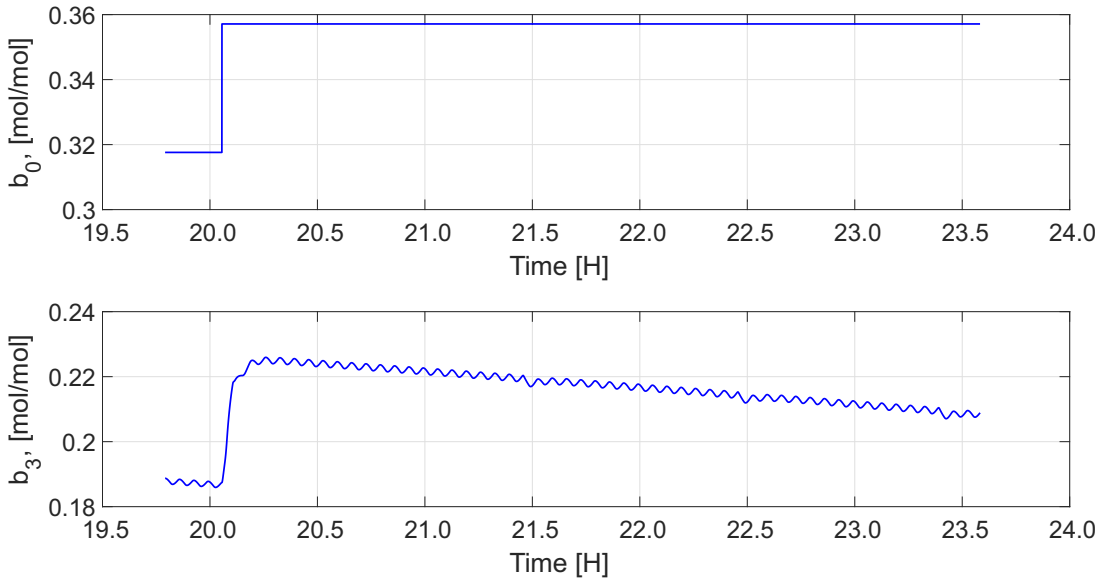

Figure 4.10: Effect of step change of input gas oxygen mole ratio (b_0) on sensor off-gas output reading (b_3)

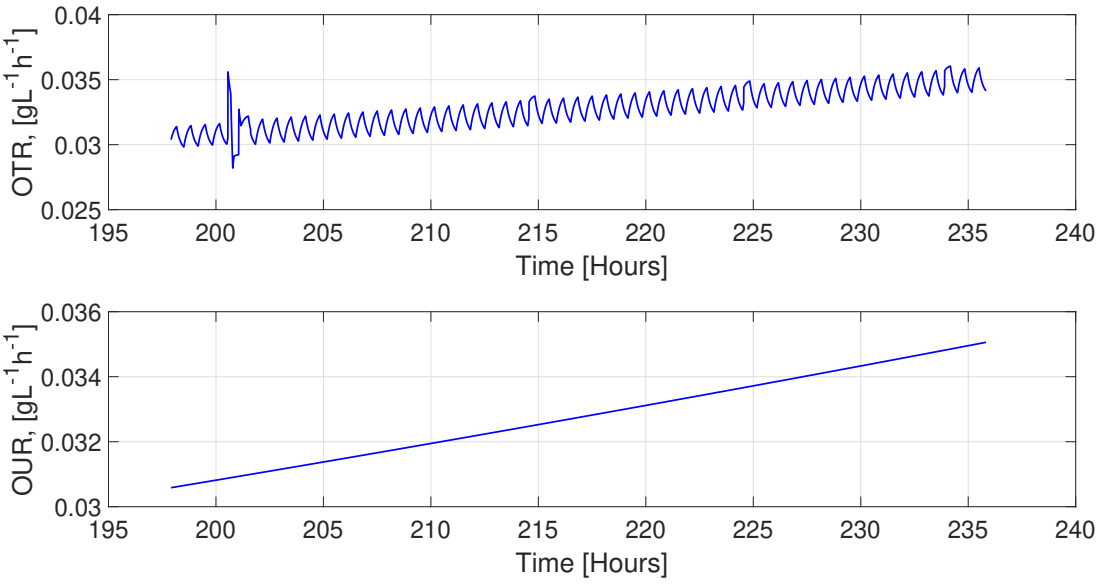

Figure 4.11: Profiles of simulated OTR and OUR signals.

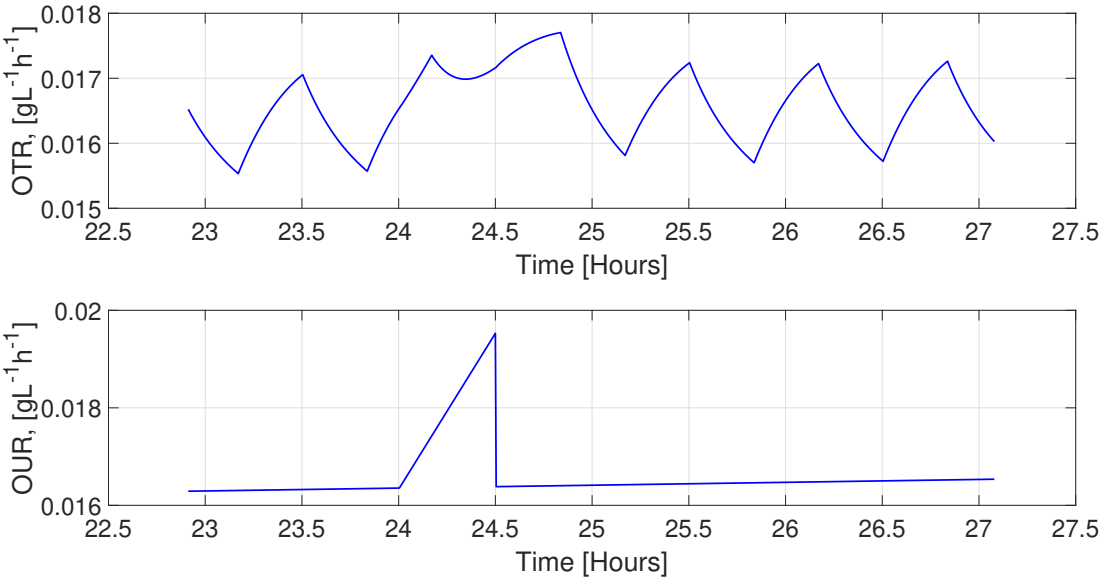

Figure 4.12: Graph of simulated OTR and OUR signals with a ramp event.

4.3.1 Accuracy

The fitting parameters α_0 and α_1 were fixed in this simulation at 2.5 and 0.0085 respectively. These values were obtained using the OTR_{offgas} data shown in Figure 4.1. The oxygen saturation concentration C^*_{cal} is fixed at 5×10^{-3}. This oxygen saturation concentration at calibration is selected to be between the oxygen saturation concentration of pure water and oxygen saturation concentration of sea water. The algorithm developed in chapter 3 was used to calculate these parameters and the percentage error between the known parameters from the simulation and calculated parameters from the algorithm was calculated as,

$$\%Error(\alpha_0) = \left(\frac{\widehat{\alpha_0} - \alpha_0}{\alpha_0}\right) \times 100 \tag{4.24}$$

$$\%Error(\alpha_1) = \left(\frac{\widehat{\alpha_1} - \alpha_1}{\alpha_1}\right) \times 100 \tag{4.25}$$

$$\%Error(C^*_{cal}) = \left(\frac{\widehat{C^*_{cal}} - C^*_{cal}}{C^*_{cal}}\right) \times 100 \tag{4.26}$$

Where $\widehat{\alpha_0}$, $\widehat{\alpha_1}$ and $\widehat{C^*_{cal}}$ are the parameters calculated using the algorithm and α_0, α_1 and C^*_{cal} are the known values used in the simulation. The algorithm was executed for several iterations. The random noise function changed the percentage error in each case.

The values calculated for $\widehat{\alpha_0}$, $\widehat{\alpha_1}$ and $\widehat{C^*_{cal}}$ and the corresponding errors are listed in the table 4.3. The error is below 5% in all cases. The errors in Table 4.3 are comparatively high since $\widehat{\alpha_0}$ and $\widehat{\alpha_1}$ were calculated as,

$$\widehat{\alpha_0} = \frac{\widehat{\bar{\alpha}_0}}{\widehat{C^*_{cal}}} \tag{4.27}$$

$$\widehat{\alpha_1} = \frac{\widehat{\bar{\alpha}_1}}{\widehat{C^*_{cal}}} \tag{4.28}$$

The algorithm computed $\widehat{\bar{\alpha}_0}$, $\widehat{\bar{\alpha}_1}$ and $\widehat{C^*_{cal}}$. There were errors associated with $\widehat{\bar{\alpha}_0}$, $\widehat{\bar{\alpha}_1}$ and $\widehat{C^*_{cal}}$. Thus, a higher error was obtained due to error propagation when these quantities were used to calculate new parameters ($\widehat{\alpha_0}$ and $\widehat{\alpha_1}$).

Simulation No.	$\widehat{\alpha_0}$	$\widehat{\alpha_1}$	$\widehat{C^*_{cal}}$	$\%Error(\alpha_0)$	$\%Error(\alpha_1)$	$\%Error(C^*_{cal})$
1	2.5553	0.0087	0.0049	4.11	2.21	2.53
2	2.5627	0.0087	0.0049	4.04	2.51	1.95
3	2.5483	0.0087	0.0049	3.64	1.93	1.98
4	2.5192	0.0085	0.0050	2.68	0.77	0.15
5	2.5573	0.0085	0.0049	4.27	2.29	3.14

Table 4.3: Calculated model parameters and corresponding errors for simulated data.

Since the values of simulation parameters (α_0, α_1 and C^*_{cal}) were known, $\bar{\alpha_0}$, $\bar{\alpha_1}$ can be calculated as,

$$\bar{\alpha_0} = \alpha_0 \times C^*_{cal} \tag{4.29}$$

$$\bar{\alpha_1} = \alpha_1 \times C^*_{cal} \tag{4.30}$$

Thus $\bar{\alpha_0} = 0.0125$ and $\bar{\alpha_1} = 4.25 \times 10^{-5}$. This allows us to compare $\bar{\alpha_0}$ and $\bar{\alpha_1}$ with $\widehat{\bar{\alpha_0}}$ and $\widehat{\bar{\alpha_1}}$ respectively. Thus, the error between these parameters can be calculated as

$$\%Error(\bar{\alpha_0}) = \Big(\frac{\widehat{\bar{\alpha_0}} - \bar{\alpha_0}}{\bar{\alpha_0}}\Big) \times 100 \tag{4.31}$$

$$\%Error(\bar{\alpha_1}) = \Big(\frac{\widehat{\bar{\alpha_1}} - \bar{\alpha_1}}{\bar{\alpha_1}}\Big) \times 100 \tag{4.32}$$

These errors are listed in Table 4.4. A less than 1% error is obtained in all the cases.

Simulation No.	$\widehat{\bar{\alpha_0}}$	$\widehat{\bar{\alpha_1}}$	$\%Error(\bar{\alpha_0})$	$\%Error(\bar{\alpha_1})$
1	0.0125	4.25E-05	0.0442	5.79E-02
2	0.0125	4.25E-05	0.0975	0.2677
3	0.0125	4.25E-05	0.0305	0.1067
4	0.0125	4.25E-05	0.102	0.2484
5	0.0125	4.25E-05	0.0666	0.2535

Table 4.4: Calculated model parameters and corresponding errors for simulated data.

The parameters calculated above were used to get an estimation of OUR and OTR. The

RMSE error between $\widehat{OTR}$ and $OTR_{Simulated}$ is calculated as,

$$RMSE(OTR) = \sqrt{\frac{1}{N}\sum_{i=1}^{N}\left(\widehat{OTR} - OTR_{Simulated}\right)^2} \tag{4.33}$$

and The RMSE error between $\widehat{OUR}$ and $OUR_{Simulated}$ is calculated as,

$$RMSE(OUR) = \sqrt{\frac{1}{N}\sum_{i=1}^{N}\left(\widehat{OUR} - OUR_{Simulated}\right)^2} \tag{4.34}$$

The RMSE error is listed for 5 iterations in Table 4.5.

Simulation No.	RMSE(OTR)	RMSE(OUR)
1	3.60E-05	8.54E-05
2	3.54E-05	8.74E-05
3	3.59E-05	7.00E-05
4	3.42E-05	8.36E-05
5	3.59E-05	8.01E-05

Table 4.5: RMSE error between $\widehat{OTR}$ and $OTR_{Simulated}$ and between $\widehat{OUR}$ and $OUR_{Simulated}$ for simulated data.

The plot for $\widehat{OTR}$ and $OTR_{Simulated}$ signals and plot for $\widehat{OUR}$ and $OUR_{Simulated}$ signals are shown in Figure 4.14. The associated stir speed and DO signal are shown in Figure 4.13. The same signals in presence of a ramp event are shown in Figure 4.15 and Figure 4.16.

As seen in Figure 4.13, DO signal periodically varies due to periodic zig-zag variations in stir speed. This effect is visible even in filtered DO signal as seen in Figure 4.13. Figure 4.14 shows the OUR and OTR graphs for the simulation over a small period of time. Very low error is obtained between the simulated OTR (OTR_{sim}) and the estimated OTR ($\widehat{OTR}$). The last part of Figure 4.14 shows the plots for the simulated OUR (OUR_{sim}) and the estimated OUR ($\widehat{OUR}$). The slight variation between $\widehat{OUR}$ and OUR_{sim} is due to noise.

Figure 4.15 portrays the effects of a sudden increase in OUR on DO signal. An increase in OUR results in a decrease in DO as expected. This effect is apparent in the filtered DO signal. Estimated OTR ($\widehat{OTR}$) and estimated OUR ($\widehat{OUR}$) signals were calculated using the algorithm discussed in Chapter 3. As seen in the last part of Figure 4.16, $\widehat{OUR}$ is a good approximation of simulated OUR. A slight delay between $\widehat{OUR}$ and OUR_{Sim} is due to lag produced by Savitzky-Golay filtering.

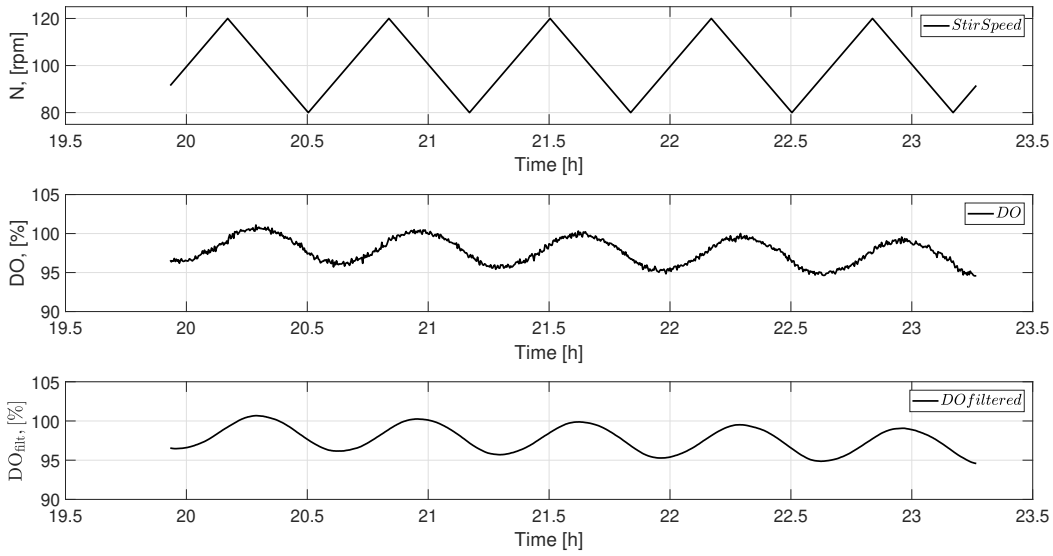

Figure 4.13: Effects of stir speed zig-zag on the filtered and unfiltered DO signals.

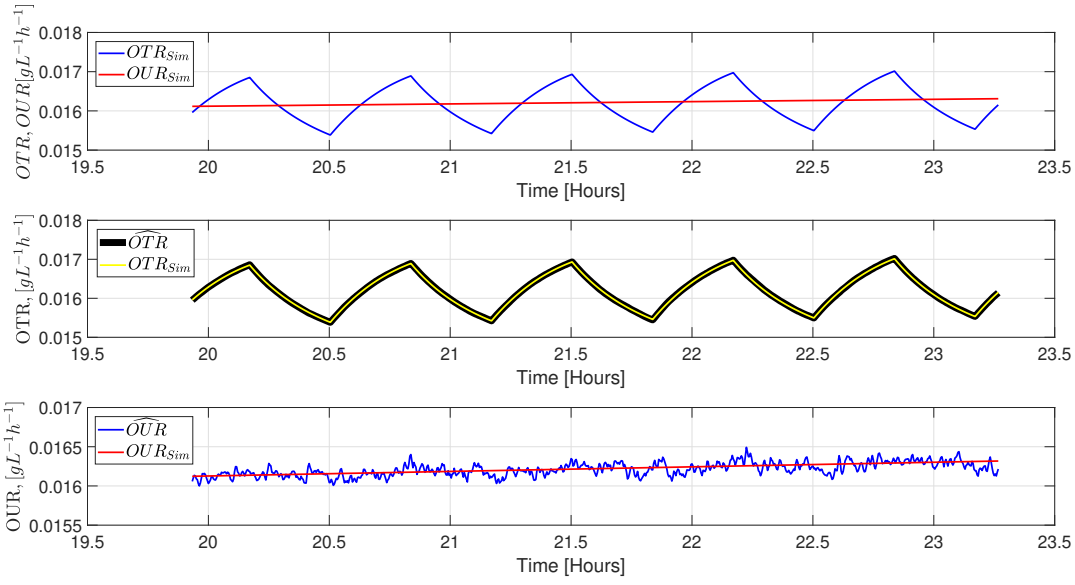

Figure 4.14: $OTR_{Simulated}$ and $OUR_{Simulated}$ signal profiles showing high variations due to stir speed in $OTR_{Simulated}$ compared to $OUR_{Simulated}$. $\widehat{OUR}$, $OUR_{Simulated}$, $\widehat{OTR}$ and $OTR_{Simulated}$ signal profiles show a comparison between estimated and simulated OUR and OTR.

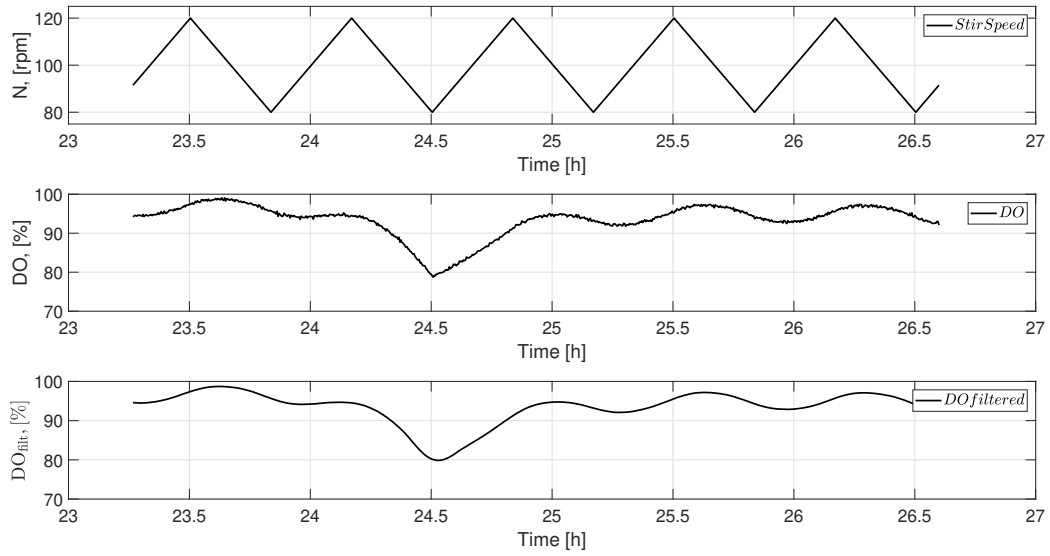

Figure 4.15: Effects of stir speed zig-zag on the filtered and unfiltered DO signals during a ramp event.

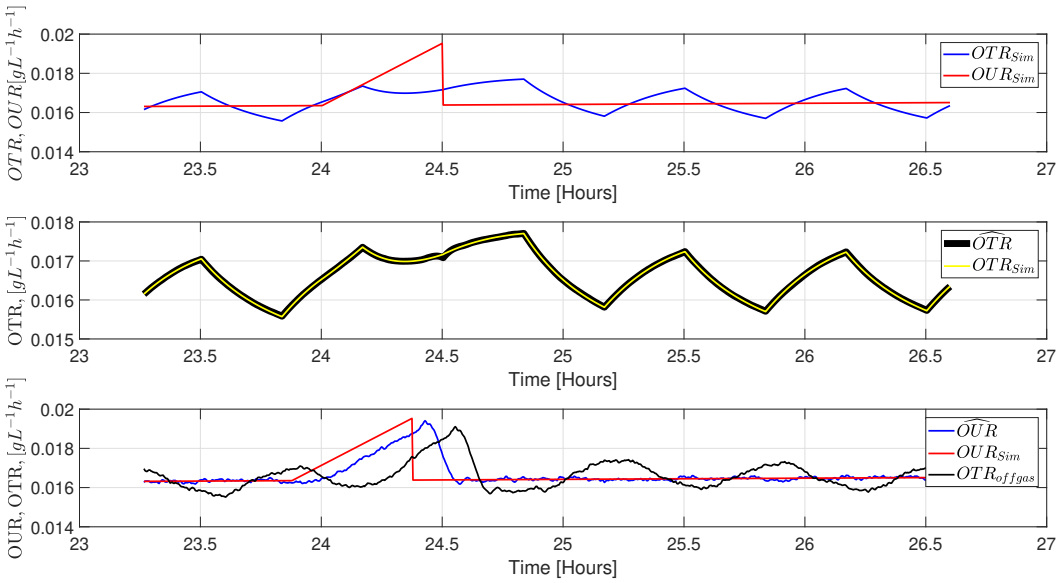

Figure 4.16: $OTR_{Simulated}$ and $OUR_{Simulated}$ signal profiles showing high variations due to stir speed in $OTR_{Simulated}$ compared to $OUR_{Simulated}$. $\widehat{OUR}$, $OUR_{Simulated}$, $\widehat{OTR}$ and $OTR_{Simulated}$ signal profiles show a comparison between estimated and simulated OUR and OTR during a ramp event.

In Summary, algorithms to estimate fitting parameters for k_La (α_0 and α_1) and C^*_{cal} were used to calculate $\widehat{\alpha_0}$, $\widehat{\alpha_1}$ and $\widehat{C^*_{cal}}$. An error of less than 1% was recorded between the known parameter values used in simulation and the parameter values obtained from the algorithm. Similarly, an estimation of OTR and OUR were calculated which had a very low RMSE error compared to the simulated OTR and OUR.

Chapter 5

Results: Estimation of k_La and C^*_{cal} for the experiment data

5.1 Experimental setup

Three experiments were conducted using CHO cells to obtain data to calculate OTR and OUR in real time. These experiments used the same cell line and media used to obtain the estimation of k_La and C^*_{cal} for the simulation constants. These experiments used constant mass flow with low error in the massflow reading.

Once the inlet gases were stabilized, the bioreactor is inoculated with cells. CHO VRC01 (NIH) cell line were used and innocuated into the bioreactor with an initial VCD (viable cell density) of approximately 6×10^5 cells/mL. Feed Boost 7a and 7b (GE) were fed 3% and 0.3% daily starting day 3. The amount of feed was increased as the cell number increased following the NIH protocol. A glucose solution with concentration of 75 g/L was used to ensure that the glucose concentration did not drop too low.The culture was fed using a pulse with modulation (PWM) controller from Simulink and DCU pumps. The feed rate and duration of the feed was calculated offline. Each of the feeding instances resembled a square pulse with constant magnitude across different feeding intervals. Thus, the total feeding rate was kept constant.

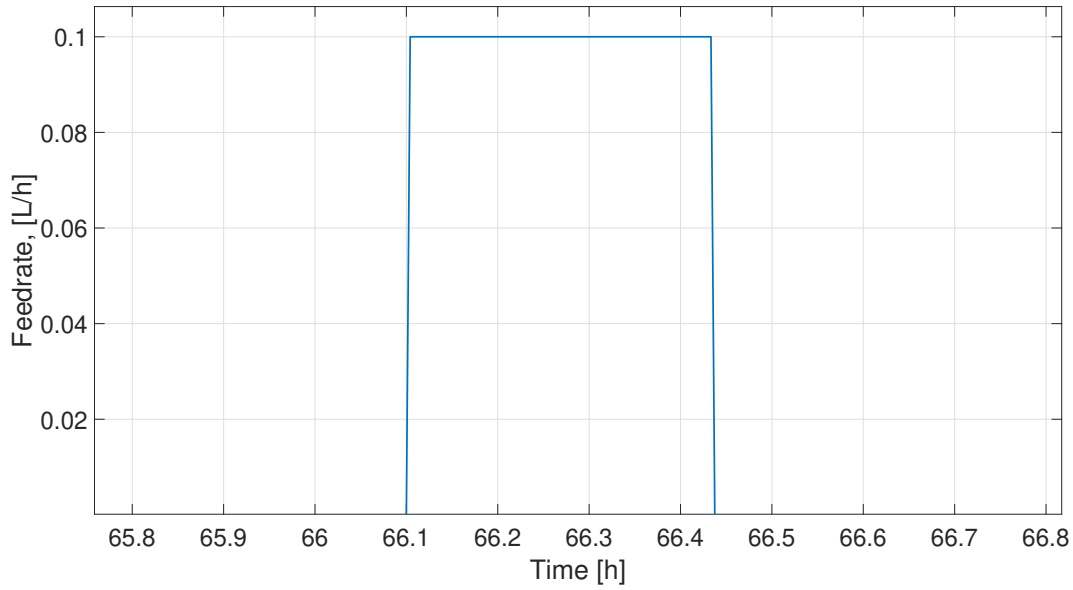

Figure 5.1: Graph of a typical feed pulse used in experiment 14. The feed rate is kept constant. This feed pulse had a duration of 20 minutes. However, depending on the glucose requirements, feed durations were changed.

5.1.1 Feeding method

A culture sample was obtained and glucose level ($C_{Initial}$)was determined before starting to feed the culture. Based on the glucose level in the culture, the required increase in the glucose concentration (C_{Final}) was determined. The change in the glucose concentration was calculated, as

$$\Delta C = C_{Final} - C_{Initial}$$

The feed rate was calculated using Equation 5.1

$$\Delta F = \frac{\Delta C \times V_{culture}}{C_{feed} \times \Delta t} \tag{5.1}$$

Where,ΔF is the feed rate [L/h], ΔC is the required change in the glucose concentration [g/L]. $V_{culture}$ is the volume of the culture [L], C_{feed} is the glucose concentration in the feed [g/L] and Δt is the feed time required to change the glucose concentration in the liquid by ΔC. In this work, the feed rate was maintained constant. Thus, Δt was calculated using a modification of 5.1

as,

$$\Delta t = \frac{\Delta C \times V_{culture}}{C_{feed} \times \Delta F} \tag{5.2}$$

The glucose concentration was measured again at the end of the pulse confirm the change in the glucose concentration. Figure 5.2 shows an example feeding profile for one of the experimental runs, experiment 14. In Figure 5.2 shorter blue pulses are Boost 7a feed and the taller red pulses are for additional glucose. During feeding period, the gas mix update controller and stir speed controller were switched to manual control and kept constant.

Experiment. No.	$VCD_{initial}$	VCD_{final}	Feeding	Stir Speed Control during BOOM events
12	6.07×10^5	1.56×10^7	No BOOM feeding	NA
13	6.05×10^5	2.03×10^7	BOOM feeding	Stir speed would change. No zigzag No gas mix change.
14	6.07×10^5	1.35×10^7	BOOM feeding	Constant stir speed. No zigzag No gas mix change.

Table 5.1: Key experiment parameters for experiments 12,13 and 14. VCD is measured in cells/ml.

The growth curve for the three experiments is shown in Figure 5.11, 5.7 and 5.3 respectively. The metabolite profiles for experiments 12, 13 and 14 are shown in Figures 5.13 to 5.14 and 5.9 to 5.10 and 5.5 to 5.6 respectively. The stir speed, pH and oxygen enrichment profiles for experiments 12, 13 and 14 are shown in Figures 5.15 to 5.17 and 5.18 to 5.20 and 5.21 to 5.23 respectively.

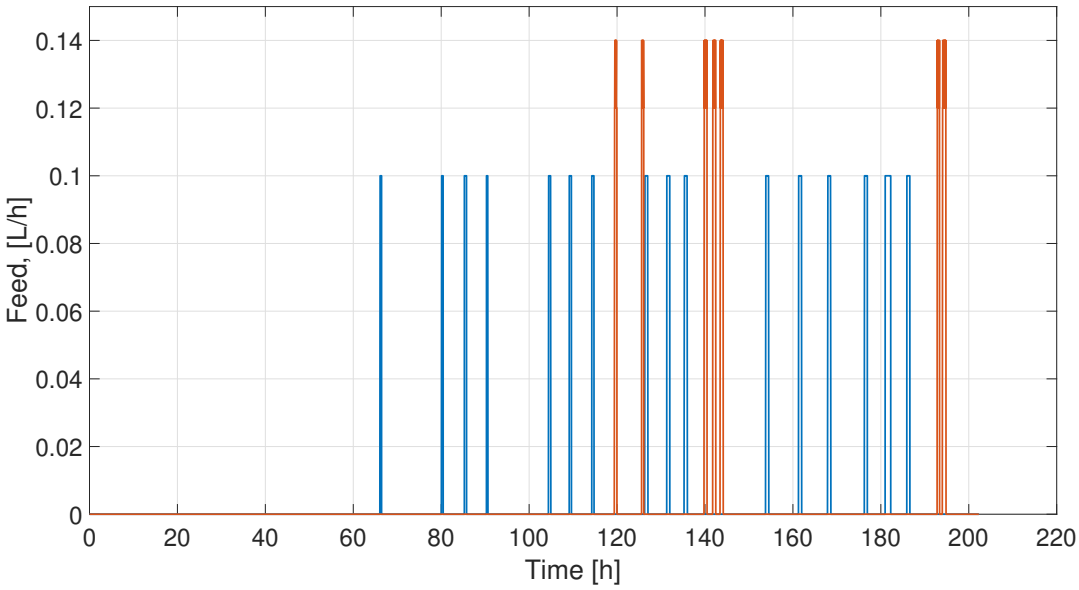

Figure 5.2: Feed profile for experiment 14.

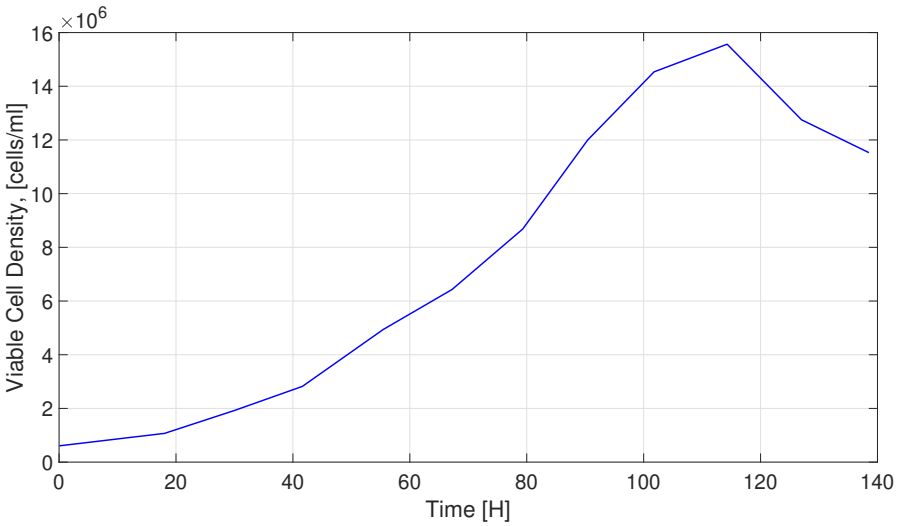

Figure 5.3: Growth profile for experiment 12.

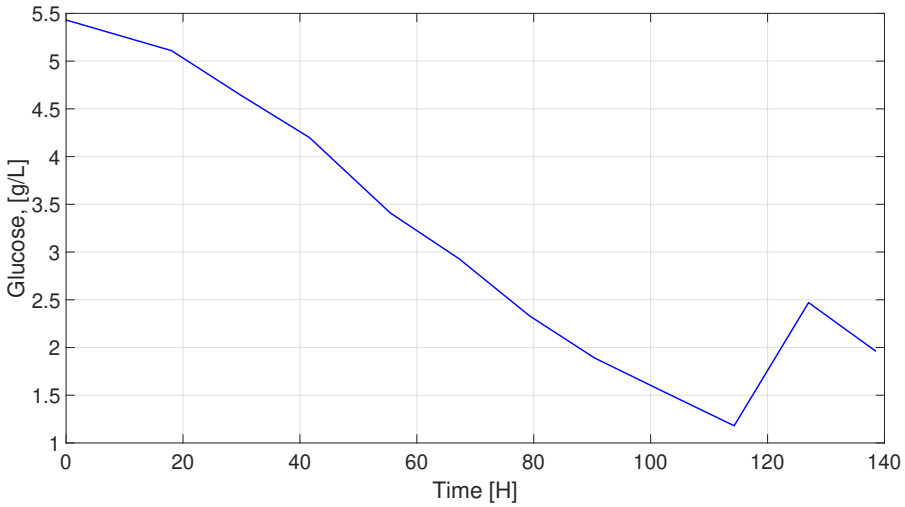

Figure 5.4: Glucose profile for experiment 12.

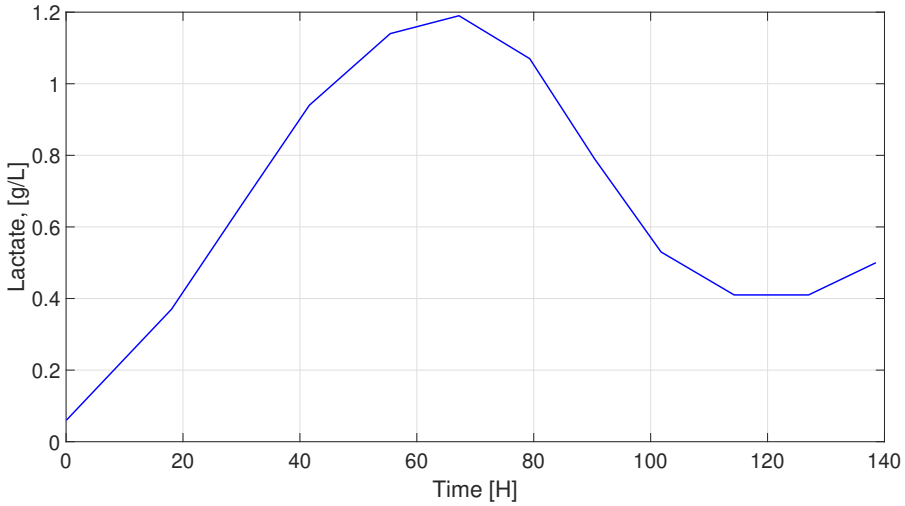

Figure 5.5: Lactate profile for experiment 12.

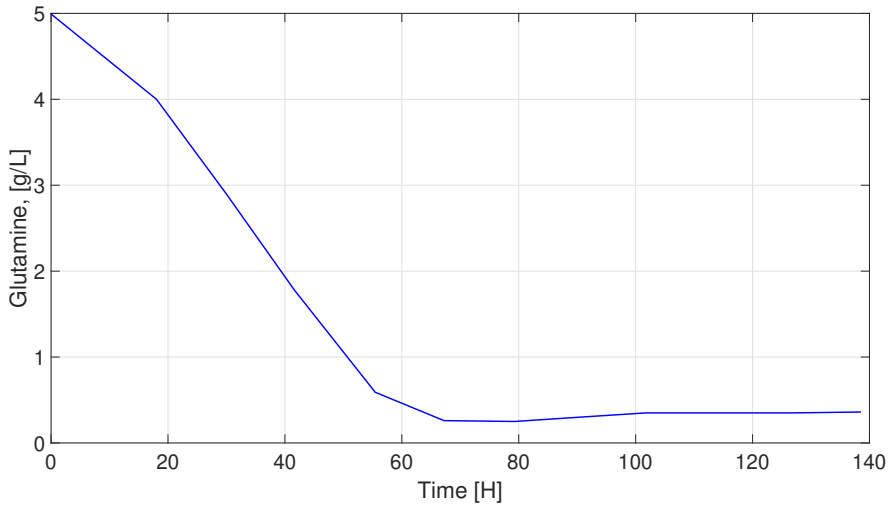

Figure 5.6: Glutamine profile for experiment 12.

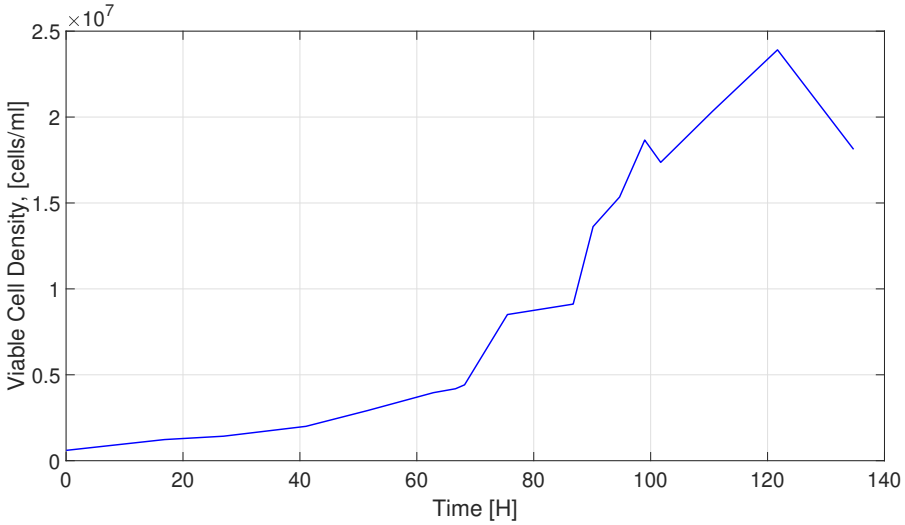

Figure 5.7: Growth profile for experiment 13.

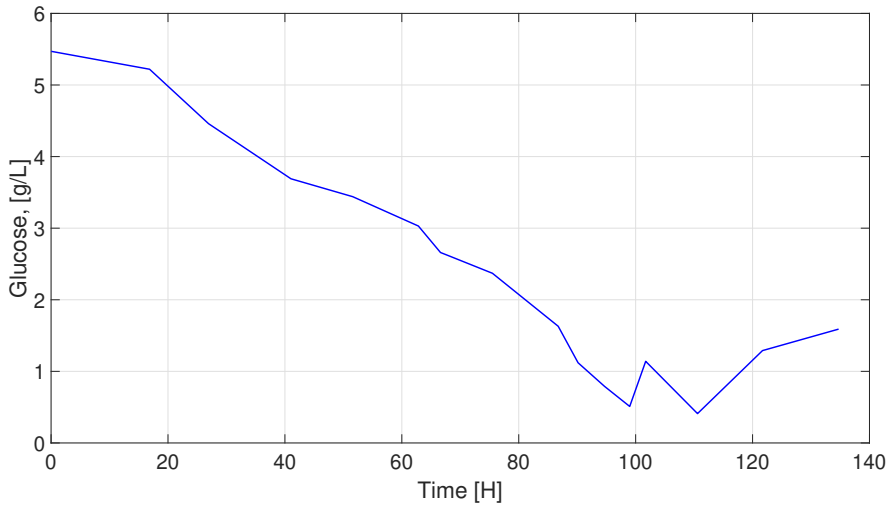

Figure 5.8: Glucose profile for experiment 13.

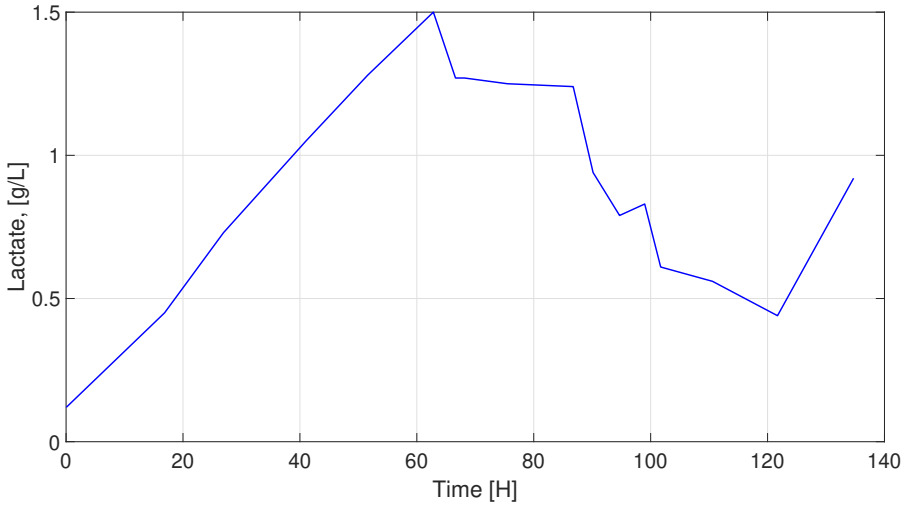

Figure 5.9: Lactate profile for experiment 13.

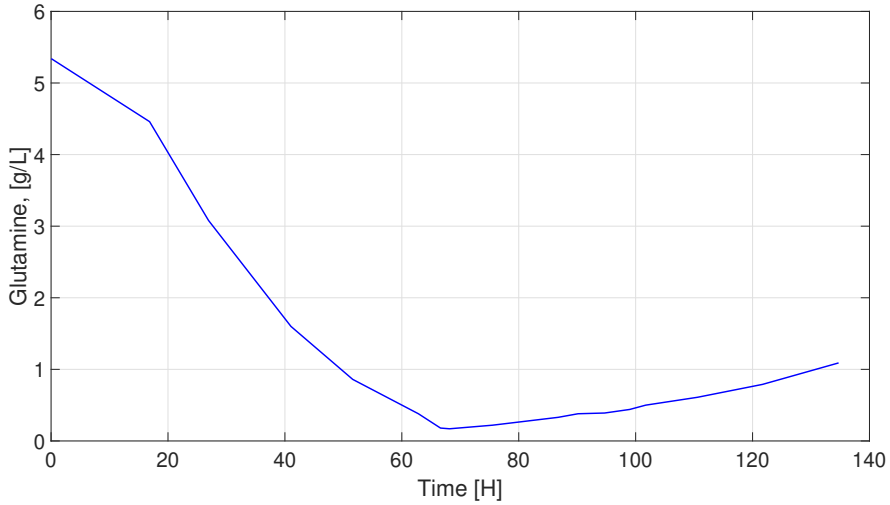

Figure 5.10: Glutamine profile for experiment 13.

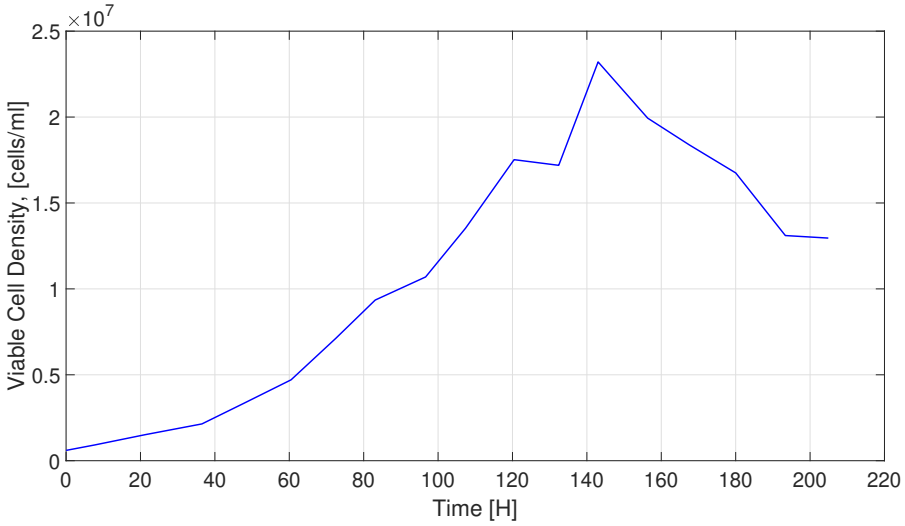

Figure 5.11: Growth profile for experiment 14.

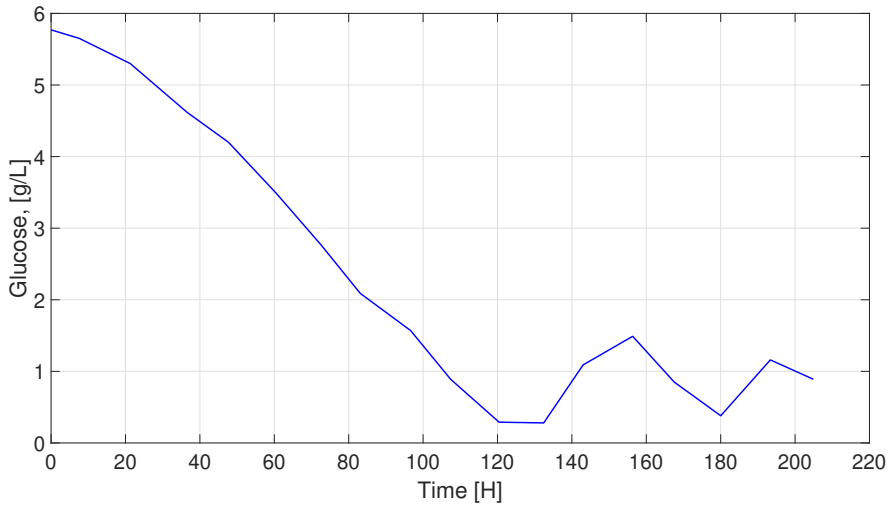

Figure 5.12: Glucose profile for experiment 14.

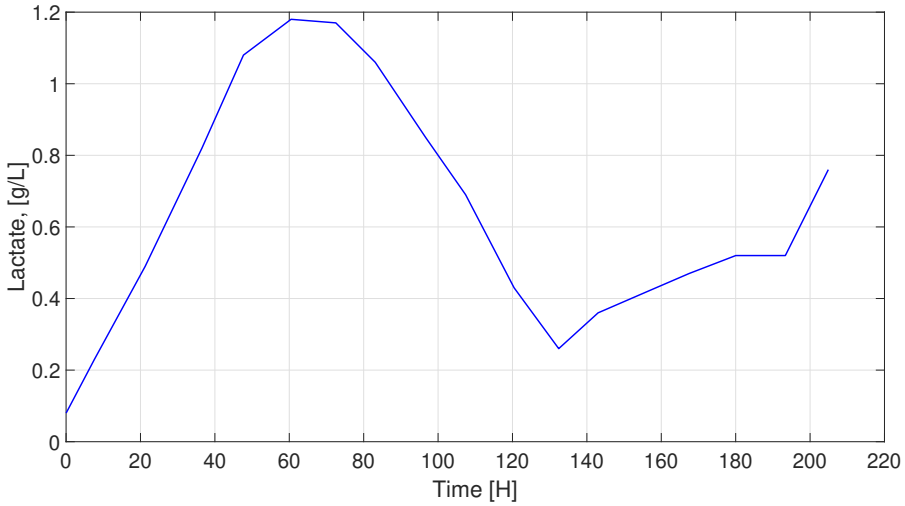

Figure 5.13: Lactate profile for experiment 14.

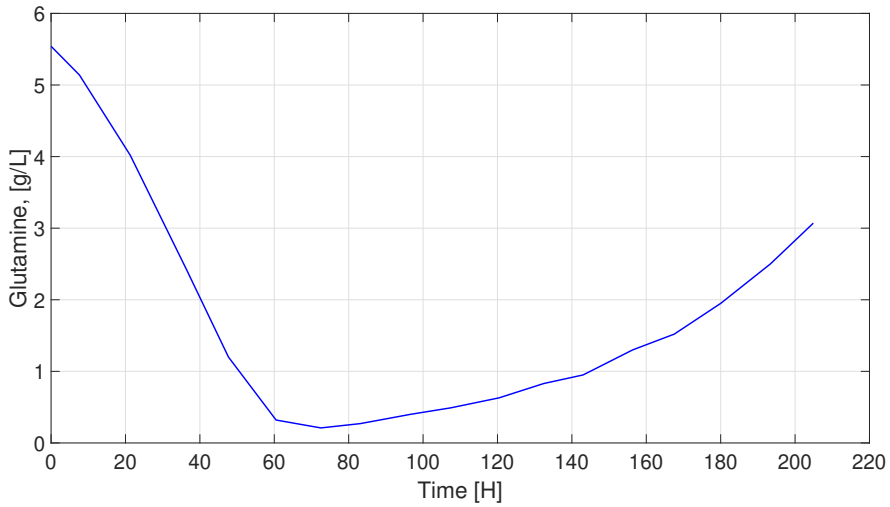

Figure 5.14: Glutamine profile for experiment 14.

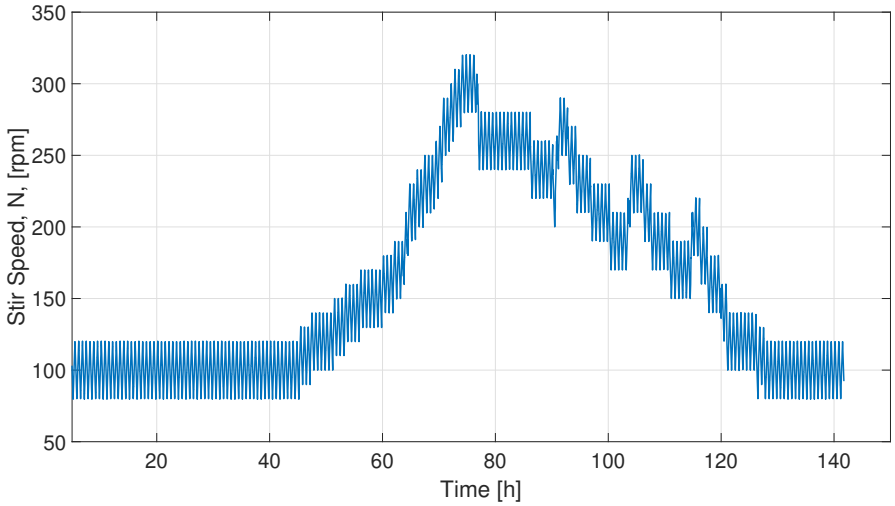

Figure 5.15: Stir speed profile for experiment 12.

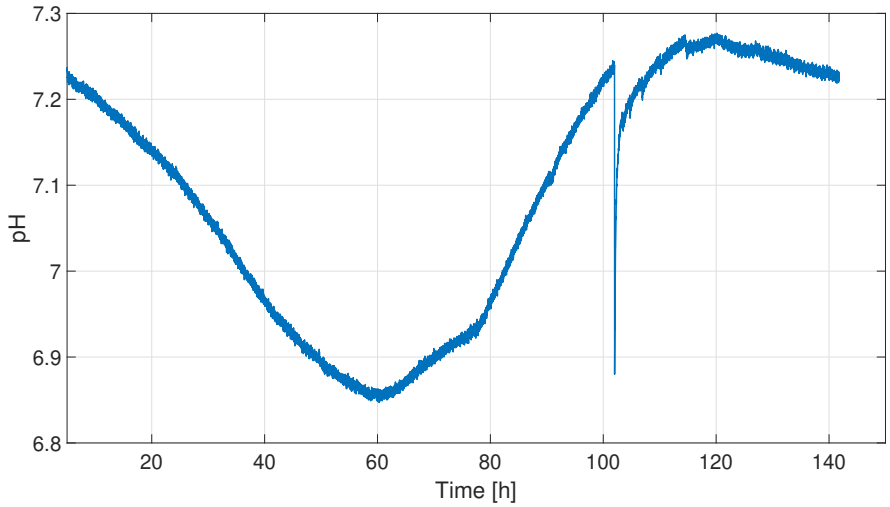

Figure 5.16: pH profile for experiment 12.

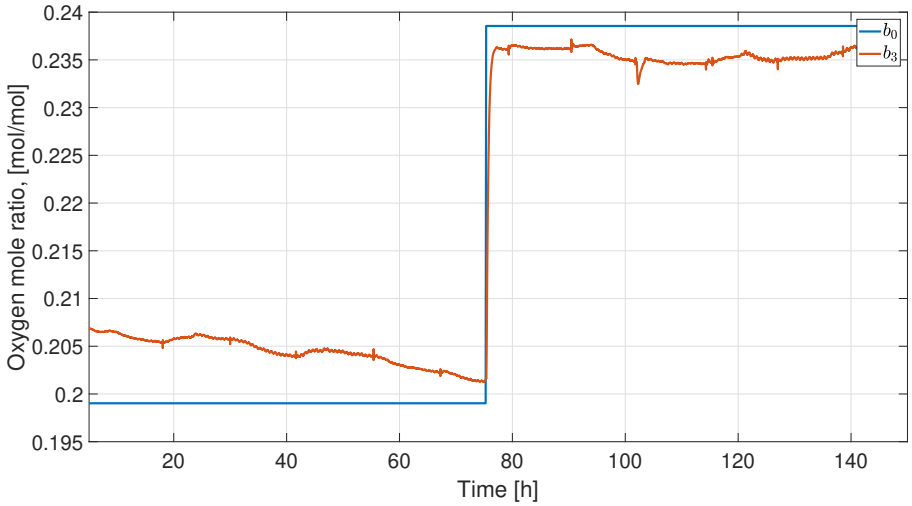

Figure 5.17: Oxygen enrichment profile for experiment 12.

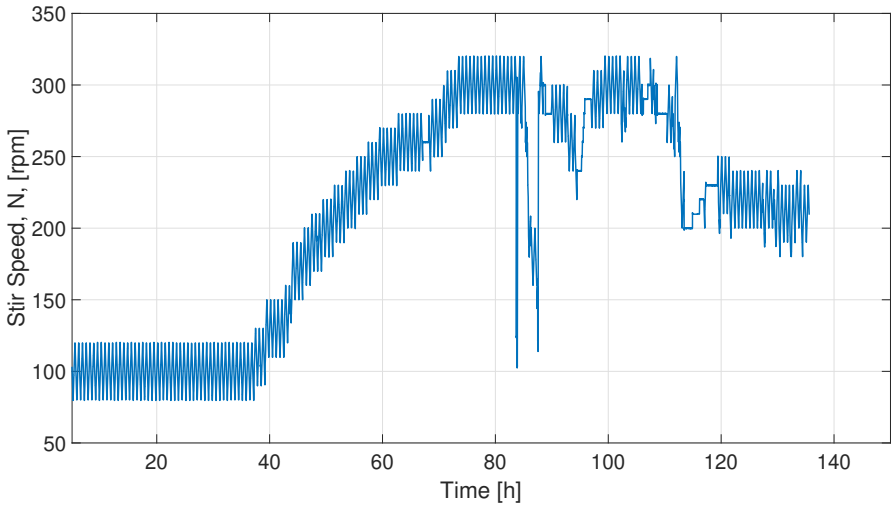

Figure 5.18: Stir speed profile for experiment 13.

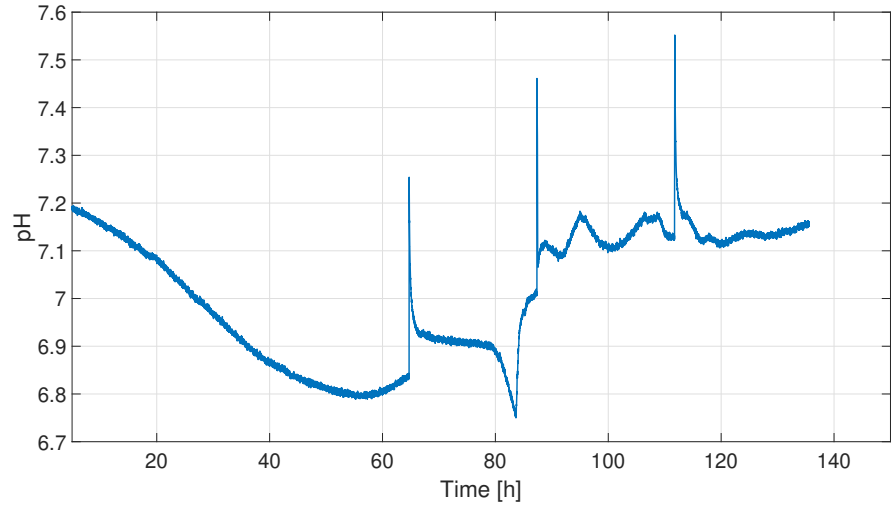

Figure 5.19: pH profile for experiment 13.

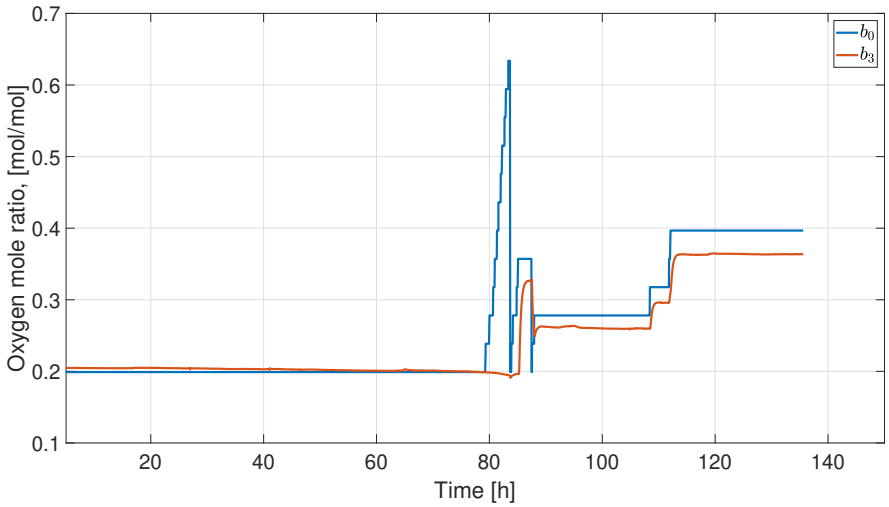

Figure 5.20: Oxygen enrichment profile for experiment 13.

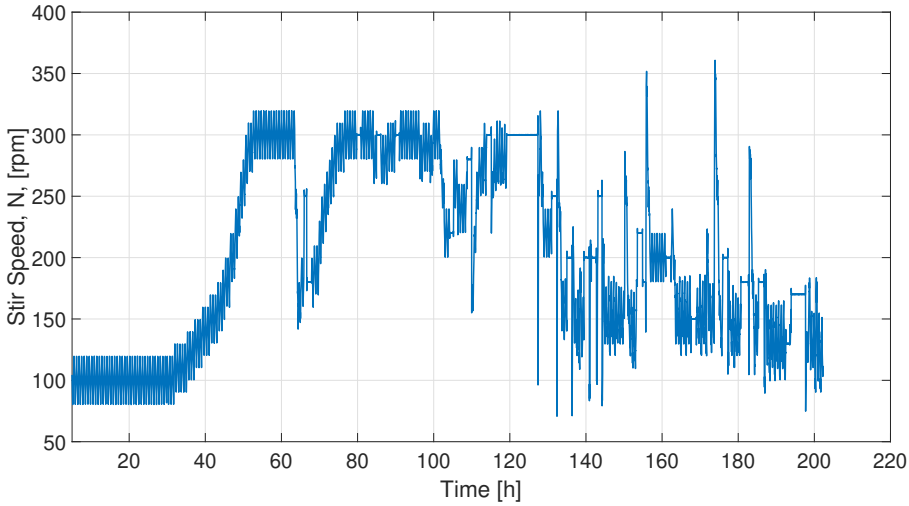

Figure 5.21: Stir speed profile for experiment 14.

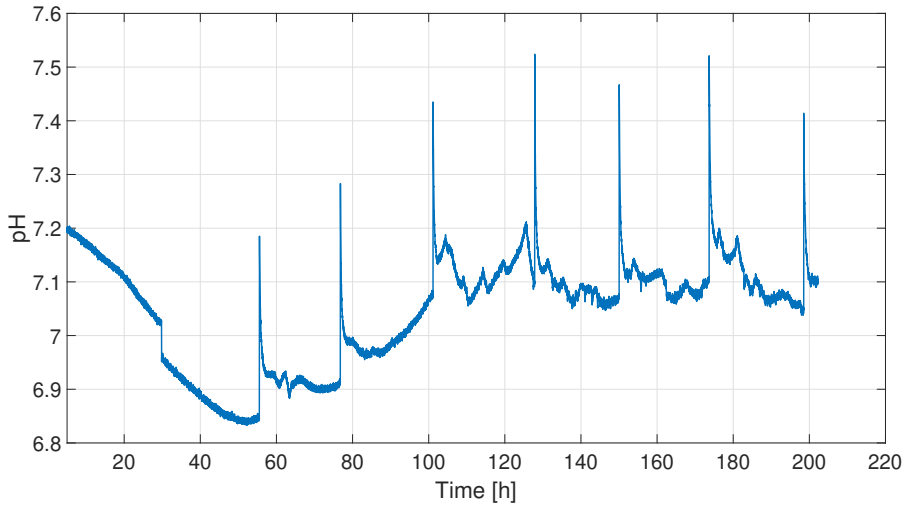

Figure 5.22: pH profile for experiment 14.

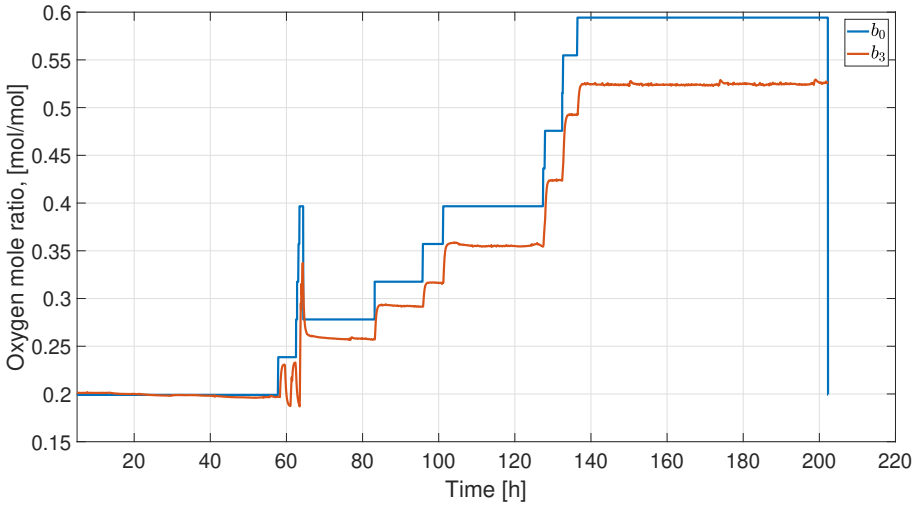

Figure 5.23: Oxygen enrichment profile for experiment 14.

5.1.2 Measurement noise in sensors

Several sensors are used for measuring signals such as off gas, dissolved oxygen, culture volume and mass flow. These sensors have an associated accuracy. Measurement noise becomes significant if the measurements have low amplitude compared to the full range of the sample. For example, in case of the oxygen mass flow controller with an accuracy of ± 1 ml/min, the flow rate

varies from 2.5 ml/min to 25 ml/min. Thus, the error in measurements can vary from 40% to 4% of the flow rate. This is a significant amount of error specially in cases where flow rate is low.

In case of volume measurement, the volume of the liquid is assumed to be constant throughout the experiment. This assumption is based on the fact that there is continuous addition of feed to compensate for the bioreactor liquid pulled out of the bioreactor during sampling. However, it is observed that the final culture volume is always less then the starting culture volume. This is due to the fact that the total amount of feed added in the bioreactor is less then the total volume withdrawn from the bioreactor during sampling. Thus, the volume measurement has an average error of 20 to 25 ml.

In this work, the offgas sensor was limited to measuring up to 0.55 oxygen mole ratio in the output gas. Additionally it had an accuracy of $\pm 2\%$ of the maximum range.Thus, the measurement error is significant during the initial stages of the experiment when the oxygen mole ratio in the sparge gas is low. The cumulative effect of the mass flow controller error and off gas sensor measurement error is significant can be observed in the initial stages of the experiment. Theoretically, the mole ratio of oxygen in the input gas (b_0) has to be larger than the mole ratio in the off-gas (b_3) due to oxygen consumption by the cells. However, as shown in figure 5.24, $b_0 < b_3$. Thus, this data cannot be used to calculate OTR_{offgas}. This error is eliminated in the later part of the experiment as the oxygen mole ratio becomes comparable to the sensor measurement precision.

5.2 Results and Discussion

The algorithm developed in Chapter 3 to estimate k_La and C^*_{cal} was applied to three experiments. These experiments used the CHO VRC01 cell line (NIH) which were cultured in GE Actipro media. The accuracy of this algorithm was checked in Chapter 4 using a simulated experiment.

5.2.1 Mass Transfer Coefficient Estimation for Experiment Data

To apply k_La estimation algorithm to experiment data it was vital to decide the length of the data subset. The algorithm cannot be applied to the entire data set because of various reasons. k_La estimate ($\widehat{k_La}$), depends on estimation of $\hat{\alpha_0}$ and $\hat{\alpha_1}$. As shown in section 3.2, $\hat{\alpha_0}$ and $\hat{\alpha_1}$ values depend on 3 major signals, (i) b_0, (ii) OTR_{offgas}, (iii) DO. In the experiment, these signals change over time. The input oxygen mole ratio (b_0) changes when there is a change in gas mix. OTR_{offgas}

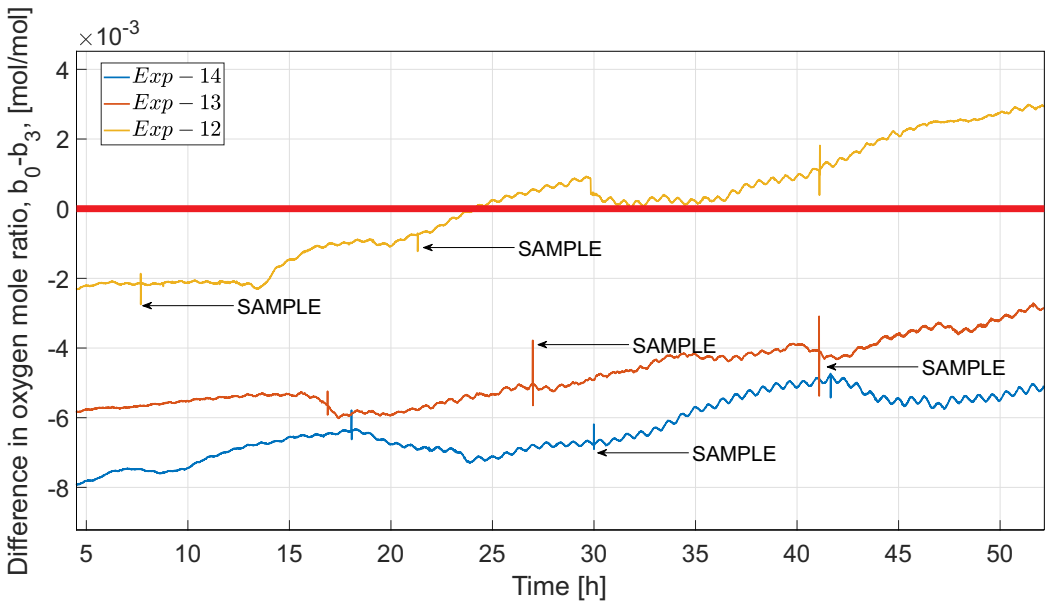

Figure 5.24: Difference in the input and output oxygen mole ratio.

changes due to increase in VCD and change in b_0. Dissolved oxygen (DO) changes due to change b_0 and VCD. To accommodate all these changes we need to obtain continuous estimation of k_La. Thus, the length of the data subset has to be decided. A very small data set leads to higher errors in $\widehat{k_La}$ and it is not feasible to apply this algorithm for online estimation if the length of the data set is too large. Thus, a trade-off has to be established to get low error results with minimum possible data set length. By applying the algorithm to various data set lengths, the final data set length was fixed at 40 minutes.

The algorithm to estimate $\widehat{k_La}$ was applied to various data subsets of 40 minutes each. These $\widehat{k_La}$ estimations computed for each experiment were then compared with $\widehat{k_La}$ estimation for the same experiment at different time periods . A graph of $\widehat{k_La}$ versus stir speed is shown in figure 5.25. The time period over which these values were computed is given in table 5.2. During these time periods, there is no gas-mix change. Thus, b_0 is almost constant. Hence the changes in OTR_{offgas} and DO signals are small. Thus, theoretically, the different $\widehat{k_La}$ values calculated over short consecutive time periods will be similar. As seen in figure 5.25, The k_La calculated over different consecutive time periods are similar. This fact can also be observed in figures 5.26 and 5.27.

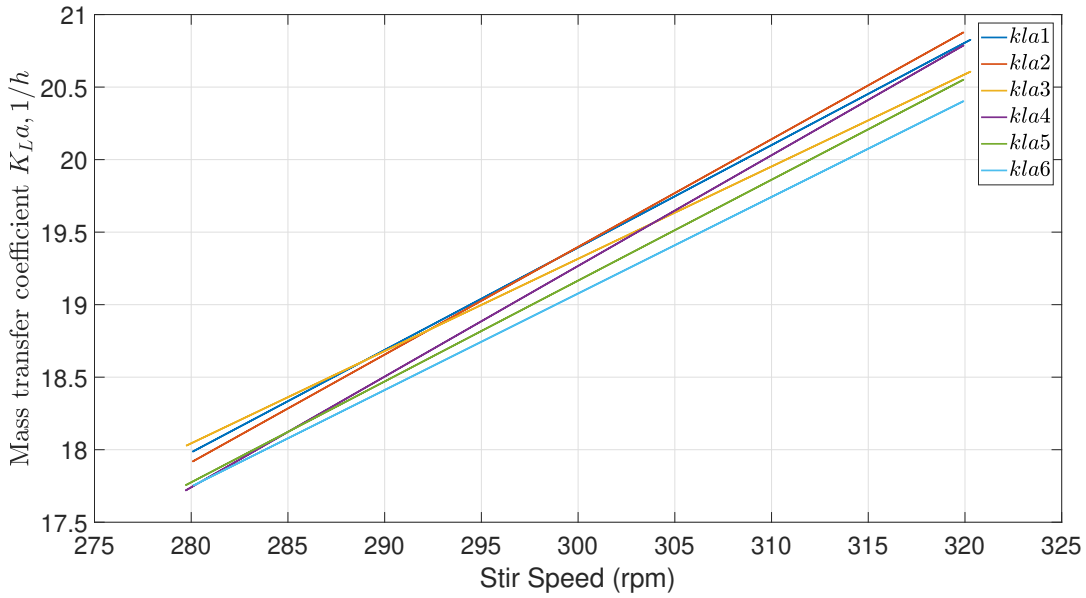

Figure 5.25: k_La estimates for experiment 14 between 91.22 and 95.22 hours. Each line represents a 40 minute time interval where the stir speed varied ± 20 rpm. These k_La calculations occured between known disturbances such as feeding, antifoam addition, air enrichment changes and sampling.

Further, $\widehat{k_La}$ was estimated for the same time period across different experiments. The plot for $\widehat{k_La}$ is shown in figure 5.28. Unlike $\widehat{k_La}$ for the same experiments shown in Figures 5.25, 5.26 and 5.27, the $\widehat{k_La}$ plots for different experiments are not clustered close together. This might be due to various changes in the physical and chemical changes in the media. Variation in k_La can occur due to change in propeller positions in the bioreactor.

Start time (h)	End time (h)	$\widehat{k_La}$
91.22	91.88	$\widehat{k_La1}$
91.88	92.55	$\widehat{k_La2}$
92.55	93.22	$\widehat{k_La3}$
93.22	93.88	$\widehat{k_La4}$
93.88	94.55	$\widehat{k_La5}$
94.55	95.22	$\widehat{k_La6}$

Table 5.2: Data subsets used to calculate $\widehat{k_La}$ for experiment 14 as shown in Figure 5.25.

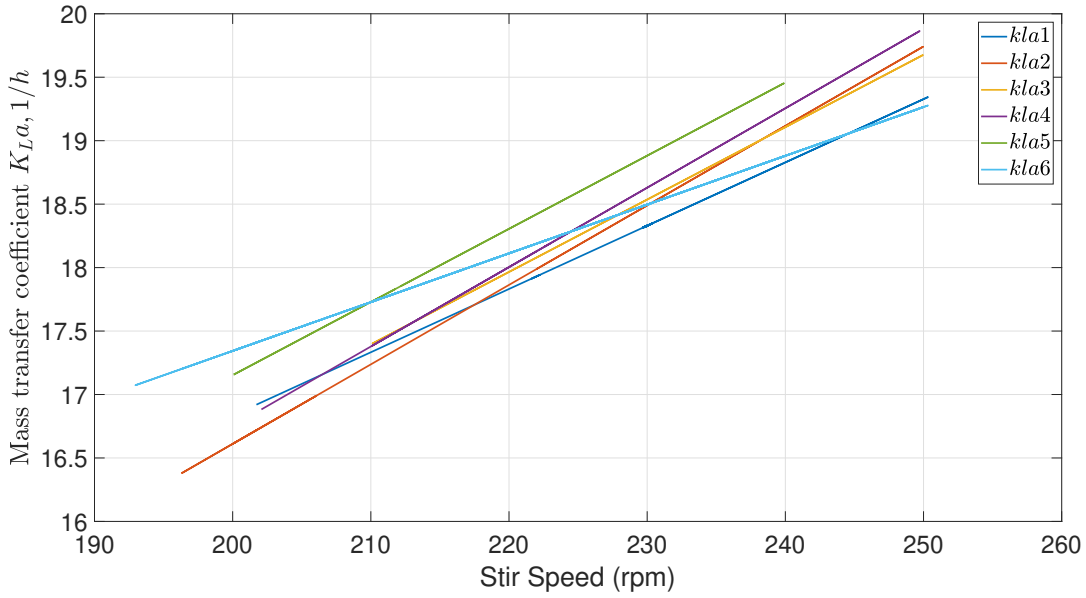

Figure 5.26: k_La estimates for experiment 13 between 89.42 and 93.42 hours. Each line represents a 40 minute time interval where the stir speed varied ± 20 rpm. These k_La calculations occured between known disturbances such as feeding, antifoam addition, air enrichment changes and sampling.

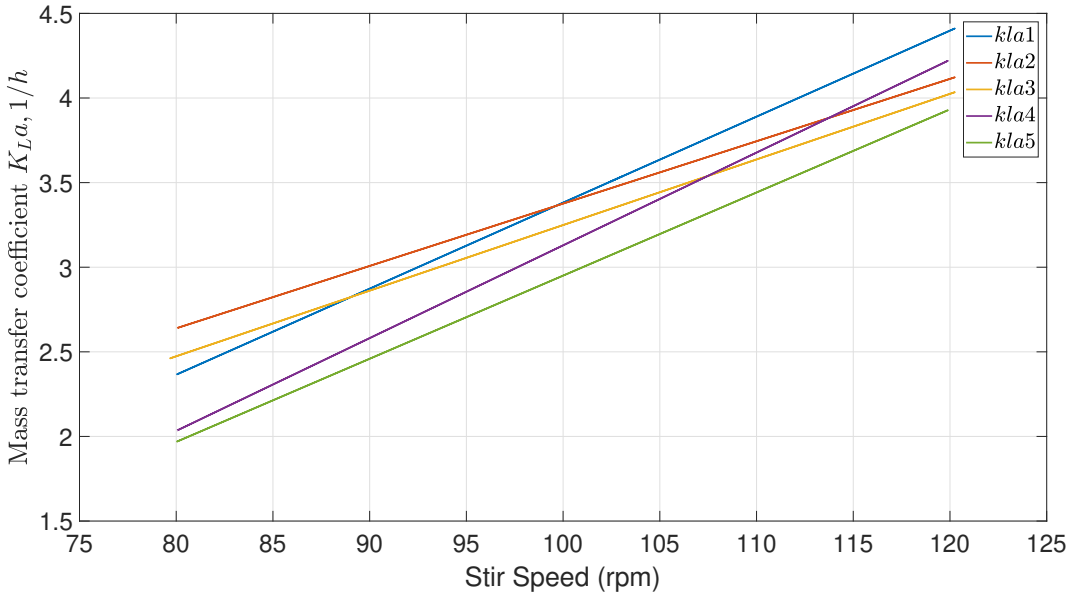

Figure 5.27: k_La estimates for experiment 12 between 136.99 and 140.33 hours. Each line represents a 40 minute time interval where the stir speed varied ± 20 rpm. These k_La calculations occured between known disturbances such as feeding, antifoam addition, air enrichment changes and sampling.

Start time (h)	End time (h)	$\widehat{k_La}$
89.42	90.08	$\widehat{k_La}1$
90.08	90.75	$\widehat{k_La}2$
90.75	91.42	$\widehat{k_La}3$
91.42	92.08	$\widehat{k_La}4$
92.08	92.75	$\widehat{k_La}5$
92.75	93.42	$\widehat{k_La}6$

Table 5.3: Data subsets used to calculate $\widehat{k_La}$ for experiment 13 as shown in Figure 5.26.

Start time (h)	End time (h)	$\widehat{k_La}$
136.99	137.66	$\widehat{k_La}1$
137.66	138.33	$\widehat{k_La}2$
138.33	138.99	$\widehat{k_La}3$
138.99	139.66	$\widehat{k_La}4$
139.66	140.33	$\widehat{k_La}5$

Table 5.4: Data subsets used to calculate $\widehat{k_La}$ for experiment 12 as shown in Figure 5.27.

Experiment No.	Start time (h)	End time (h)
12	75.66	76.33
13	77.33	78
14	75.33	76

Table 5.5: Data subsets used to calculate $\widehat{k_La}$ for experiment 12, 13 and 14 corresponding to figure 5.28

5.2.2 Oxygen saturation concentration estimation for experiment data.

As discussed in section 3.3, the oxygen saturation concentration can be obtained by minimizing the variations between OUR_{linfit} and $\widehat{OUR}$. A fixed data subset length is selected based on the reasoning discussed in section 5.2.1. A very small data set leads to higher errors in $\widehat{k_La}$ and it is not feasible to apply this algorithm for online estimation if the length of the data set is too large. Thus, a trade-off has to be established to get low error results with minimum possible data set length. By applying the algorithm to various data set lengths, the final data set length was fixed at 40 minutes. Furthermore, the frame-length and order of the fitting polynomial for Savitzky-Golay filtering has to be fixed. In this experiments stir speed was continuously varied by

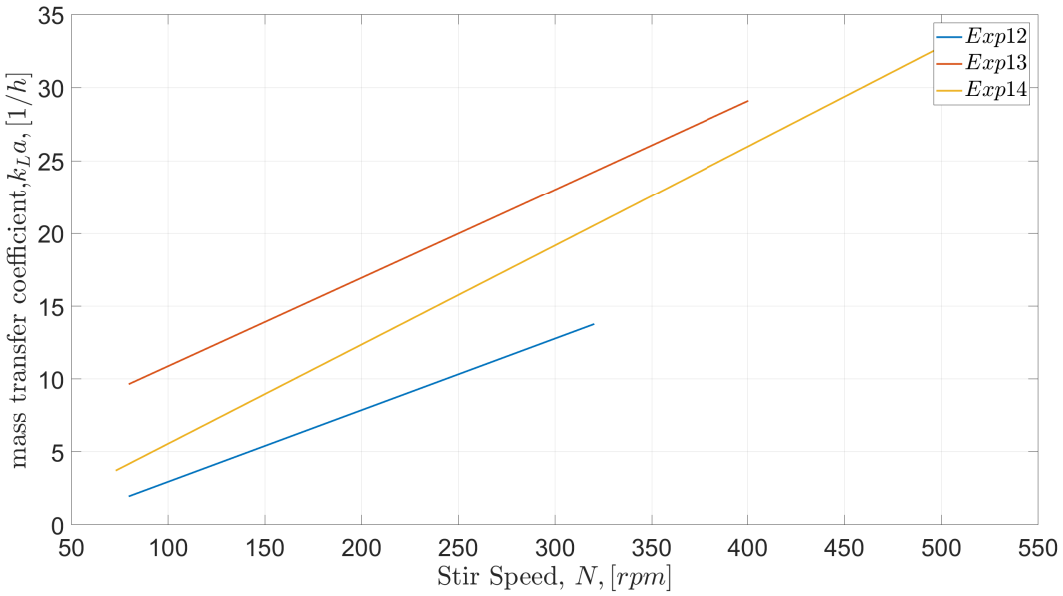

Figure 5.28: k_La versus stir speed for experiment 12, 13 and 14. The k_La values are extrapolated for comparison. The data subsets are chosen during a similar time frame for all the experiments.

adding a triangular wave with a period of 40 minutes to the stir speed signal. This was to ensure that $\widehat{k_La}$ estimation problem was well formed. This stir speed variations lead to a similar variation in DO signal reading. Thus, it is important to make sure that the filter frame-length is not very large. A large frame-length will not filter the DO signal correctly at its peak where the DO signal changes slope. A very small frame-length will not filter the noise to deliver a smooth DO signal. Thus, through trial and error a frame length of 11 samples (time period = 165 seconds) was chosen. A second order filtering polynomial was chosen to better fit the typical DO signal.

The algorithm to estimate $\widehat{C^*_{cal}}$ was applied to various data subsets of 40 minutes each. These $\widehat{C^*_{cal}}$ estimations computed for each experiment were then compared with $\widehat{C^*_{cal}}$ estimation for the same experiment at different time periods. Table 5.6 lists the estimated $\widehat{C^*_{cal}}$ values for experiment 14. The $\widehat{C^*_{cal}}$ are almost constant with a error between successive values of approximately $\pm 5\%$. These values are calculated on day 4 of the experiment. Thus, the oxygen saturation concentration is very low due to addition of feed and other compounds. The oxygen saturation concentration also decreases as the VCD increases. On day 4 of experiment, the VCD is 10.7×10^6. Similar results were observed for experiment 13 and 12 as shown in table 5.7 and 5.8.

The estimated oxygen saturation concentration in the bioreactor liquid ($\widehat{C^*_{cal}}$) is compared

Start time (h)	End time (h)	$\widehat{C^*_{cal}}$ (g/L)
91.22	91.88	2.99×10^{-3}
91.88	92.55	3.21×10^{-3}
92.55	93.22	2.90×10^{-3}
93.22	93.88	2.78×10^{-3}
93.88	94.55	2.92×10^{-3}
94.55	95.22	2.97×10^{-3}

Table 5.6: Data subsets used to calculate $\widehat{C^*_{cal}}$ and the estimated $\widehat{C^*_{cal}}$ for experiment 14.

Start time (h)	End time (h)	$\widehat{C^*_{cal}}$ (g/L)
89.42	90.08	3.19×10^{-3}
90.08	90.75	3.09×10^{-3}
90.75	91.42	3.02×10^{-3}
91.42	92.08	2.86×10^{-3}
92.08	92.75	2.49×10^{-3}
92.75	93.42	2.77×10^{-3}

Table 5.7: Data subsets used to calculate $\widehat{C^*_{cal}}$ and the estimated $\widehat{C^*_{cal}}$ for experiment 13.

Start time (h)	End time (h)	$\widehat{C^*_{cal}}$ (g/L)
136.99	137.66	3.49×10^{-3}
137.66	138.33	3.49×10^{-3}
138.33	138.99	3.14×10^{-3}
138.99	139.66	2.92×10^{-3}
139.66	140.33	2.68×10^{-3}

Table 5.8: Data subsets used to calculate $\widehat{C^*_{cal}}$ and the estimated $\widehat{C^*_{cal}}$ for experiment 12.

for different time periods across experiments 13 and 14. As seen from tables 5.6 and 5.7, the $\widehat{C^*_{cal}}$ estimate is constant over approximately the same time range. These time ranges are listed in Table 5.9

Experiment 13			Experiment 14		
Start time(h)	End time(h)	$\widehat{C^*_{cal}}$ (g/L)	Start time(h)	End time(h)	$\widehat{C^*_{cal}}$ (g/L)
91.22	91.88	3.08×10^{-3}	91.42	92.08	3.21×10^{-3}
92.55	93.22	2.83×10^{-3}	92.08	92.75	3.01×10^{-3}
125.75	126.42	3.28×10^{-3}	124.33	124.99	3.09×10^{-3}

Table 5.9: Data subsets used to calculate $\widehat{C^*_{cal}}$ and the estimated $\widehat{C^*_{cal}}$ for experiment 12.

5.2.3 $\widehat{OTR}$ and $\widehat{OUR}$

The estimated values of $\widehat{k_La}$ and $\widehat{C^*_{cal}}$ are used to calculate $\widehat{OTR}$ and $\widehat{OUR}$. A small subset of $\widehat{OTR}$ and $\widehat{OUR}$ signals calculated during feeding pulses is shown in Figure 5.29 to 5.32. The $\widehat{OUR}$ signal for all the feed pulses are compiled in appendix B. It can be observed from all the feed pulses that OTR_{offgas} is a filtered version of $\widehat{OTR}$ and hence OTR_{offgas} lags behind $\widehat{OTR}$. The estimated values of $\widehat{k_La}$ and $\widehat{C^*_{cal}}$ calculated using the algorithm discussed in sections 3.2 and 3.3 reduce the variation in $\widehat{OUR}$. As seen in figure 5.32, $\widehat{OTR}$ has high variation. However, a smooth $\widehat{OUR}$ signal is obtained. The high variation in $\widehat{OTR}$ for pulse 8 is due to quantization error in stir speed value.

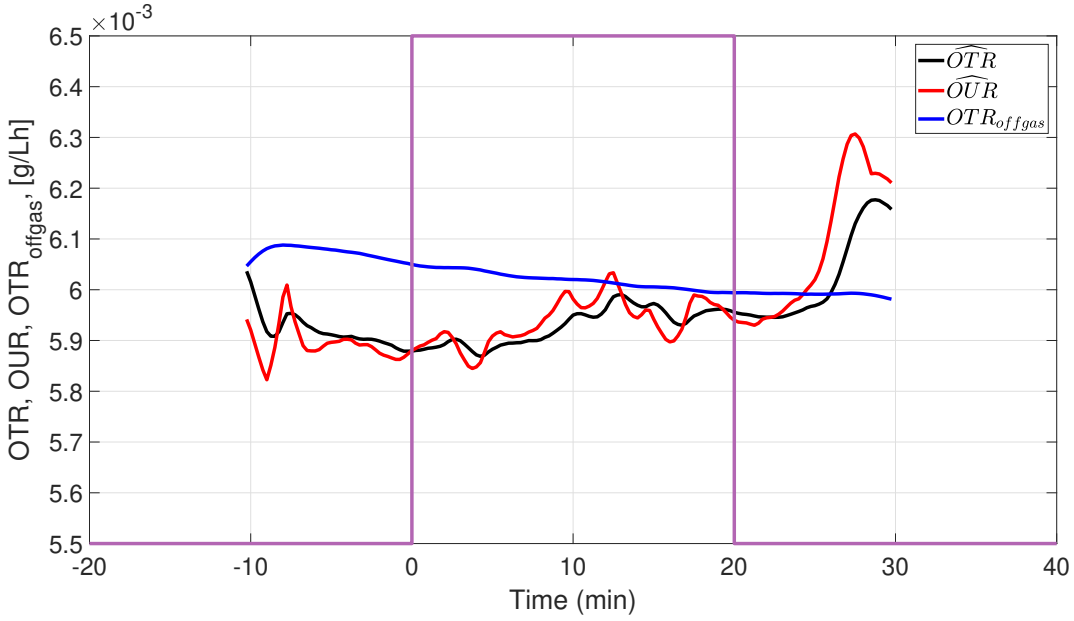

Figure 5.29: OUR, OTR and OTR_{offgas} for feed pulse 4 of experiment 14. The purple line represents a feeding pulse. Start time for the pulse was 96.95 hours and the end time for the pulse was 97.28.

This is a small sampling of OUR, OTR and OTR_{offgas} signals calculated for different feed pulses of experiment 14. All the pulses and the corresponding signals are compiled in Appendix B.

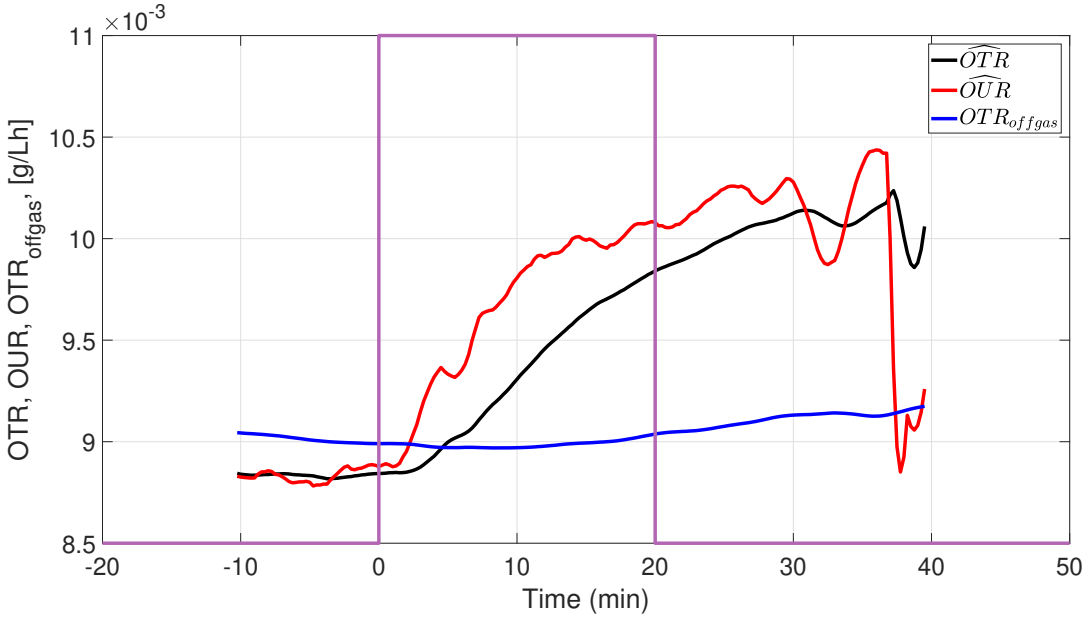

Figure 5.30: OUR, OTR and OTR_{offgas} for feed pulse 5 of experiment 14. The purple line represents a feeding pulse. Start time for the pulse was 111.05 hours and the end time for the pulse was 111.55.

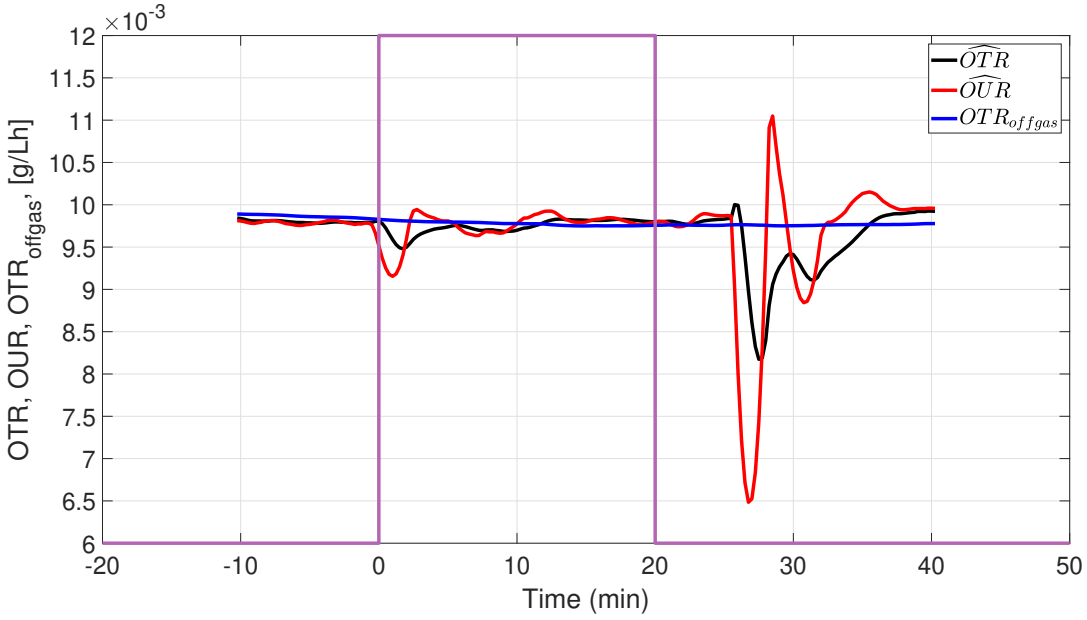

Figure 5.31: OUR, OTR and OTR_{offgas} for feed pulse 7 of experiment 14. The purple line represents a feeding pulse. Start time for the pulse was 120.90 hours and the end time for the pulse was 121.23.

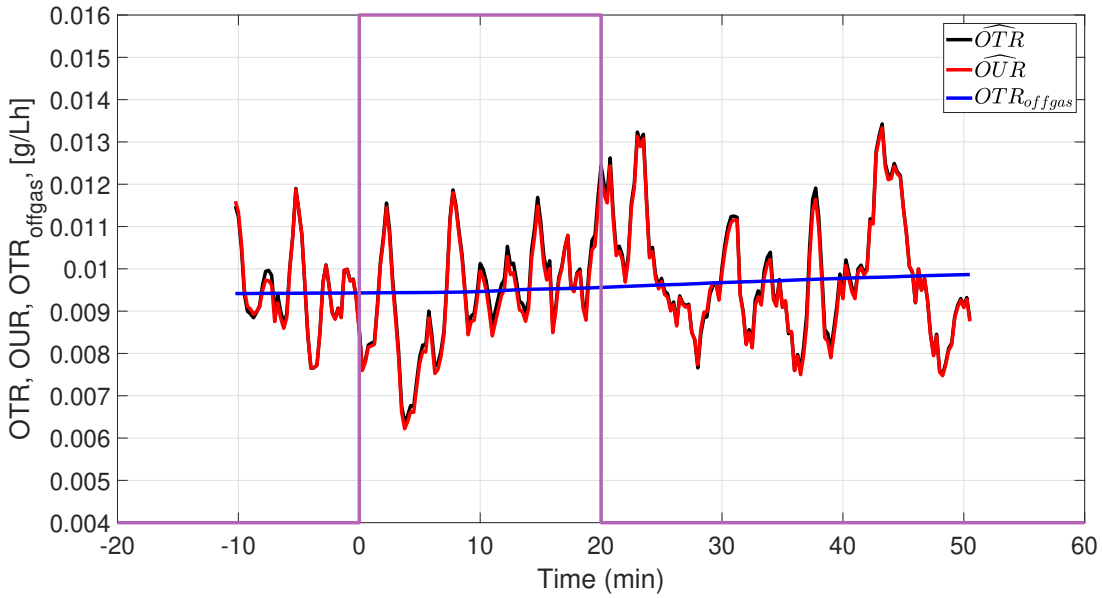

Figure 5.32: OUR, OTR and OTR_{offgas} for feed pulse 8 of experiment 14. The purple line represents a feeding pulse. Start time for the pulse was 133.18 hours and the end time for the pulse was 134.01.

Chapter 6

Conclusion and Future Work

6.1 Conclusion

In this thesis, a new method was proposed to estimate $\widehat{k_La}$ and $\widehat{C^*_{cal}}$ based on minimizing the variations in $OUR_{linfit} - \widehat{OUR}$. The dynamics of headspace delay and off-gas sensor measurement delay were included in the design. A Simulink simulation environment was used to simulate a bioreactor experiment and the algorithm to compute $\widehat{k_La}$ and $\widehat{C^*_{cal}}$ was tested against known values from this simulation. A noise model was developed based on the dissolved oxygen reading of the actual bioreactor experiment to mimic the effects of noise in laboratory experiments. It was found that, the algorithm converged and estimated the correct values of $\widehat{k_La}$ and $\widehat{C^*_{cal}}$ even in the presence of noise. This established the accuracy of the algorithm.

It is important to note here that a data range is used apply this algorithm and predict $\widehat{k_La}$ and $\widehat{C^*_{cal}}$. To apply this algorithm online and to quickly get estimates for $\widehat{k_La}$ and $\widehat{C^*_{cal}}$ this data range has to be minimized. Through trial and error it was determined that using only 40 minutes of previously acquired data can give good estimate of $\widehat{k_La}$ and $\widehat{C^*_{cal}}$. The algorithm used to estimate $\widehat{k_La}$ does not directly use the value of C^*_{cal}, instead it uses a product of α_0 & C^*_{cal} and α_1 & C^*_{cal}. Thus, any errors in initial estimation of C^*_{cal} is automatically balanced by changing α_0 and α_1. The algorithm automatically adjusts these values thus eliminating dependence of the algorithm on initial estimation of C^*_{cal}.

This algorithm was used to find $\widehat{k_La}$ and $\widehat{C^*_{cal}}$ for three laboratory experiments with NIH igG cell line and GE Actipro media. First, the $\widehat{k_La}$ values for different data subsets in the same

experiments were determined and compared for consistency. It was observed that, consequent data subsets provided similar values of $\widehat{k_La}$ in the same experiment. This fact was observed for different experiments. Thus, $\widehat{k_La}$ estimation helped establish the consistency of the algorithm. Next, estimated $\widehat{k_La}$ values from different experiments but same time period were compared with each other. It was found that Experiment 12 had the lowest value of $\widehat{k_La}$ followed by $\widehat{k_La}$ for experiment 14. Experiment 13 had the highest $\widehat{k_La}$. This could be one of the reasons why VCD for experiment 13 was highest followed by experiment 14 and experiment 12.

Next, $\widehat{C^*_{cal}}$ was calculated for different experiments using different data subsets. It was observed that $\widehat{C^*_{cal}}$ was almost constant over short data ranges. It is difficult to establish the accuracy of this results since there are no published values of $\widehat{C^*_{cal}}$ for the media used. Second, the culture composition changes over time, thus it is not possible to know the actual oxygen saturation concentration in the bioreactor culture. However, the estimated values of $\widehat{C^*_{cal}}$ over short data subsets were consistent. On comparing the values of $\widehat{C^*_{cal}}$ from different experiments but from approximately same time period, it was observed that $\widehat{C^*_{cal}}$ values are similar for same culture conditions for different experiments.

The estimated values of $\widehat{C^*_{cal}}$ and $\widehat{k_La}$ were used to calculate $\widehat{OTR}$ and $\widehat{OUR}$. The algorithm was used to minimize the variation between $OUR_{linfit} - \widehat{OUR}$ to provide a correct $\widehat{OUR}$ signal. It was observed that even when $\widehat{OTR}$ variations are high due to changing stir speed or noise, the algorithm provided a smooth $\widehat{OUR}$ signal. This establishes the accuracy of the algorithm. Thus, the algorithm estimated a correct values of $\widehat{k_La}$ and $\widehat{C^*_{cal}}$ and provided a smooth $\widehat{OUR}$ signal.

6.2 Future Work

6.2.1 Change in oxygen saturation concentration over time.

This work estimates $\widehat{C^*_{cal}}$ which is then used to calculate $\widehat{OUR}$. The oxygen saturation concentration, however, changes over time changing the effect of increase in gas mix on $\widehat{OTR}$. This effect can be mathematically stated by modifying equation 3.4,

$$OTR = (\alpha_0 + \alpha_1(N - N_0))({C_{cal}}^* \frac{b_0}{b_{0i}} - {C_{cal}}^* \frac{DO}{100}) \tag{6.1}$$

As seen in equation 3.4, $\widehat{C^*_{cal}}$ affects the gas mix change given by $\frac{b_0}{b_{0i}}$ and the DO change

which in turn affects $\widehat{OTR}$ estimation. However, the effect of oxygen saturation concentration on gas mix change is not same over time. This is because the oxygen saturation concentration changes due to various reasons like feed addition and increase in VCD throughout the experiment. The changing oxygen saturation concentration can be mathematically represented using a new variable K_0. K_0 is a function of different parameters such as salinity of the culture, temperature, pressure etc. Thus equation 3.4 can be rewritten as,

$$OTR = (\alpha_0 + \alpha_1(N - N_0))(K_0 \times {C_{cal}}^* \frac{b_0}{b_{0i}} - {C_{cal}}^* \frac{DO}{100}) \tag{6.2}$$

Initially during calibration K_0 is 1. It should decrease with time to represent a the decrease in oxygen saturation concentration over time. In this work K_0 is assumed to be constant and equal to 1. However, a new method needs to be developed which estimates K_0 value.

6.2.2 Online implementation of the algorithm

This algorithm can be implemented online during a bioreactor experiment. A small data subset of 40 minutes can be acquired and various parameters like $\hat{\alpha_0}$, $\hat{\alpha_0}$ and $\widehat{C^*_{cal}}$ can be estimated. The algorithm uses Savitzky-Golay filtering to reduce noise in DO signal and compute $\dot{DO}$. A framelength of 11 samples or 165 seconds will suffice to compute $\dot{DO}$ online. Thus, $\widehat{OTR}$ and $\widehat{OUR}$ can be estimated online.

This algorithm can be implemented on multiple consequent data subsets to verify the calculated parameters. This will help determine the metabolic state of the bioreactor culture and enable the estimator-controller pair to update the feed rate.

Appendices

Appendix A Simulation Blocks to simulate bioreactor experiment.

A set of simulation blocks were used to simulate an experiment. The block used in this simulation are explained in this section with their corresponding alphabet.

A: First, all the fixed parameters are predetermined and fixed. These parameters include α_1, α_0, temprature, pressure, gas constant, mass flow etc.

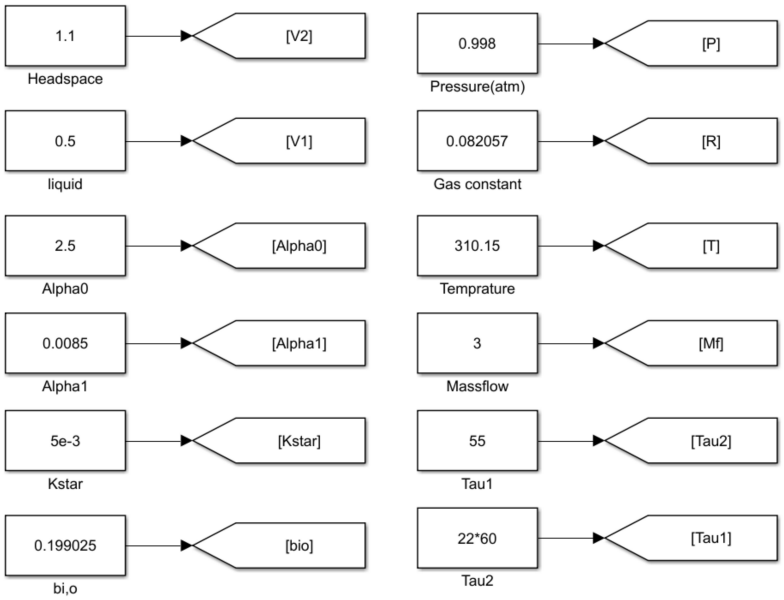

Figure A1: Block A

B: k_La is computed using equation equation 4.4.

C: The input oxygen mole ratio was calculated using the oxygen and air percentages. The driving force is calculated as a function of oxygen saturation concentration [Kstar].

D: The oxygen uptake rate $[OUR_1]$ is modeled as shown.

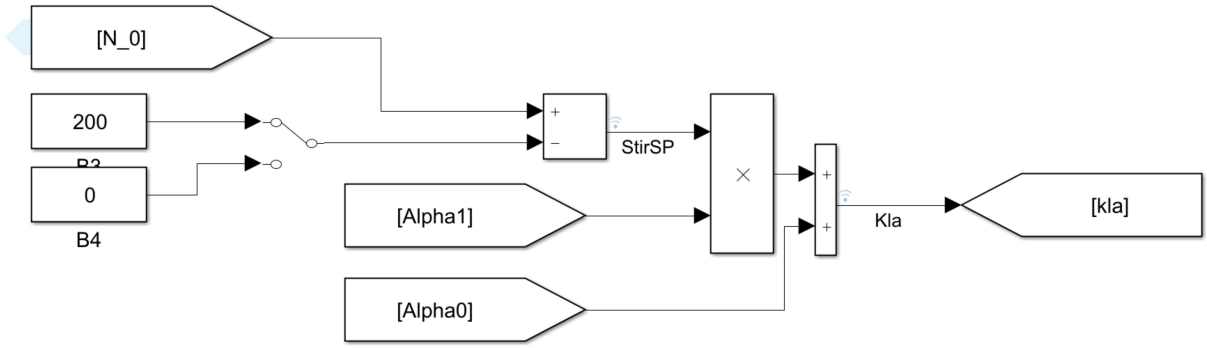

Figure A2: Block B

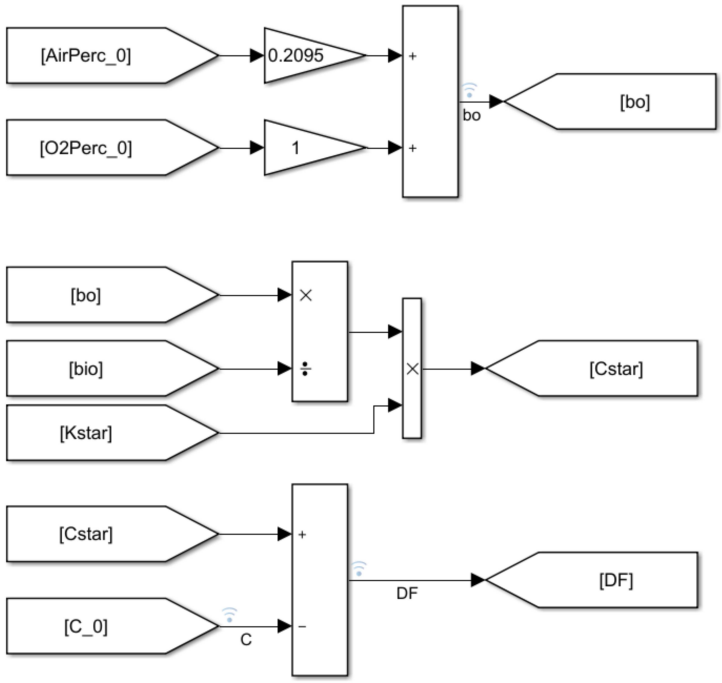

Figure A3: Block C

E: The change in oxygen concentration [Cdot] is calculated as $OTR - OUR_0$.This signal is then integrated to calculate the oxygen concentration [Ct].

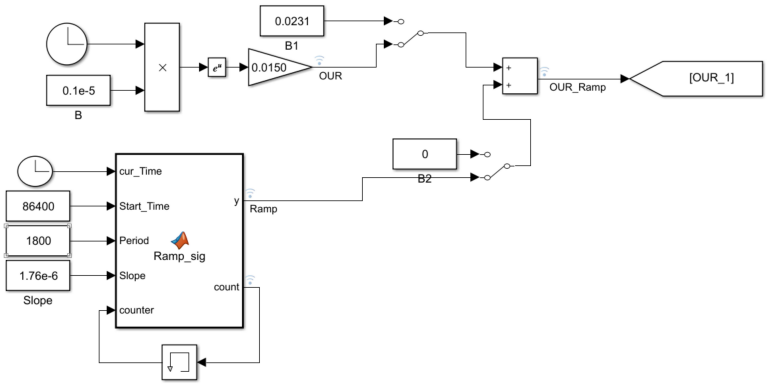

Figure A4: Block D

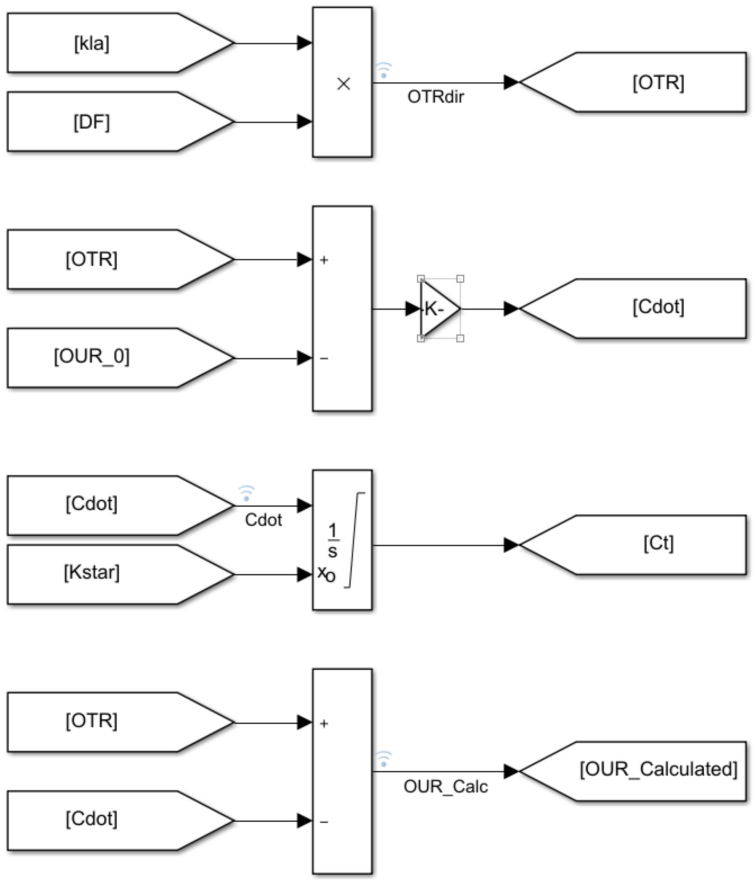

Figure A5: Block E

F: The oxygen concentration [Ct] is used to update dissolved oxygen [DO].

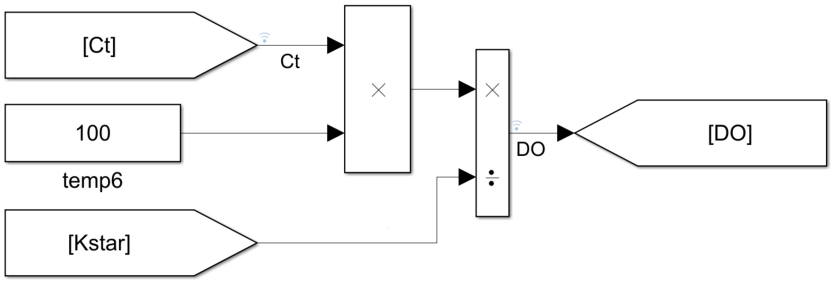

Figure A6: Block F

G: The updated [DO] signal is used to update stir speed and oxygen and air percentages in the sparge gas. A triangular signal is superimposed on the stir speed output signal to mimic persistent agitation in the experiments. The update logic code is given below:

```
function [StirSP,AirSP,O2SP] = ControlStir(Stir,DO,Air,O2)
upper_DO_lim = 50;
lower_DO_lim = 40;
StirSP = Stir;
AirSP = Air;
O2SP = O2;
if (DO >= lower_DO_lim && DO < upper_DO_lim)
   % Do nothing
elseif (DO <40 && Stir<=300)
    StirSP = Stir+20;
elseif (DO<40 && Stir>300)
    AirSP = Air-0.05;
    O2SP = O2+0.05;
elseif (DO > upper_DO_lim && Stir > 100)
    StirSP = Stir-5;
end
```

```
end
```

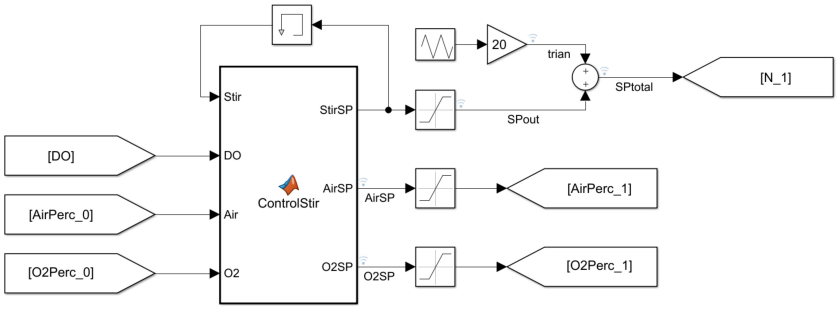

Figure A7: Block G

H: The offgas sensor reading are simulated by first calculating the oxygen mole ratio at the surface of the bioreactor culture. Then, the signal is passed through two low pass filters to allow simulate headspace mixing dynamics and offgas sensor measurement delay.

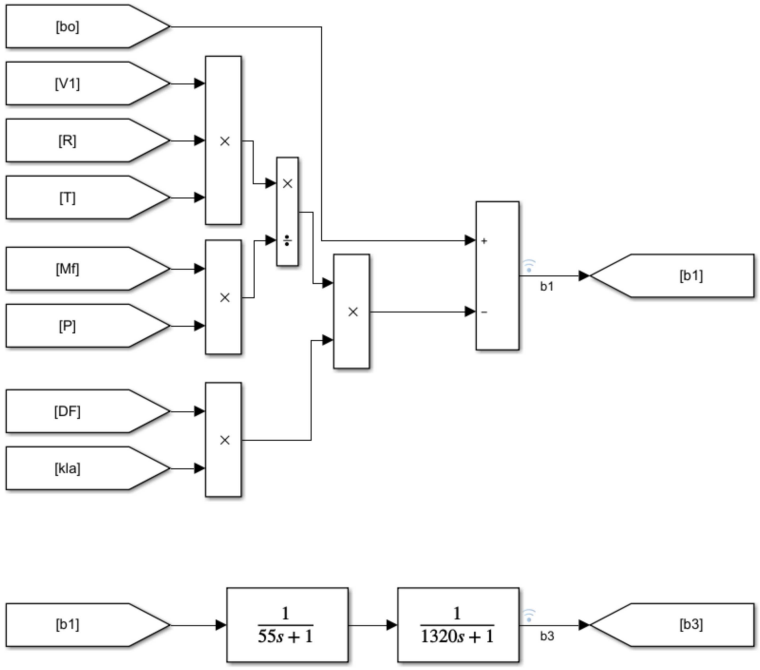

Figure A8: Block H

Appendix B $\widehat{OUR}$ plots for all feed pulses of experiment 14

This sections provides a catalog of all the feed pulses of experiment 14. The oxygen uptake rate is normalized to make analysis easy.

Pulse No.	Start Time [h]	End Time [h]	Initial Glucose concentration (g/L)	Final Glucose concentration (g/L)	Initial OUR [g/Lh]
1	72.63	72.96	2.77	2.80	0.0037
2	86.80	87.13	1.73	1.89	0.0047
3	91.88	92.38	1.53	1.82	0.0056
4	96.95	97.28	1.57	1.77	0.0059
5	111.05	111.55	0.85	0.54	0.0088
6	115.82	116.32	0.49	0.69	0.0095
7	120.90	121.23	0.29	0.51	0.0098
8	133.18	134.01	0.28	0.73	0.0116
9	137.90	138.73	0.46	0.81	0.0116
10	142.02	142.69	0.63	1.09	0.0119
11	153.80	154.47	0.63	1.09	0.0166
12	167.95	168.62	0.85	1.25	0.0164
13	176.30	176.97	0.16	0.44	0.0166
14	181.00	181.67	0.19	0.90	0.0163
15	185.90	187.07	0.78	1.16	0.0150

Table 1: List of feed pulses and corresponding initial and final glucose concentration and initial OUR.

Pulse No.	$VCD_{initial}$ [cells/mL]	$Lactate_{initial}$ [g/L]	$Lactate_{initial}$ [g/L]
1	7.12×10^6	1.17	1.02
2	9.35×10^6	0.97	0.92
3	– – –	1.01	0.9
4	1.07×10^7	0.85	0.75
5	– – –	0.45	0.29
6	– – –	0.4	0.39
7	1.75×10^7	0.43	037
8	1.72×10^7	0.26	0.25
9	– – –	0.43	0.39
10	2.32×10^7	0.46	0.36
11	1.99×10^7	0.42	– – –
12	1.84×10^7	0.47	– – –
13	1.67×10^7	– – –	0.52
14	– – –	0.37	– – –
15	– – –	0.38	– – –

Table 2: Feed pulses and corresponding VCD and lactate.

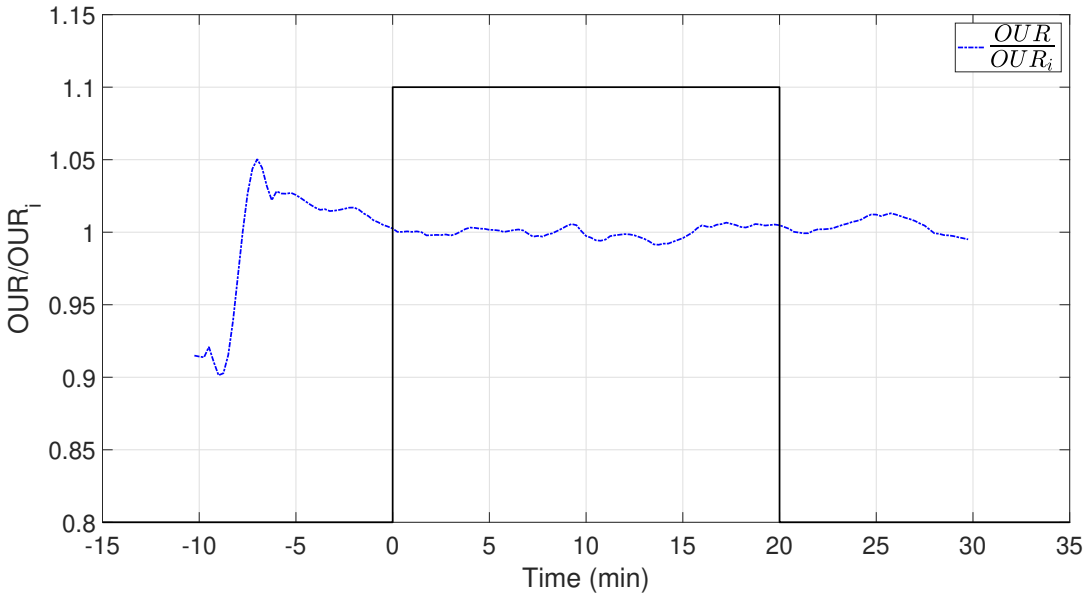

Figure A9: Pulse 1

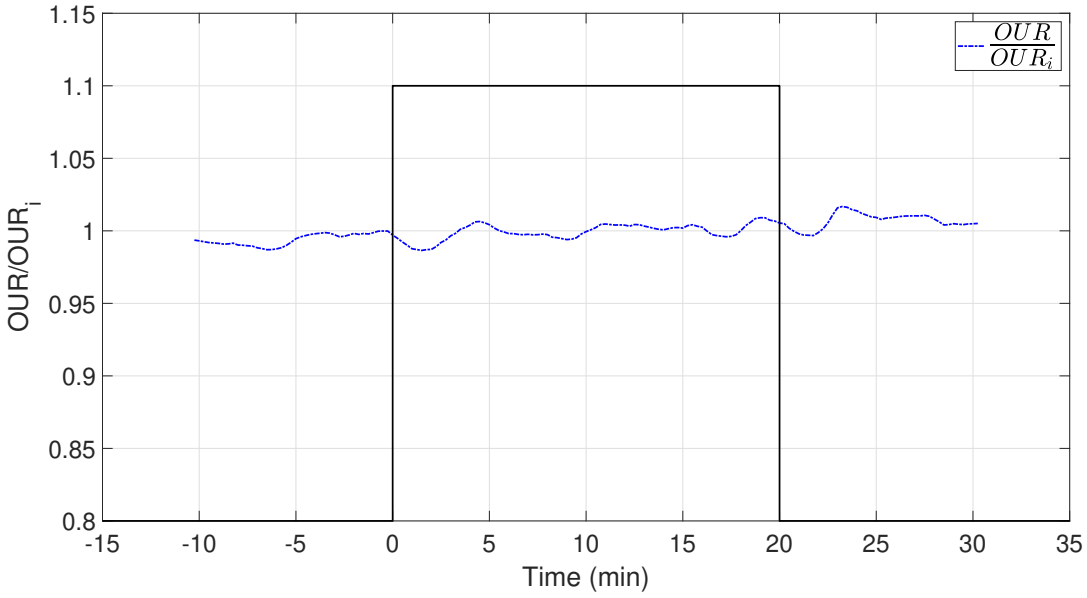

Figure A10: Pulse 2

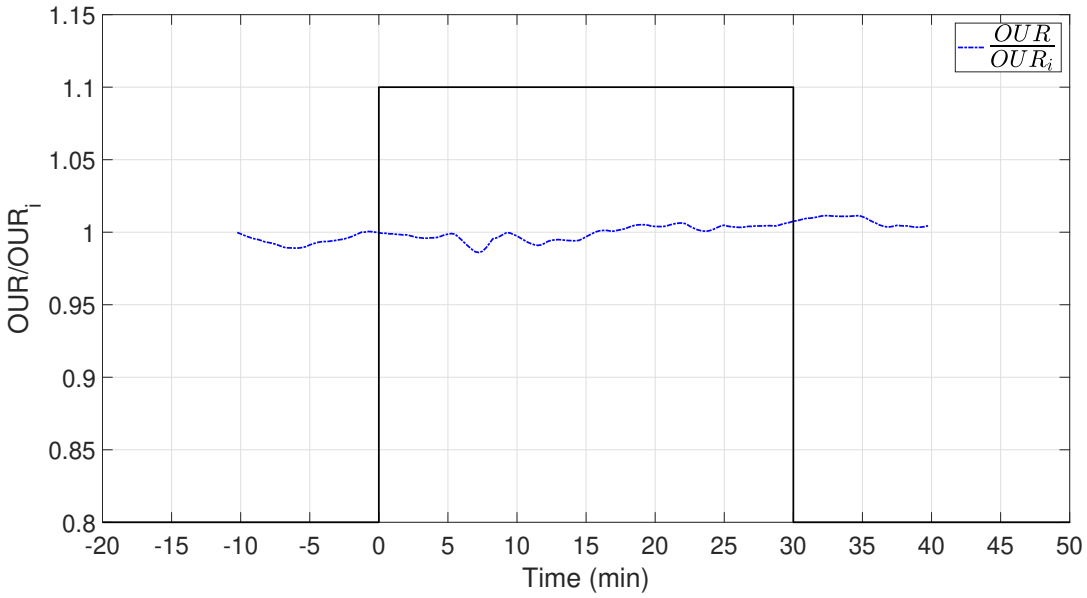

Figure A11: Pulse 3

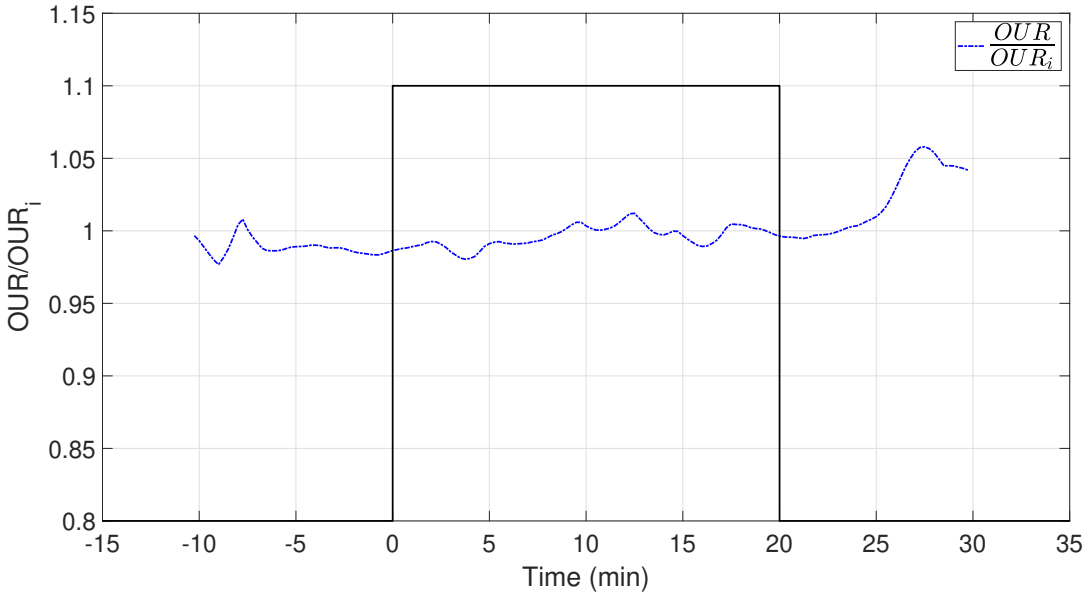

Figure A12: Pulse 4

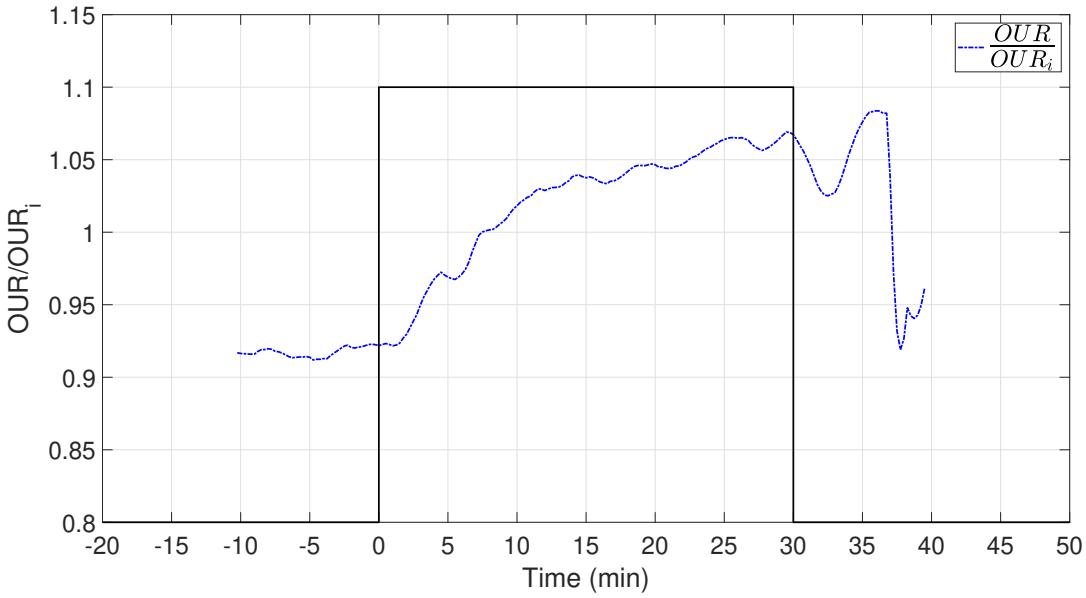

Figure A13: Pulse 5

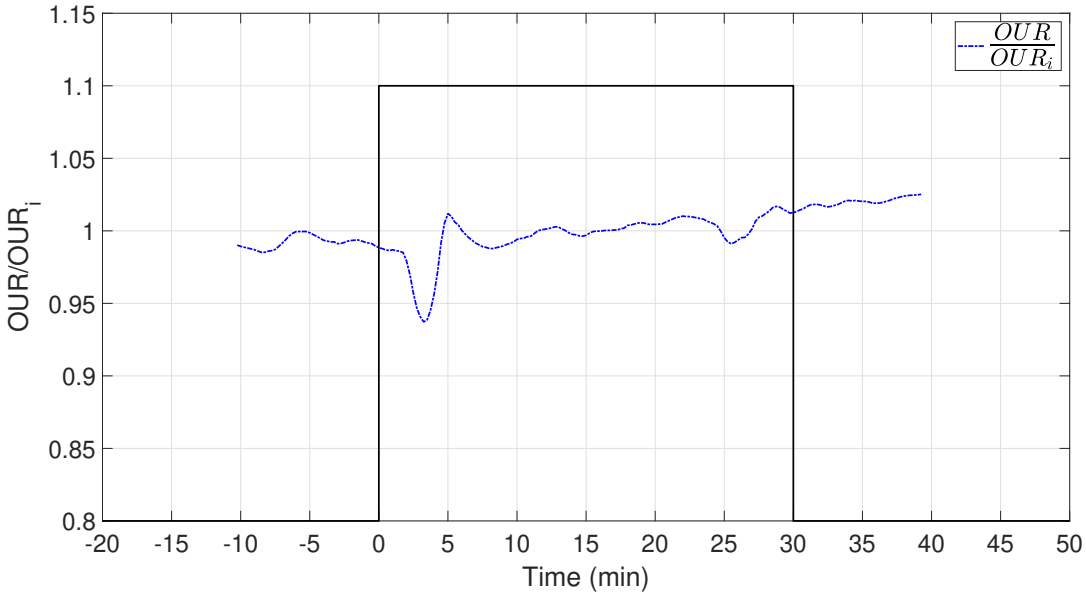

Figure A14: Pulse 6

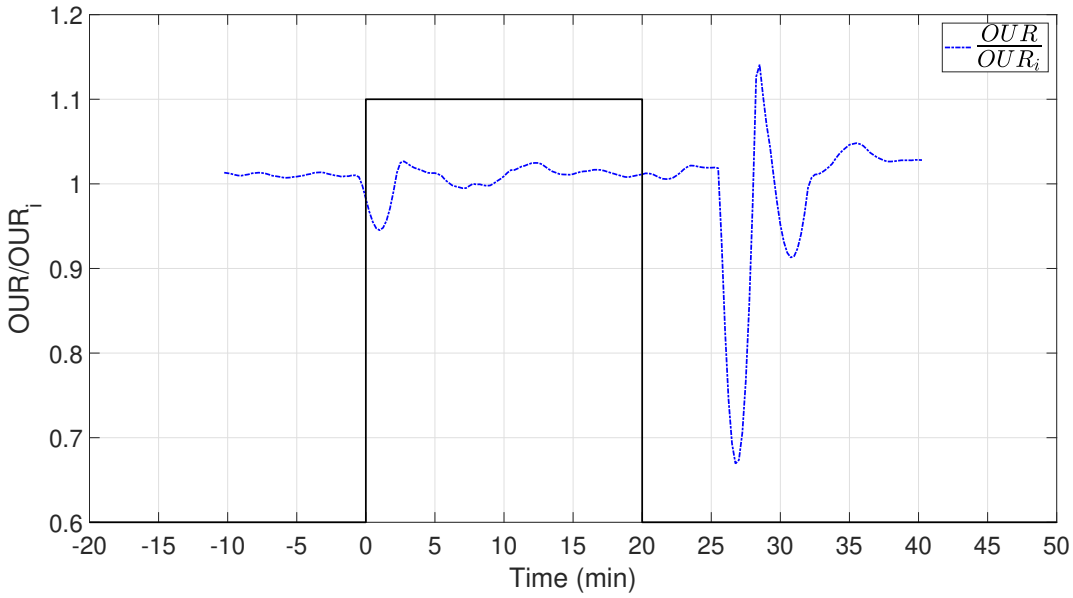

Figure A15: Pulse 7

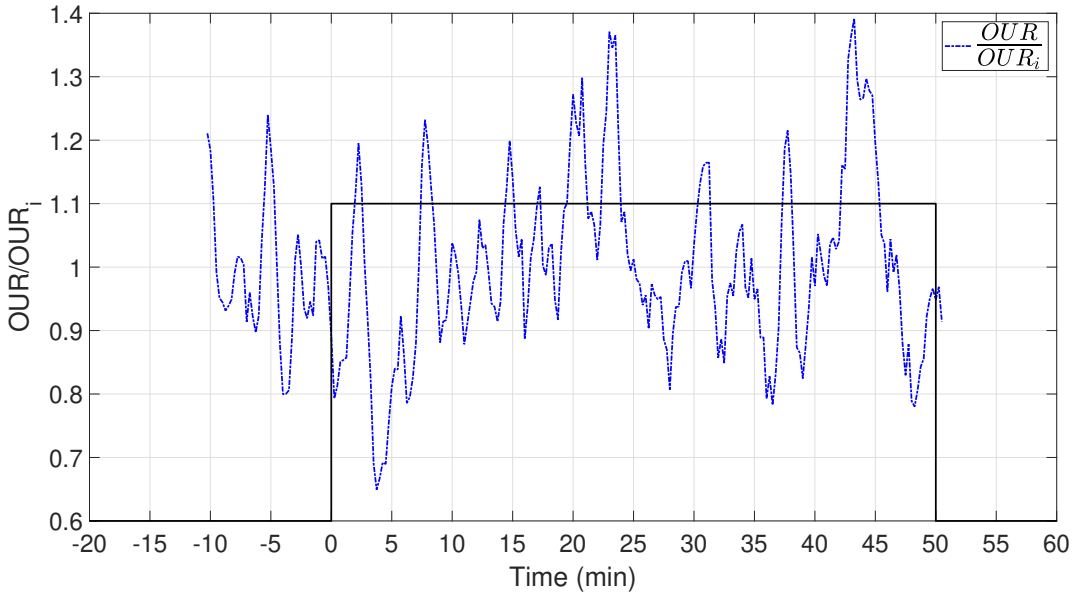

Figure A16: Pulse 8

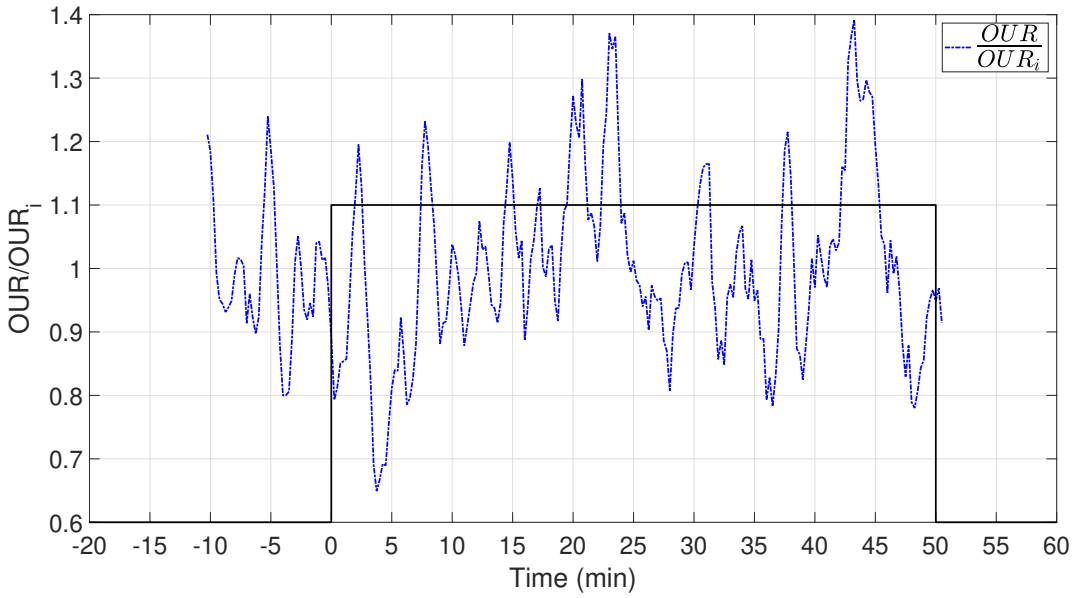

Figure A17: Pulse 9

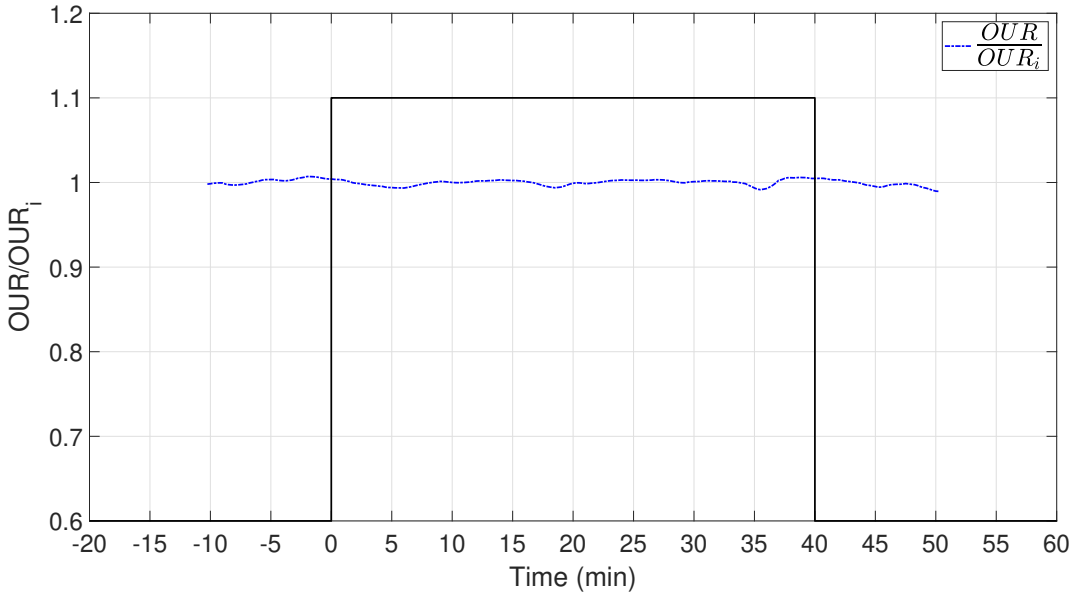

Figure A18: Pulse 10

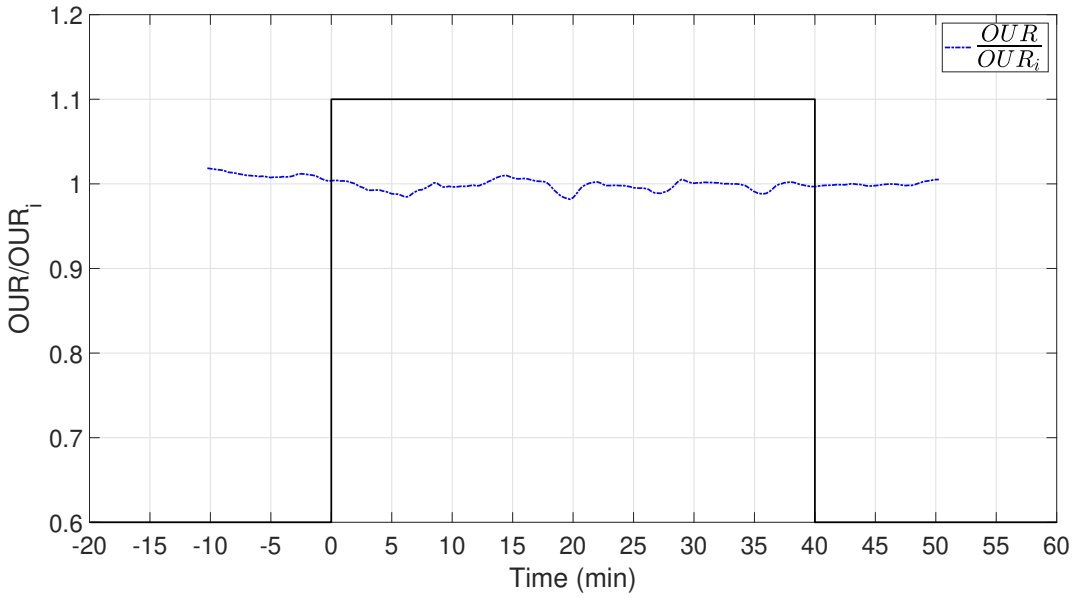

Figure A19: Pulse 11

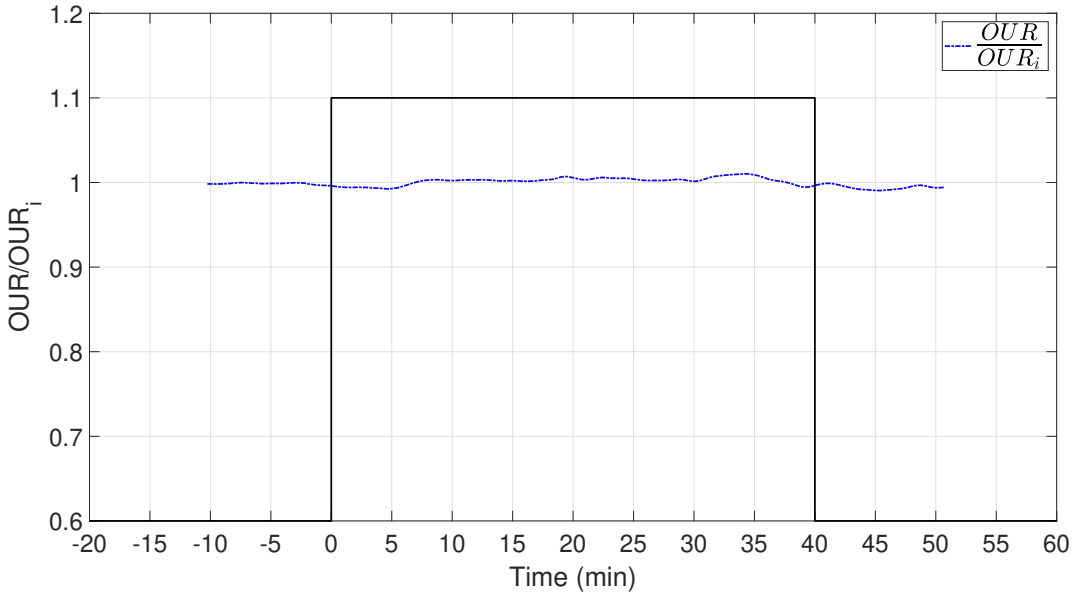

Figure A20: Pulse 12

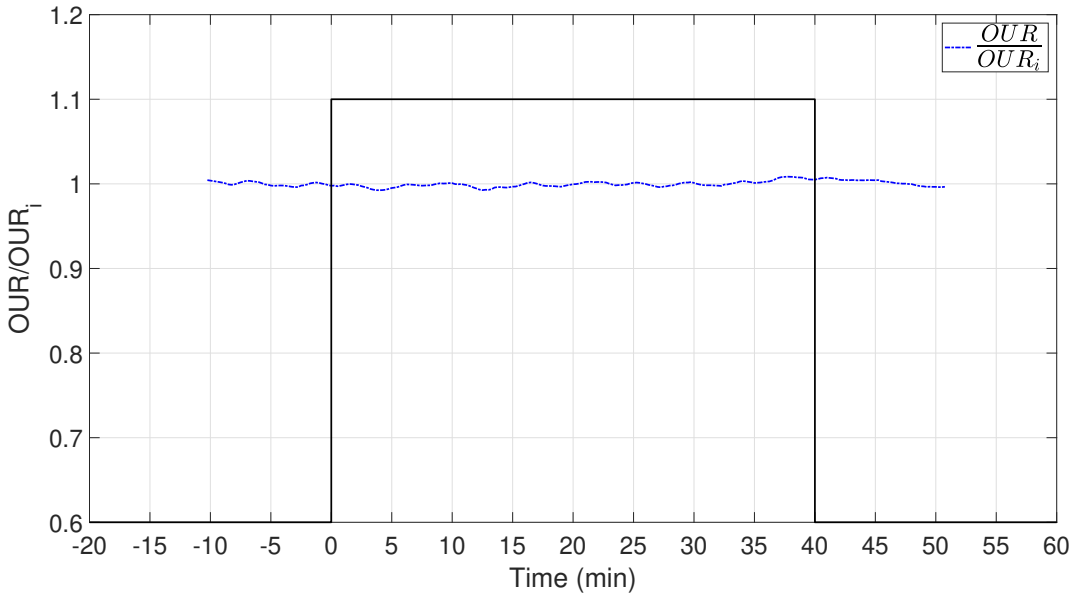

Figure A21: Pulse 13

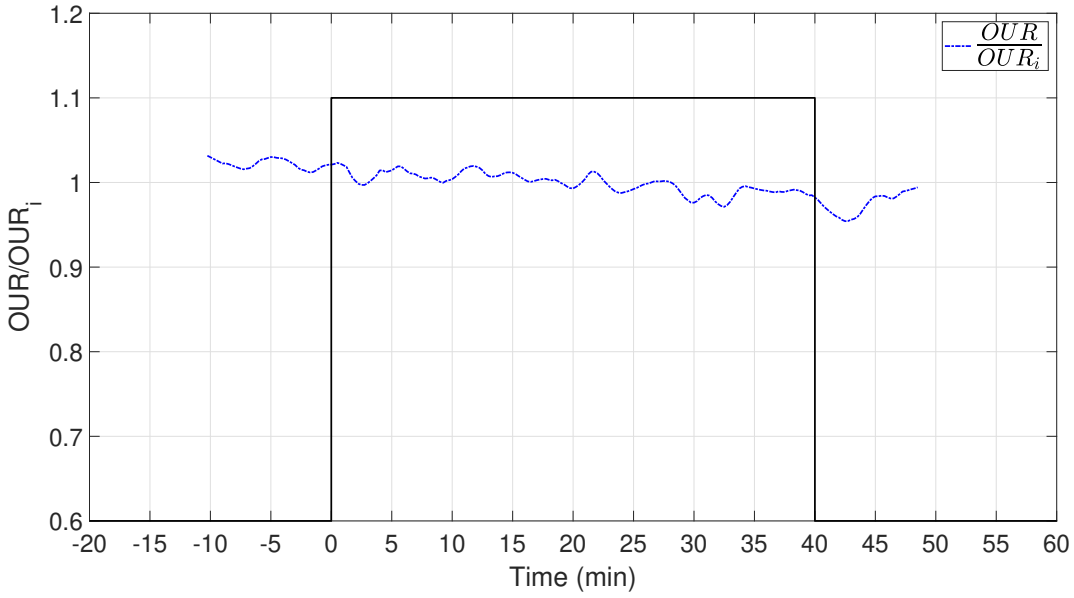

Figure A22: Pulse 14

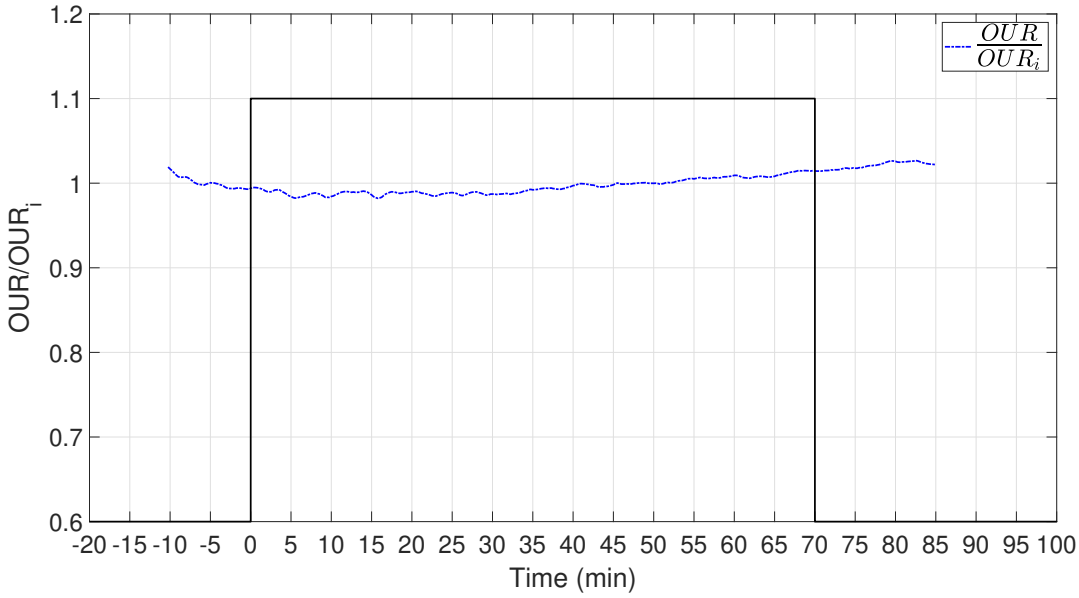

Figure A23: Pulse 15

Bibliography

[Aehle, 2010] Aehle, M. (2010). Application of bluesens analyzers in a cell culture process. *BlueSens Report 1*, pages 22–28.

[Al-Rubeai et al., 2015] Al-Rubeai, M., Jäger, V., Büssow, K., Schirrmann, T., and McDonnell, S. (2015). *Animal Cell Culture*. Springer International Publishing, Belmont. DOI 10.1007/978-3-319-10320-4.

[Badino et al., 2000] Badino, A. C., Facciotti, M., and Schmidell, W. (2000). Improving kla determination in fungal fermentation, taking into account electrode response time. *Journal of Chemical Technology and Biotechnology*, 75(6):469–474.

[Bandyopadhyay et al., 1967] Bandyopadhyay, B., Humphrey, A., and Taguchi, H. (1967). Dynamic measurement of the volumetric oxygen transfer coefficient in fermentation systems. *Biotechnology and bioengineering*, 9(4):533–544.

[Brunner et al., 2016] Brunner, M., Fricke, J., Kroll, P., and Herwig, C. (2016). Investigation of the interactions of critical scale-up parameters (ph, po2 and pco2) on cho batch performance and critical quality attributes. *Bioprocess and Biosystems Engineering*, pages 1–11.

[Castan et al., 2002] Castan, A., Näsman, A., and Enfors, S.-O. (2002). Oxygen enriched air supply in escherichia coli processes: production of biomass and recombinant human growth hormone. *Enzyme and microbial technology*, 30(7):847–854.

[Dorresteijn et al., 1994] Dorresteijn, R. C., Gooijer, C. D. D., Tramper, J., and Beuvery, E. C. (1994). A simple dynamic method for on-line and off-line determination of kla during cultivation of animal cells. *Biotechnology techniques*, 8(9):675–680.

[Doverskog et al., 1997] Doverskog, M., Ljunggren, J., Öhman, L., and Häggström, L. (1997). Physiology of cultured animal cells. *Journal of Biotechnology*, 59:103–115.

[Fontova et al., 2018] Fontova, A., Lecina, M., López-Repullo, J., bIvánMartínez Monge, Comas, P., Bragósa, R., and Cairób, J. J. (2018). A simplified implementation of the stationaryliquid mass balance method for on-line our monitoring in animal cell cultures. *SOCI Journal*.

[Friesewinkel et al., 2010] Friesewinkel, P., Niu, H., Drugmand, J.-C., and Bogaerts, P. (2010). Simple metabolic modelling of vero cell growth on glucose in fixed-bed bioreactors. In *The 11th IFAC Symposium on Computer Applications in Biotechnology (CAB2010)*.

[Goldrick et al., 2018] Goldrick, S., Lee, K., Spencer, C., Holmes, W., Kuiper, M., Turner, R., and Farid, S. S. (2018). On-line control of glucose concentration inhigh-yielding mammalian cell cultures enabledthrough oxygen transfer rate measurements. *Biotechnology Journal*.

[Handlogten et al., 2018] Handlogten, M., Zhu, M., and Ahuja, S. (2018). Intracellular response of cho cells to oxidative stress and its influence on metabolism and antibody production. *Biochemical Engineering Journal*, 133(1):12–20.

[Hu et al., 2011] Hu, W., Berdugo, C., and Chalmers, J. J. (2011). The potential of hydrodynamic damage to animal cells of industrial relevance: current understanding. *Cytotechnology*.

[Ju et al., 1991] Ju, L. K., Lee, J. F., and Armiger, W. B. (1991). Enhancing oxygen transfer in bioreactors by perfluorocarbon emulsions. *Biotechnology Progress*, 7(4):323–329.

[Lara et al., 2011] Lara, A. R., Knabben, I., Regestein, L., Sassi, J., Caspeta, L., Ramírez, O. T., and Büchs, J. (2011). Comparison of oxygen enriched air vs. pressure cultivations to increase oxygen transfer and to scale-up plasmid dna production fermentations. *Engineering in Life Sciences*, 11(4):382–386.

[Lashkari, 2017] Lashkari, S. G. (2017). Controlling recombinant escherichia coli cultures to the boundary of oxidative and overflow metabolism (boom) for robust efficient growth. Master's thesis, Clemson University.

[Ljunggren and Häggström, 1992] Ljunggren, J. and Häggström, L. (1992). Glutamine limited fed-batch culture reduces the overflow metabolism of amino acids in myeloma cells. *Cytotechnology*, 8:45–56.

[Mayyan, 2017] Mayyan, M. (2017). On-line estimation of oxygen transfer rate with oxygen enriched air using off-gas sensor for escherichia coli. Master's thesis, Clemson University.

[Narendra and Annaswamy, 2012] Narendra, K. S. and Annaswamy, A. M. (2012). *Stable adaptive systems*. Courier Dover Publications.

[Nasser and El-Moghaz, 2010] Nasser, A. and El-Moghaz (2010). Factors effects the growth of chinese hamster ovary (cho) cell on microcarriers culture. *Advances in Bioresearch*, 1:182–188.

[Patel and Thibault, 2009] Patel, N. and Thibault, J. (2009). Enhanced in situ dynamic method for measuring kla in fermentation media. *Biochemical Engineering Journal*, 47(1):48–54.

[Pepper, 2015] Pepper, M. E. (2015). *Designing a Minimal-Knowledge Controller to Achieve Fast, Stable Growth for Recombinant Escherichia coli Cultures*. PhD thesis, Clemson University.

[Redmon et al., 1983] Redmon, D., Boyle, W. C., and Ewing, L. (1983). Oxygen transfer efficiency measurements in mixed liquor using off-gas techniques. *Journal (Water Pollution Control Federation)*, pages 1338–1347.

[Riet, 1979] Riet, K. V. (1979). Review of measuring methods and results in nonviscous gas-liquid mass transfer in stirred vessels. *Industrial and Engineering Chemistry Process Design and Development*.

[Wang, 2014] Wang, L. (2014). Design and implementation of a real-time adaptive oxygen transfer rate estimator. Master's thesis, Clemson University.